# IDENTIFYING INHIBITORS OF BREAST TUMOR-INITIATING CELLS

# A HIGH-THROUGHPUT SCREEN TO IDENTIFY SMALL MOLECULES THAT SELECTIVELY TARGET TUMOR-INITIATING CELLS IN A MOUSE MODEL OF HER2-INDUCED BREAST CANCER

By

Andrew Oswald Giacomelli, B.Sc. (Hons.)

A Thesis Submitted to the School of Graduate Studies in Partial Fulfillment of the Requirements for the Degree Master of Science

McMaster University

MASTER OF SCIENCE (2011) McMaster University (Biochemistry)
Hamilton, Ontario

Title: A high-throughput screen to identify small molecules that selectively target tumor-initiating cells in a mouse model of Her2-induced breast cancer

Author: Andrew Oswald Giacomelli, B.Sc. (Hons.)

Supervisor: Dr. John A. Hassell

Number of pages: vi, 132

**ABSTRACT**

**A growing body of evidence suggests that most human tumors, including those of the breast, are organized as cellular hierarchies. Positioned at the apex of these hierarchies are tumor-initiating cells (TICs), which are capable of limitless self-renewal and also differentiate, to give rise to various populations of non-tumorigenic cells that make up the bulk of the tumor. Importantly, recent findings have demonstrated that TICs are refractory to current best practice therapies, and thus likely account for high rates of tumor recurrence following remission. Therefore, it will likely be important to identify novel means of targeting TICs in order to achieve durable cancer cures.**

**Using a highly sensitive transplantation assay, our laboratory previously showed that mammary tumors arising in various strains of transgenic mice comprise a very high fraction of TICs, and that when cells from these tumors are propagated in serum-free medium as tumorspheres, the high frequency of TICs is maintained. We therefore sought to use mouse mammary tumorspheres as an *in vitro* system with which to identify TIC-targeted agents and carried out a high-throughput screen of nearly 32,000 small molecules. To eliminate compounds showing general toxicity, we employed mouse mammospheres, which primarily comprise normal mammary epithelial stem and progenitor cells, in a secondary screen. Using this platform, we identified a small molecule that selectively targeted tumorsphere-derived cells *in vitro* and led to tumor growth arrest and tumor cell death *in vivo*. This study illustrates the utility of mouse models and high throughput screening to identify compounds which may target TICs but spare untransformed stem cells.**

**ACKNOWLEDGEMENTS**

I owe a great debt of gratitude to those individuals whose contributions have made this work possible. First, I would like to thank my supervisor, Dr. John Hassell, whose constant guidance, and wealth of experience and knowledge have helped shape me as a scientist. I would also like to thank the members of my supervisory committee, Dr. Sheila Singh and Dr. Gerry Wright for their invaluable advice and insights into my research. Acknowledgement is also due to all the members of the Hassell lab who have contributed directly or indirectly to this work. I would particularly like to thank Robin Hallett for conducting and analyzing the *in vivo* experiments in N#202 tumors (Figure 7-8), Craig Aarts for conducting and analyzing immunostains of Compound X-treated spheres (Figure 6C-F), Adele Girgis-Gabardo for isolating and preparing cells for the high-throughput screen (Figure 5, Table 1) and for conducting and analyzing countless sphere-forming assays (Figure 6A-B, Table 4), Allison Nixon for preparing the catalase expression vector (Figure 19) and TOP-FLASH reporter vector (Figure 21), and Dr. Anna Dvorkin for performing gene set enrichment analysis (Table 8). Thanks are also due to additional members of the Hassell group, past and present, for their willingness to partake in stimulating scientific discussion and for their commitment to the research goals of our laboratory, namely Dr. Bonnie Bojovic, Dr. Anita Bane, Dr. Natasza Kurpios, Dr. Dora Ilieva, Dr. Duane Hewitt, Maria Kondratyev, Stephen Rogers, Antonija Kreso, Salma Trabelsi, and Ali Lessan.

Ultimately, this work would not have been possible without the help of our collaborators at the McMaster Institute for Infectious Disease Research (Dr. Eric Brown, Dr. Kalinka Koteva, Jan Blanchard, Cecilia Murphy, Jenny Wang, Inga Kireeva), the McMaster Chemistry Department (Dr. Fred Capretta, Nick Todorovic), and the Ontario Institute for Cancer Research Medicinal Chemistry Division (Dr. Rima Al-Awar, Dr. David Uehling , Dr. Ahmed Mami), and they too are owed a great deal of thanks.

Finally, I would like to thank my family for supporting me in my decision to pursue a career in research.

*This thesis is dedicated to Ophelia Giacomelli and Rita Hunsperger, whose stories impel me to find a cure for breast cancer.*

**TABLE OF CONTENTS**

**LIST OF FIGURES**

**LIST OF TABLES**

**LIST OF ABBREVIATIONS**

ALDH1 – aldehyde dehydrogenase 1
AML – acute myeloid leukemia
aS MA – alpha smooth muscle actin
bFGF – basic fibroblast growth factor
BSA – bovine serum albumin
CI – 95% confidence interval
CMV – cytomegalovirus
CSC – cancer stem cell
DAPI – diamidinophenylindoline
DFF-dA – difluorofluorescein diacetate
DMEM – Dulbecco's Modified Eagle Media
DMSO – dimethyl sulfoxide
EDAC – 1-ethyl-3-(3-dimethylaminopropyl) carbodiimide
EDTA – ethylenediaminetetraacetic acid
EGF – epidermal growth factor
EGFR – epidermal growth factor receptor
ESA – epithelial specific antigen
FACS – fluorescence activated cell sorting
FBS – fetal bovine serum
GPX – glutathione peroxidase
GSH – glutathione (reduced)
GSK3β – glycogen synthase kinase 3-β
GSSG – glutathione (oxidized)
GST – glutathione S-transferase
H&E – hematoxylin and eosin
HTS – high-throughput screening
$IC_{50}$ – concentration that inhibits activity/viability by 50%
IgG – immunoglobulin gamma
MMS – mammospheres
MMTV – mouse mammary tumor virus
MOPS – 3-(N-morpholino)propanesulfonic acid
NHS – *N*-hydroxysuccinimide
NOD/SCID – non-obese diabetic/severe combined immune-deficient
NSG – NOD/SCID/interleukin-2 receptor $\gamma^{KO/KO}$
PBS – phosphate buffered saline
ROS – reactive oxygen species
SCM – stem cell media
SDS – sodium dodecyl sulfate
SFE – sphere-forming efficiency
TMS – tumorspheres
TUNEL – terminal dUTP nick-end label

# 1. INTRODUCTION

## *1.1. Tumor cell heterogeneity and the cancer stem cell model*

Human tumors are often complex tissues that, in addition to supporting stromal, endothelial, and hematopoietic cells, comprise a collection of clonally derived, but phenotypically distinct cancer cells. This phenomenon was first realized in the early 20$^{th}$ century, but has only recently been linked to disease progression and response to therapy (Dick 2008). The cancer stem cell hypothesis proposes that this cellular heterogeneity is the result of an abnormal developmental program, initiated by cancer cells with stem cell-like properties, equivalently termed cancer stem cells (CSCs), tumorigenic cells, or tumor-initiating cells (TICs) (Reya et al. 2001). In a process that mirrors normal organogenesis and tissue repair, TICs give rise to all the various tumor cell types through a defined, albeit aberrant program of differentiation (Figure 1). Just as somatic stem cells are unique in their ability to generate and maintain complete normal tissues for the lifetime of an organism, in the abnormal hierarchy of a tumor, only the TICs are thought to possess long term self-renewal and tumor reconstitution potential (Reya et al. 2001). The remaining cancer cells, although capable of rapid short-term proliferation, are thought to be incapable of sustaining tumor growth or initiating malignant metastases. Whereas recent evidence suggesting that TICs may be generated from non-tumorigenic cells has rendered the absoluteness of this hypothesis somewhat contentious (Roesch et al. 2010; Vermeulen et al. 2010; Chaffer et al. 2011; Iliopoulos et al. 2011), it nevertheless represents a significant advance in our understanding of tumor biology and also appears to have important clinical ramifications.

Support for the CSC hypothesis has been garnered through the application of functional tests of developmental potential and self-renewal to populations of tumor cells. Analogous to assays for somatic stem cells, *bona fide* tumorigenic cells must be able to engraft an immune-compromised or syngeneic recipient animal and generate a secondary tumor that recapitulates the tumor of origin, in terms of its cellular heterogeneity and capacity for serial transplantation. Although autologous tumor cell transplantation experiments, which would be considered unethical by today's standards, initially suggested that human tumors comprise rare populations of TICs (Dick 2008), John Dick and colleagues at the University of Toronto were the first to rigorously apply the principles of stem cell biology to isolate and quantify TICs in human tumors (Lapidot et al. 1994). Using a combination of fluorescence activated cell sorting (FACS) and limiting-dilution xenotransplant assays, this group was able to reproducibly separate human acute myeloid leukemia (AML) samples into tumorigenic and non-tumorigenic cell fractions (Lapidot et al. 1994). The cells having tumorigenic potential were characterized by high expression of CD34 and low expression of CD38, a cell surface phenotype normally associated with hematopoietic stem cells. When transplanted into immune-compromised mice, as few as 1000 $CD34^+/CD38^-$ cells could engraft and reproduce the cellular heterogeneity of the primary tumor, whereas $CD34^+/CD38^+$ and $CD34^-$ cells never engrafted, even when up to a million cells were transplanted. Since this initial demonstration, analogous protocols have illustrated that minority TIC populations can also be purified from a variety of solid tumor types, including those of the breast (Al-Hajj et al. 2003), brain (Singh et al. 2003), neural crest (Hansford et al. 2007), head and neck (Prince et al. 2007), skin (Quintana et al. 2008; Schatton et al. 2008), colon (O'Brien et al. 2007), and prostate (Collins et al. 2005).

In human breast cancer, cells having tumorigenic potential were first prospectively purified from pleural effusions using antibodies against lineage (Lin) markers (CD2, CD3, CD10, CD16, CD18, CD31, CD64, and CD140b), the epithelial specific antigen, ESA, the hyaluronic acid receptor, CD44, and the heat stable antigen, CD24 (Al-Hajj et al. 2003). Those cells which displayed a $Lin^-/ESA^+/CD44^+/CD24^-$ marker profile were capable of generating serially transplantable xenografts in non-obese diabetic/severe combined immune deficient (NOD/SCID) mice 10- to 50-fold more efficiently than unsorted tumor cells, or cells from other sorted fractions. Interestingly, the $CD44^+/CD24^-$ surface phenotype is also associated with basal cells in the mammary gland as well as mammary epithelial cells experimentally induced to undergo an epithelial-to-mesenchymal transition (Mani et al. 2008). Moreover, the $CD44^+/CD24^-$ populations of normal mammary epithelial cells and breast cancer cells have an enhanced capacity to form non-adherent spherical colonies when cultured in serum-free medium, suggesting that they may be stem-like (Dontu et al. 2003; Fillmore and Kuperwasser 2008; Mani et al. 2008).

A complementary approach to enrich for normal and tumorigenic human mammary stem-like cells uses the Aldefluor™ assay, in which a weakly fluorescent substrate is converted to a more highly fluorescent form in cells having high aldehyde dehydrogenase 1 (ALDH1) activity (Ginestier et al. 2007). Upon transplant, FACS-sorted $Aldefluor^{hi}$ cells have an increased capacity for generating xenografts in NOD/SCID mice as compared to unsorted cells, whereas $Aldefluor^{lo}$ cells do not engraft. Notably, the Aldefluor assay has also been used to further enrich the purity of TICs in the $CD44^+/CD24^-$ population of breast tumor xenografts, and in one experiment, as few as twenty $Lin^-/Aldefluor^{hi}/CD44^+/CD24^-$ cells were capable of generating

tumors in subsequent recipients. Interestingly, $CD44^+/CD24^-$ and $ALDH1^+$ cells are more often found in breast tumors of the basal molecular subtype (Lee et al. 2011), however, it is presently unclear whether this reflects an increased frequency of TICs in basal versus luminal breast cancer, or whether TICs in luminal breast cancers express different cell-surface markers or functional activities.

Importantly, numerous pre-clinical and clinical studies have demonstrated that many front-line chemotherapeutics, including anthracyclines, alkylating agents, taxanes, antiestrogens, and nucleoside analogues can increase the frequency of $CD44^+/CD24^-$, $ALDH1^+$, and/or sphere-forming cells in human breast cancer cell lines (Fillmore and Kuperwasser 2008), xenografts (Yu et al. 2007), and patient tumors (Li et al. 2008; Creighton et al. 2009; Lee et al. 2011), suggesting that although these agents can shrink tumors, they may be ineffective at targeting rare TICs. Given that TICs are capable of limitless expansion and possess tumor-reconstitution potential, these findings offer an explanation for the eventual failure of current therapeutic regimens and stress the importance of finding novel means of targeting these stem-like cells in order to achieve long-lasting cures. Moreover, because cancer stem cells and normal somatic stem cells likely share many but not all attributes, and the latter cells are critical for the maintenance of normal tissue homeostasis, it would be advantageous to identify agents which target TICs but not untransformed stem cells (Figure 2).

*1.2 Mouse models of human breast cancer*

Unfortunately, extensive molecular characterization of TICs from tumors generally, and in particular human breast tumors, has been hindered by an inability to obtain sufficiently pure populations with which to perform analyses – and this in turn has impeded drug discovery

efforts. The difficulties stem primarily from the relative rarity of TICs within human breast tumors (1 in $10^4$ – 1 in $10^5$ cells), the small quantity of tumor tissue made available following surgical resection (<1 $cm^3$), the failure of current culture techniques to permit maintenance or expansion of the number of TICs *in vitro*, and the lack of unambiguous markers to distinguish TICs from the more abundant non-tumorigenic cells. By contrast, mammary tumors that arise in various strains of transgenic mice can be grown to larger sizes (~5 $cm^3$) and comprise a very high fraction of TICs (Kurpios et al. 2011). As determined by limiting-dilution cell transplant assay, approximately 30% of bulk tumor cells from each of 3 independent strains are functional TICs, and remarkably, single unpurified tumor cells can generate large tumors in as little as 16 weeks. One such transgenic strain, in which Her2 is overexpressed and activated in mammary epithelial cells, serves as a good illustration of how mouse models of breast cancer can be used to circumvent some of the issues associated with working with human breast tumors, and can serve as tool to aid in discovery of agents that target breast TICs.

Her2 (c-ErbB2, Neu) is a receptor tyrosine kinase of the epidermal growth factor receptor (EGFR) family that is amplified and/or overexpressed in approximately 20-30% of human breast cancers, and whose expression is inversely correlated with patient survival (Slamon et al. 1987). Two targeted therapies are currently approved to treat patients with Her2-positive breast tumors: Trastuzumab (Herceptin™), a humanized monoclonal antibody directed against the extracellular domain of Her2 (Hortobagyi 2001), and Tykerb (Lapatinib™) (Strecker et al. 2009), a dual-specificity EGFR1/Her2 kinase inhibitor. Although these therapies are often able to prolong survival, they are rarely curative, and patients generally relapse with resistant disease (Harris et al. 2011). These observations suggest that tumorigenic cells may be spared by these

treatments and emphasizes the need to develop new approaches to treat patients whose tumors overexpress Her2.

Several mouse models of Her2-overexpressing breast cancer have been developed (reviewed in (Ursini-Siegel et al. 2007), and for a variety of reasons we have chosen to focus on the N#202 strain developed by Bill Muller and colleagues (Guy et al. 1992). This particular strain expresses the cDNA for normal rat Neu under transcriptional control of the mouse mammary tumor virus (MMTV) promoter/enhancer, and was initially developed as an alternative to earlier MMTV-Neu-NT models, which were engineered to express a mutant and constitutively active form of Neu (Muller et al. 1988). In the latter model, transgenic females develop synchronous multi-focal mammary tumors with early onset and high penetrance, however in the N#202 strain, mammary tumors arise after a long latency period (50% of virgin mice develop tumors by 205 days of age), often comprise a single focus, and have a propensity to metastasize to the lung, suggesting that additional mutagenic events are required for frank tumor development. Interestingly, the majority of N#202 tumors feature in-frame mutations in the transgene, which eliminate or add an odd number of cysteine residues in the extracellular juxtamembrane region of the Neu protein (Siegel et al. 1994). This causes intermolecular disulfide bonds to form between receptors and leads to constitutive, ligand-independent activation of Neu tyrosine kinase activity and downstream signaling events, including the Phosphatidyl-inositol-3 kinase (PI3K) and Src pathways.

Given that the same or similar processes lead to tumor formation in most mice of this strain, it is not surprising that global transcriptomic analyses demonstrated a homogeneous pattern of gene expression among nearly all N#202 tumors examined (9 of 10) (Herschkowitz et

al. 2007). This suggests that studies of tumor progression or response to therapy in this model are likely to yield similar results across individual mice, which in turn simplifies the interpretation of experimental results. Furthermore, by comparing the gene expression profiles of this and 12 other mouse models of breast cancer with those of 184 primary human breast tumors, it was demonstrated that N#202 tumors cluster most closely with human luminal B tumors, which overexpress Her2, lack estrogen and progesterone receptor expression, and exhibit poor prognosis. Thus, this strain provides an accurate and experimentally tractable model of a clinically relevant subset of human breast cancers.

*1.3. Sphere culture for propagation of normal and malignant mammary stem cells*

As mentioned above, results from our laboratory have demonstrated that approximately 30% of freshly-isolated primary N#202 tumor cells are functional TICs. Moreover, the proportion of tumorigenic cells can be maintained indefinitely by culturing these cells in serum-free, chemically-defined medium containing epidermal growth factor (EGF), basic fibroblast growth factor (bFGF), and B27 nutrient supplement (Kurpios et al. 2011); a medium initially developed to propagate normal mouse neuronal stem cells *in vitro* as neurospheres (Reynolds and Weiss 1992) and later used to propagate normal human mammary epithelial cells as mammospheres (MMS) (Dontu et al. 2003). Under these growth conditions, individual tumor cells give rise to non-adherent colonies we previously termed tumorspheres (TMS) (Youn et al. 2005) (Figure 3), which according to global gene expression profiling, very closely mimic the primary tumor from which they were derived. Importantly, in this model, TMS-forming cells co-fractionate with tumorigenic cells, suggesting that sphere-formation is likely a good surrogate assay for TICs (Liu et al. 2007). It is also noteworthy that in contrast to cells grown in serum-

containing medium in two-dimensional (2D) culture systems, which are depleted by orders of magnitude in TICs (Kurpios et al. 2011), cells within TMS bear a striking morphological resemblance to tumor cells *in situ*. Collectively, these findings provided us with a compelling rationale to use mouse mammary TMS as a renewable source of breast TICs for study *in vitro*.

Using the same media and growth conditions that promote neurosphere and TMS formation, we have been able to propagate normal mouse mammary epithelial stem and progenitor cells as MMS (Figure 3). The functionality of these cells is preserved for several passages *in vitro,* and when transplanted orthotopically into the cleared fat pads of syngeneic recipient mice, MMS-derived cells can give rise to duct-limited outgrowths, lobule-limited outgrowths, or complete mammary outgrowths that include both ducts and lobules (Liao et al. 2007) (N. Kurpios and J. A. Hassell, unpublished data). These outgrowths can be serially transplanted in successive recipient animals, formally demonstrating that MMS comprise functional stem and progenitor cells. Furthermore, recent work suggests that mammosphere-initiating cells, identified by their relative quiescence in culture, represent a population of *bona fide* mammary epithelial stem cells (Cicalese et al. 2009). Because these cells likely represent the precursors to breast TICs *in vivo* and are not transformed through *in vitro* sphere culture, MMS are presumed to be an excellent normal cell control for studies carried out in TMS.

## 2. MATERIALS AND METHODS

### *2.1. alamarBlue proliferation assay*

Thoracic #3 and abdominal #4 mammary glands isolated from 6-8 week old virgin FVB/N females, or mammary tumors isolated from transgenic N#202 females were diced by razor

blade, digested enzymatically (trypsin/collagenase), washed in F12 (Gibco), and resuspended in mouse stem cell media (mSCM) [low glucose DMEM (Gibco)/F12 (Gibco) (3:1) containing mouse EGF (Invitrogen) (20 ng/mL), bFGF (Invitrogen) (40 ng/mL), B27 (Gibco) (4 ng/mL), fungizone (Gibco) (1 mg/mL), penicillin/streptomycin (Gibco) (1%), and Heparin (Sigma) (4 ng/mL)].

Human breast cancer cell line spheres are grown in human Stem Cell Media (hSCM) [low glucose DMEM/F12 (3:1) containing human EGF (Invitrogen) (20 ng/mL), bFGF (10 ng/mL), human insulin (Sigma) (40 μg/mL), B27 (2 ng/mL), fungizone (1 mg/mL), penicillin/streptomycin (1%), and Heparin (4 ng/mL)].

Adherent human breast cancer cell lines were propagated in RPMI (Gibco) supplemented with 10% FBS (Gibco), fungizone (1 mg/mL), and penicillin/streptomycin (1%).

In preparation for alamarBlue assays, sphere cultures were centrifuged and dissociated, or adherent cell cultures trypsinized, washed, and resuspended. Total viable cell number was measured by Trypan Blue (Gibco) exclusion and cell number determined using a hemocytometer. Cells were then diluted 20,000 cells/mL and 50 μL pipetted into wells of a black 384-well plastic dish using a Beckman Coulter Biomek 3000 or Biomek FX. Following addition of cells and compound, the plates are incubated for 24 hours at 37°C, 5% $CO_2$. alamarBlue (5 μL) (Gibco) is then added to each well, and plates are incubated for a further 24 hours. Fluorescence is read at $\lambda_{excitation}$ = 535 nm and $\lambda_{emission}$ = 600 nm using a Perkin Elmer EnVision or a Beckman Coulter Multimode Detector Dx. High (+) control wells contain cells in media and vehicle without compound, low (–) control wells contain media and vehicle with no cells.

$$\% \text{ Residual Activity} = (\text{Relative Fluorescence Units} - \mu_- / (\mu_+ - \mu_-) \times 100\%$$

$$\% \text{ Inhibition of Proliferation} = 100\% - \% \text{ Residual Activity}$$

$$Z' = 1 - ((3\sigma_+ + 3\sigma_-) / |\mu_+ - \mu_-|)$$

$\mu$ refers to the mean Relative Fluorescence Units of the controls, $\sigma$ represents their standard deviation.

Dose response curves are generated using GraphPad Prism™ non-linear regression analysis software (unconstrained, variable Hill slope).

*2.2. Sphere-forming assay*

In preparation for sphere-forming assays, single cell suspensions derived from primary tumors, primary mammary epithelial cells, or established TMS and MMS cultures were obtained as in the alamarBlue assay. Cells were pipetted into wells of a 96-well clear plastic plate using a Beckman Coulter Biomek 3000, and serially diluted compound was then added into triplicate wells. Following 4-7 day incubation at 37°C, 5% $CO_2$, spheres were counted and normalized to vehicle-treated control wells.

*2.3.Animal studies*

All experiments were carried out under the auspices of the Canadian Council on Animal Care (CCAC). Mice were housed in the central animal facility at McMaster University and provided food and water *ad libitum*. Female FVB/N mice were used as recipients for N#202 tumor cells and NOD/SCID/IL-2$\gamma^{KO/KO}$ (NSG) mice were used as recipients for HCC1954 cells. Single cell suspensions were prepared at a 2X concentration in phosphate buffered saline (PBS)/5% FBS

prior to being mixed with Matrigel™ (BD Biosciences) at a 1:1 ratio. One hundred microlitres of the resulting 1X cell suspensions were injected subcutaneously into recipient mice, which were then monitored for tumor growth.

Drug treatments were initiated when tumors reached ~1 $cm^3$. In these instances, mice were treated with Compound X (4 mg/kg in 10 µL DMSO (FVB/N) or 2 mg/kg in 5 µL DMSO (NSG)) or an equivalent volume of DMSO vehicle by intraperitoneal injection using a Hamilton syringe. Following treatment, animals were sacrificed by carbon dioxide suffocation and tumors were harvested for fixed tissue or live cell analysis. Serial transplantation assays using cells from these tumors were similarly conducted, however no further treatment was administered to the recipient mice.

*2.4. Immunofluorescence microscopy*

Formalin-fixed paraffin-embedded tissue fragments were cut into 5 µm sections and placed onto glass slides. Following dewaxing in xylenes and incubation in antigen retrieval solution (Vectashield), sections were washed in PBS (2 x 5 minutes), blocked for 1 hour in blocking buffer (PBS/0.03% Tween-20/3% normal goat serum) prior to incubation with primary antibodies (1.5 hours at room temperature). Sections were then washed (3 x 5 minutes) in PBS prior to incubation with fluorochrome-coupled secondary antibodies (45 minutes at room temperature). After final washes in PBS (3 x 5 minutes), slides were dried, spotted with mounting media containing DAPI (Vectashield), and sealed with coverslips. Primary antibodies and dilutions were as follows: CK8 - polyclonal rat anti-human (Troma hybridoma supernatant) 1/15, aSMA - monoclonal mouse anti-human (Sigma) 1/750. Secondary antibodies (used at a 1/200 dilution) were as follows: goat anti-mouse AlexaFluor 488 (Invitrogen), goat anti-rat AlexaFluor 568

(Invitrogen). TUNEL staining was carried out according to the manufacturers protocol (Millipore). All fluorescence images were taken on Leica DMIRB fluorescence microscope.

*2.5. Combination matrix models*

Where $I_A$ and $I_B$ indicate the % Inhibition of Proliferation achieved by either single agent, and $I_{Model}$ indicates the predicted % Inhibition of Proliferation:

$$I_{Highest\ Single\ Agent} = max\ (I_A, I_B) \qquad I_{Bliss\ Indepedence} = I_A + I_B - (I_A I_B)$$

To provide the highest stringency for quantifying synergy or antagonism, the Highest Single Agent model was applied when antagonistic interactions were inferred, whereas the model for Bliss independence was used for additive or synergistic interactions.

*2.6. Affinity purification*

Mammary tumors from female N#202 mice weighing approximately 1 g were placed in 1 mL of hypotonic lysis buffer (25 mM MOPS, pH = 7.2, 15 mM EDTA, 15 mM $MgCl_2$, Protease inhibitors (Roche) 1/10, Phosphatase inhibitors (Roche) 1/10, 0.5% NP-40) and homogenized on ice using a tissue homogenizer (5 second bursts followed by 10 second recovery/cooling periods). Vials were left on ice for 1 hour prior to being centrifuged at 14,000 rpm for 10 minutes at 4$^{o}$C. Supernatants were then collected as cytoplasmic extracts and, when nuclear extracts were required, the pellet was resuspended in hypertonic lysis buffer (same as above but containing 400 mM NaCl) for a further 20 minutes prior to centrifugation and supernatant collection. Protein concentration in the lysates was estimated using a Bradford assay (BioRad), and was typically 25-50 mg/mL.

Prior to the binding assay, lysates were diluted to 2-4 mg/mL in cold (4$^{o}$C) binding buffer (50 mM Tris, pH = 7.4, 150 mM NaCl, 5 mM EDTA, Protease inhibitors (Roche) 1/10, Phosphatase inhibitors (Roche) 1/10, 0.5% NP-40) and Compound X (200 µM unless otherwise indicated) or an equivalent volume of DMSO vehicle was added to the lysates. Affinity probe-coupled magnetic beads (~2 x $10^{8}$ beads per reaction) were washed 3 times in cold binding buffer, collected by magnet, resuspended in lysate and incubated at 4$^{o}$C for 1 hour using slow-tilt rotation. The beads were then collected by magnet and washed 3 times in cold PBS to remove non-specifically-bound proteins. Beads were then resuspended in SDS buffer containing reducing agent (Invitrogen) and incubated for 5 minutes at 90$^{o}$C to elute specifically-bound proteins. Lysate (at various dilutions) was similarly incubated in reducing SDS buffer. Beads were then collected a final time by magnet and the supernatants removed for analysis.

Lysates, eluates from the beads, and protein standard ladder (Frogga Biosciences) were then loaded into wells of 4-12% Bis-Tris polyacrylamide gel (BioRad) for electrophoresis. Subsequently, gels were subjected either to silver staining or Western blot.

*2.7. Silver stain*

Following electrophoresis, gels were removed from their casing and fixed in 50% methanol/12% acetic acid/0.05% formalin for 2 hours, washed in 35% ethanol (3 x 20 minutes), sensitized in 0.02% $Na_2S_2O_3$ for 2 minutes, washed in milliQ water (3 x 5 minutes), and stained in 0.2% $AgNO_3$/0.076% formalin for 20 minutes. Gels were then washed again in milliQ water (2 x 1 minute) and developed in 6% $Na_2CO_3$/0.05% formalin/0.0004% $Na_2S_2O_3$. Staining was terminated by incubating in 50% methanol/12% acetic acid for 5 minutes. Gels were then

imaged using a Canon CanoScan scanner and stored in 1% acetic acid until bands were excised and sent for proteolytic digestion and mass spectrometry.

*2.8. Western blot*

Following electrophoresis, proteins in polyacrylamide gels were transferred onto polyvinylidine fluoride membranes (Millipore) and then incubated for 2 hours at 37$^{o}$C in blocking buffer (PBS/0.1% Tween-20/5% BSA). Membranes were then placed in blocking buffer containing primary antibodies and incubated overnight at 4$^{o}$C. These were then washed (3 x 10 minutes) in PBS/0.1% Tween-20 before being placed in blocking buffer containing fluorochrome-coupled secondary antibodies and incubated for 1 hour at room temperature. After a final series of washes in PBS/0.1% Tween-20 (8 x 5 minutes), membranes were imaged using an Odyssey scanner (Leica). Primary antibodies and dilutions were as follows: CK5 - monoclonal rabbit anti-human (AbCam) 1/500, CK79 - polyclonal mouse anti-human (AbCam) 1/500, E-cadherin - monoclonal mouse anti-human (Invitrogen) 1/1000, β-catenin - polyclonal rabbit anti-human (Invitrogen) 1/1000, Serum Albumin - polyclonal goal anti-mouse (AbCam) 1/1000. Secondary antibodies (all used at a 1/5000 dilution) were as follows: goat anti-rabbit AlexaFluor 680 (Invitrogen), goat anti-mouse AlexaFluor 680 (Invitrogen), donkey anti-goat AlexaFluor 680 (Invitrogen), goat anti-mouse Infrared Dye 800 (Sigma).

*2.9. Reactive oxygen species detection assay*

MCF7 cells were seeded in 384-well plates in DMEM/10% FBS and allowed to adhere for 24 hours. Media was removed and cells were washed in PBS. DFF-dA probe (Invitrogen) (10 μM in PBS) was then added and cells incubated for 1 hour before this was removed and fresh PBS

added. Compound X, $H_2O_2$, or Fervenulin X was then added and fluorescence measurements were taken after 24 hours. Oxidized DFF-dA signal for each assay was normalized to the signal generated by the DMSO control in that assay.

*2.10. Wnt reporter assay*

Stable cell lines were generated by infecting either adherent MCF7 breast cancer cells or HCT116 colon carcinoma cells with lentivirus particles encoding a TOP-FLASH reporter containing 7 repeats of the TCF4 consensus sequence driving expression of firefly Luciferase and a CMV-driven puromycin resistance gene (Invitrogen) at a multiplicity of infection of less than 1 particle/cell. Infected cells were then cultured under puromycin selection as populations comprising greater than 500 clones. Prior to reporter assays, cells were trypsinized and seeded into wells of 384-well plates at 5000 cells/well. Compound dilutions were then added and plates incubated for 22 hours. alamarBlue was then added to each well and cells were incubated for 2 hours further prior to reading fluorescence and performing luminescence assays using SteadyGlo luciferin (Promega). Fluorescence and luminescence readings were obtained using a Beckman Coulter Multimode Detector Dx.

*Note: Experiments were conducted a minimum of two times and a representative experiment shown unless otherwise stated in figure captions.*

**3. RESULTS**

*3.1. Chemical screens*

Using the murine sphere cultures as model systems, we set out to identify small molecular weight compounds that would target breast TICs but not normal mammary epithelial

cells. To this end, we developed an alamarBlue-based high throughput screening (HTS) assay that quantifies cell proliferation and metabolism during the time that spheres are formed (Figure 4). Using this assay, we carried out a primary screen of nearly 32,000 compounds in duplicate in TMS at a concentration of 5 μM, and in so doing, employed TMS preparations from 10 different primary tumors. Z' values, which take into account replicate error and signal to noise ratio, were greater than 0.5, indicating excellent assay quality (Zhang et al. 1999). The libraries screened include the Canadian Compound Collection, which comprises novel synthetic compounds from Chembridge and Maybridge as well as known bioactive molecules from BIOMOL, Sigma, Prestwick, and MicroSource; the Johns Hopkins Clinical Compound Collection, a library comprising approved drugs, pharmaceutical excipients, and food additives; a library of approved drugs from Dr. Aaron Schimmer at the University of Toronto; and three natural product-inspired synthetic libraries from Prabhat Arya of the National Research Council of Canada. A scatterplot (Figure5A) and histogram (Figure 5B) of the primary screen illustrate that the activity of all tested compounds conformed to a Gaussian distribution centered at ~94% residual activity with a standard deviation of ~15%.

Compounds that inhibited proliferation by greater than 75% in the primary screen were identified as hits and selected for follow up dose-response alamarBlue assays carried out in TMS and MMS in parallel. In addition, we assayed compounds that enhanced proliferation by greater than 250%. Importantly, cells from established TMS and MMS preparations exhibit nearly identical sphere-forming efficiencies (~1 in 100), and over the course of the 48 hour assay display very similar growth kinetics (A. Kreso and J. A. Hassell, unpublished data). As such, a comparative chemical sensitivity analysis between TMS- and MMS-derived cells is unlikely to be

biased by differences in the cellular proliferation rates or the number of sphere-forming units present in these two populations.

*3.2. Chemical biology identifies similarities among hit compounds*

The screening campaign yielded more than 250 hits, nearly 200 of which had $IC_{50}$ values (the concentration required to inhibit proliferation by 50%) of less than 5 µM in TMS and MMS (Table 1, Appendix 1). Furthermore, we found that several compounds having agonistic effects in the primary screen elicited dose dependent increases in proliferation in the follow-up assays (Figure 5H). Although the vast majority of compounds were found to act similarly on both populations (Figure 5C), and several compounds were more potent in MMS than in TMS (Figure 5F), we nevertheless sought commonalities among our hits at both the structural and mechanistic levels.

Structural similarity searches were carried out with the aid of PowerMV™ software, and the results were manually curated to eliminate false positives. This exercise allowed us to identify 38 classes of structurally related compounds, each of which comprises two or more structural analogues (Table 2). As a small molecule's structure is often related to its biological function, hit compounds that exhibit significant structural relatedness and have comparable potencies might be expected to share a common molecular target.

As a complementary approach, we carried out literature searches to discover common biological indications among structurally distinct hits (Figure 5D, Table 3). In this way, we identified a number of molecular targets, cellular processes, and signaling pathways that likely play important roles in breast TIC and mammary epithelial stem and progenitor cell biology.

Several of these have been previously implicated in human breast cancer and mammary gland development, including the estrogen receptor and NFκB transcription factors, as well as topoisomerase II. However, in addition, this approach implicated a number of molecular targets whose roles in the normal or malignant mammary epithelium have not been well established. Most notable among these are several classes of G-protein coupled receptors (GPCRs) including serotonin, histamine, dopamine, and adrenergic receptors. In fact, one of the largest classes of structurally related hit compounds included phenothiazines and thioxanthenes, whose actions on a subset of these neurotransmitter receptors are thought to confer them with antipsychotic (i.e. Thioridazine) or anti-emetic (i.e. Triflupromazine) properties.

Because these and many other hit compounds are drugs approved for a variety of indications other than cancer, and have well defined pharmacological, toxicological, and drug interaction profiles (Regenthal et al. 1999), it may be a worthwhile exercise to determine whether they could be safely re-purposed to treat breast cancer patients (Chong and Sullivan 2007). For example, we found that Disulfiram, an alcohol deterrent and reported alcohol dehydrogenase (Sharkawi 1980) and proteasome inhibitor (Chen et al. 2006), exhibited an $IC_{90}$ of less than 200 nM in TMS (Figure 4H), a concentration 8 to 10 times lower than the plasma concentration that elicits toxic side effects in humans (Regenthal et al. 1999). Notably, clinical trials involving this compound as a single agent or as a component of combination therapy are underway in prostate (ClinicalTrials.gov Identifier: NCT01118741) and liver (NCT00742911) cancer patients, and have been completed in melanoma (NCT00256230) and lung cancer (NCT00312819) patients, although data from the latter trials are not yet published.

*3.3. Identification and characterization of Compound X*

Whereas the screening campaign successfully identified hundreds of potent hits, only one compound in all the libraries (Chembridge 5234104, a structural analogue of toxoflavin that we termed Compound X) exhibited significant TMS-selectivity ($IC_{50\text{-}TMS}$ = 63 nM (95% Confidence Interval (CI) = 19-210 nM) and $IC_{50\text{-}MMS}$ = 1.4 µM (CI = 1.3-2.3 µM)) (Figure 5E). Sphere-forming assays confirmed that Compound X selectively blocks the formation of TMS as compared to MMS, whether from primary cell isolates or established sphere cultures (Figure 6A-B), suggesting that this compound preferentially targets TMS-forming cells relative to MMS-forming cells. In addition, at doses similar to those which inhibited mouse mammary TMS formation, we found that Compound X effectively blocked sphere formation in a panel of 9 human breast cancer cell lines representative of the various molecular subtypes of human breast cancer (Table 4), and inhibited the proliferation of 14 human breast cancer cell lines and 2 quasi-normal human breast epithelial cell lines growing adherently in serum-containing medium (Table 5), demonstrating that the activity of this compound is not limited to murine breast tumor cells. Although adherent cell cultures may be depleted in TICs, the rationale for performing proliferation assays under these conditions was provided by the wealth of knowledge related to breast cancer cell lines propagated in serum-containing medium, including detailed portraits of their genomic aberrations, as well as transcriptomic and protein expression profiles (Neve et al. 2006).

To establish the extent to which the activity and selectivity of Compound X might be explained by its chemical structure, and to determine whether we could find more potent or more selective analogues, we assayed a compendium of small molecules that share structural features with the screening hit. Interestingly, we discovered that the unsubstituted parent

molecule, toxoflavin, although active was not selective (Figure 6C ii), whereas a number of analogues having aromatic ring substitutions at the 3-position on the azapteridine ring were both active and selective (Figure 6C iv-vi), though none to the same extent as Compound X. By contrast, analogues retaining aromatic substitutions but having a fervenulin core rather than a toxoflavin core were unable to inhibit cell proliferation, even at doses up to 100 µM (Figure 6C iii). Collectively, these observations demonstrate that the toxoflavin core is required for activity and that the aromatic substitutions confer selectivity. Furthermore, this analysis suggested that the most promising compound in the series was in fact Compound X, prompting us to focus on this molecule for the remainder of our study.

*3.3.1. Compound X alters the morphology, marker expression patterns, and apoptotic index of sphere-resident cells*

To identify phenotypic changes that occur in TMS- and MMS-resident cell populations upon exposure to Compound X, we examined histological sections of 4-day old spheres that had been treated *in vitro* for 24 hours with varying concentrations of the compound. Analysis of hematoxylin and eosin (H&E) stained sphere sections revealed distinct morphological differences between Compound X- and vehicle-treated spheres (Figure 6D-E). Whereas cells within vehicle-treated TMS and MMS were densely packed, had high nuclear-to-cytoplasmic ratios, and stained intensely with hematoxylin, cells within Compound X-treated spheres were larger, more loosely associated, exhibited lower nuclear-to-cytoplasmic ratios, and stained less intensely. These observations suggest that Compound X altered the nature of sphere-resident cells in both TMS and MMS.

To determine whether the morphological changes induced by Compound X were accompanied by differences in the expression of lineage markers, we stained sphere sections with antibodies to alpha-smooth muscle actin (aSMA), which identifies myoepithelial- and mesenchymal cells in the mouse mammary gland, and cytokeratin 8 (CK8), which identifies mammary epithelial cells of the luminal lineage (Figure 6D-E). Whereas TMS-resident cells normally co-express aSMA and CK8 in all cells, treatment with 2.5 µM Compound X caused a segregation of these markers into distinct TMS-resident cell populations (Figure 6D, 5Fi). Interestingly, upon treatment, cells at the periphery of TMS retained expression of CK8 but lost expression of aSMA, whereas cells in the centers of spheres lost expression of CK8 and retained expression of aSMA.

Unlike TMS, MMS generally express myoepithelial-, but not luminal-lineage markers (Figure 6E, 5Fii). When treated with Compound X however, some MMS-resident cells were found to express CK8. These changes in marker expression in TMS and MMS may be due to the induction of a program of differentiation, or could alternatively be a byproduct of cell death.

To determine whether the differential activity of Compound X on TMS- and MMS-derived cells was a result of selective induction of cell death, we performed quantitative terminal dUTP nick-end label (TUNEL) staining on sphere sections. Whereas TUNEL-positive cells were rare in dimethyl sulfoxide (DMSO)-treated TMS and MMS (<1 %), exposure to Compound X increased their abundance in a dose-dependent manner (Figure 6G). Notably, 24 hours after treatment with 2.5 µM Compound X, fragmented DNA could be detected in nearly 90% of TMS-resident cells. By contrast, when MMS were treated with 2.5 µM Compound X, fewer than 10% of MMS-resident cells became TUNEL-positive, suggesting that the selective activity of this

compound was likely due to preferential induction of cell death in TMS-resident cells. Notably, the observation that Compound X induced cell death in the vast majority of TMS-resident cells implies that all tumor cell types present in TMS, including TICs (which represent ~30% of TMS-resident cells) and non-tumorigenic cells (which represent the remaining ~70%) are sensitive to the compound.

*3.3.2. Compound X inhibits the growth of mouse mammary tumors*

The results of our *in vitro* analyses suggested that Compound X may target tumor cells more readily than normal cells, which we hypothesized might manifest itself as a high therapeutic index *in vivo*. Using the $LD_{50}$ (dose which is lethal to 50% of animals) of toxoflavin as a starting point, we determined the maximum tolerated dose (MTD) of Compound X to be between 2 and 4 mg/kg by intraperitoneal injection, depending on the strain of mouse used the in the study (Figure 7A). To assess the therapeutic potential of Compound X in mammary tumor-bearing mice, we seeded subcutaneous tumors using two general models: primary murine N#202 tumor cells transplanted into syngeneic, immune-competent FVB/N recipients at 10,000 cells/injection, and human Her2-positive HCC1954 sphere-derived breast cancer cells transplanted into immune-compromised NOD/SCID/IL-2$\gamma^{KO/KO}$ (NSG) recipients at 50,000 cells/injection. When tumor grafts reached ~1$cm^3$, mice were treated with Compound X at 4 mg/kg/day (FVB/N) or 2 mg/kg/day (NSG) by intraperitoneal injection, for two cycles of 5 days on and 2 days off. Over this period, control animals were injected with an equivalent volume of DMSO vehicle (10 or 5 µL, resepectively). Tumor dimensions were measured every 2-5 days, and volumes were inferred (l x w x h) and normalized to the volume of the tumor at the time treatment began. Six hours after the last treatment in FVB/N recipients, or 48 hours after the

last treatment in NSG recipients, mice were sacrificed and their tumors were harvested for analysis.

In the N#202 model, using three independent primary tumors, Compound X significantly inhibited tumor growth by comparison to DMSO-treated controls ($p < 0.0001$) (Figure 7B-C), and induced a marked change in gross tumor morphology and cellular composition as judged by histological analysis (Figure 7D-E). Whereas tumors from DMSO-treated animals were composed almost entirely of tumor epithelial cells, those of the Compound X-treated mice contained a mixture of tumor and reparative/regenerative tissue – features which are similar to those seen in human breast tumors excised following chemotherapy (Anita Bane, personal communication).

Immunostaining patterns were also different in DMSO- and Compound X-treated tumors. Whereas the DMSO-treated tumors were devoid of cells expressing aSMA, Compound X-treated tumors contained streaks of aSMA-positive cells that covered approximately 10% of the tumor sections (Figure 8A). Although this marker is used to identify mature myoepithelial cells in the mouse mammary gland and ostensibly differentiated N#202 tumor cells (Kondratyev et al. 2011), it also stains fibroblasts. Because the aSMA-positive cells were elongated, had cytoplasmic projections, and were localized to regions of the tumor that showed signs of repair and regeneration, we concluded that this antibody was most likely marking the latter cells.

CK8 is a marker of luminal-lineage epithelial cells in the mouse mammary gland and is ubiquitously expressed in N#202 tumor cells *in situ*. Whereas in DMSO-treated tumors, CK8 was expressed throughout the tumor, in Compound X-treated tumors it was not expressed in aSMA-positive cells but was expressed at normal levels in the remaining 90% of cells present in the sections (Figure 8A). Finally, we observed intense TUNEL staining in the reparative regions of

Compound X-treated tumors, indicating the presence of fragmented DNA. Interestingly, this stain was localized not only to nuclear regions, but also to cytoplasmic and apparently extracellular regions. These observations suggest that the treatment caused tumor cells to undergo cell death *in vivo*, and that the nucleic acid debris had not been fully cleared from the affected region of the tumor (Figure 8B). Incidentally, we did not observe a difference in the Ki67 proliferation index between Compound X- and vehicle-treated tumors (data not shown).

Contrasting the findings in the N#202/FVB/N model, in the HCC1954/NSG model, no clear differences in tumor size were observed between DMSO- and Compound X-treated cohorts (Figure 9A-B), nor were there overt differences in their hematoxylin & eosin- (Figure 9C-D), CK8-, aSMA- or TUNEL-staining patterns (Figure 10A-B). Several differences between the mouse-in-mouse and human-in-mouse models might explain these disparities. First, the twofold reduced dose of Compound X required to treat the NSG mice may not have provided sufficient drug to the site of action to trigger tumor cell response. Second, immune cells present in FVB/N but not NSG mice, including mature B- and T-cells, may be critical in mediating the effects of the compound. Third, although HCC1954 tumor cells overexpress Her2, they are classified as basal, whereas N#202 tumors are luminal – thus, the nature of these tumor cells is fundamentally different, and while Compound X similarly blocks sphere formation by N#202 and HCC1954 cells *in vitro*, there may be differences in their response to the compound *in vivo* as a result of their genetic makeup or gene expression profiles. Finally, we cannot exclude the possibility that some cells within the HCC1954 tumors may have been targeted by the compound, but that these cells may have been so rare as to have yielded no obvious phenotype.

Despite the apparent lack of activity against HCC1954 tumors, the observation that Compound X effectively halts the growth of N#202 tumors and induces tumor cell death argue that this compound might show promise in treating a subset of breast cancer patients whose tumors are classified as luminal B and Her2-positive.

*3.3.3. Treatment with Compound X* in vivo *does not increase the number of sphere-forming cells resident in tumors and does not cause the emergence of resistant sphere-forming cells*

Because Compound X treatment induced tumor cell death and led to a reduction in N#202 tumor volume relative to vehicle-treated controls, we questioned whether this regimen also reduced the number of tumor-resident TICs. Because TMS formation can be used as a surrogate assay for TICs, we attempted to address this query by quantifying the sphere-forming efficiencies of cells isolated from compound- and vehicle-treated tumors (Figure 11A).

Vials of tumor fragments (~250 mg), which had been frozen and stored in 90% FBS/10% DMSO at -80$^{o}$C, were thawed at 37$^{o}$C, washed in F12, and processed to single cells using mechanical and enzymatic dissociation. Four matched pairs of tumors were analyzed – two from cohort 811, one from cohort 7782B, and one from cohort 890 – each pair consisting of a Compound X-treated and a vehicle-treated tumor. Once processed, the isolated cells were seeded in chemically-defined medium at 100,000 viable cells/mL in ultra-low attachment 96-well dishes and after 7 days, the spheres were counted.

Notably, the percentage of viable cells recovered from these tumors ranged from 20 to 40%, which contrasts with the viability obtained from fresh tumors, which typically exceeds 90%. Furthermore, cells from the 890 cohort yielded no spheres, and the sphere-forming

efficiencies of cells from the remaining tumors averaged approximately 1 in 500, or about 5-fold lower than normally observed. Collectively these observations imply that the freeze-thaw procedure had highly deleterious consequences to both the viability and functionality of sphere-forming cells in tissue fragments. Nonetheless, it is interesting to note that the frequency of sphere-forming cells was not significantly different among Compound X- and vehicle-treated tumors ($SFE_{DMSO}$ = 1/560 (1/290 – 1/6,700) and $SFE_{Compound\ X}$ = 1/480 (1/340 – 1/833)), implying that, all deleterious consequences being equal, compound treatment did not alter the frequency of TICs in these tumors relative to those in vehicle-treated controls. However, because treatment halted tumor growth and in many cases caused tumors to regress, the compound may have led to a reduction in the absolute number of sphere-forming cells resident in tumors.

It is conceivable that the viable sphere-forming cells which remained in the tumors of Compound X-treated animals might have survived treatment because of an intrinsic or adapted resistance to the compound. To rule out this possibility, we also subjected the cells isolated above to sphere-forming assays in the presence of varying concentrations of Compound X. In these assay, cells isolated from Compound X- and vehicle-treated tumors were approximately equally sensitive to the compound when treated *in vitro* ($IC_{50\text{-}DMSO}$ = 1 μM (CI = 0.6-1.7 μM) and $IC_{50\text{-}Compound\ X}$ = 1.4 μM (CI = 1.1-1.8 μM)) (Figure 11B). Therefore the compound did not cause the emergence of resistant clones. It is notable that the $IC_{50}$ observed in these assays was considerably higher than previously observed from freshly-isolated tumor cells, however a number of differences between the experiments may account for this disparity, including the higher cell density and ultra-low attachment plates used in these latter assays. These alterations to the protocol were intended to counteract the low cell viability and functionality, since in a

previous experiment using cells isolated from frozen tumor samples, incubating cells at a lower cell density in normal tissue-culture treated dishes caused many of the cells to adhere to the plastic and prevented them from forming spheres (data not shown).

*3.3.4. Compound X-treated tumor cells form tumors more efficiently than cells from vehicle-treated tumors*

To more formally address whether *in vivo* treatment had affected the frequency of TICs present in N#202 tumors, we performed comparative serial transplantation assays in parallel to the experiments described above. Cells isolated from the four matched pairs of tumors were transplanted into 6-8 week old female FVB/N recipient mice at 5,000 and 50,000 viable cells per subcutaneous injection. Four mice were injected per condition, and the animals were monitored for tumor growth over the course of the next 20 weeks. All mice in a given condition were sacrificed when the first mouse in that group reached endpoint.

Notably, cells from both Compound X- and vehicle-treated 890 tumors did not form tumors upon re-transplant, paralleling their inability to form spheres in suspension culture. Furthermore, in the remaining samples, the latency to tumor incidence was considerably longer than expected, likely because the TIC frequency was reduced. Thus, the transplantation assays appear to have suffered from the poor cell viability and loss of functionality that plagued the sphere-forming assays.

Disappointingly, in two of the three cohorts which did engraft (each comprising a Compound X- and a vehicle-treated tumor) tumor cells isolated from Compound X-treated animals formed large secondary tumors faster than those isolated from vehicle-treated animals

(Figure 11C-D), whereas in the third cohort the opposite was true (Figure 11E). Because data from our laboratory has previously suggested a direct correlation between the number of TICs injected, and either the time to frank tumor onset or the size of the resulting tumor (Kurpios et al. 2011), the observations made in former two cases suggest that the compound may have preferentially ablated non-tumorigenic cells, resulting in an enrichment in TICs. However, results from the third experiment call this into question and suggest that the compound may have led to a modest reduction in TICs. Although these experiments have not shown a consistent trend, collectively they suggest that Compound X does not lead to a dramatic increase or decrease in the frequency TICs in N#202 tumors. In addition, it bears mention that the *in vivo* treatment regimen may not have been optimized, and thus we cannot rule out the possibility that a longer treatment period may eventually have eliminated all TICs resident in these tumors.

*3.4. Identifying the molecular target and mechanism of action of Compound X*

To the best of our knowledge, Compound X's molecular target and mechanism of action in mammalian cells has not been fully characterized. However, it is a structural analogue of toxoflavin, a toxin that has been isolated from certain pathogenic bacteria including strains of *Pseudomonas* and *Burkholderia* (Latuasan and Berends 1961; Levenberg and Linton 1966; Garcia et al. 1999).

In addition to its ability to act as an electron carrier (Latuasan and Berends 1961), toxoflavin and its analogues have been reported to affect the activity of numerous proteins including Hepatitis C Virus RNA-dependent RNA-Polymerase (HCV RdRP) (Middleton et al. 2007), human RNA-Polymerase II (PolII) (Middleton et al. 2007), Polo-Like Kinase 1 (Plk1) (Goh et al. 2004), and a number of other kinases, phosphatases, and transcription factors (Lepourcelet et

al. 2004; Pharmaceutica 2004b, a; Frank 2008). As a first pass attempt to identify the molecular target of this compound, we sent several milligrams to Millipore so that it could be subjected to a series of *in vitro* kinase assays at a concentration of 2 μM. The rationale for assaying this compound against kinases is related to the reported importance of various kinases in human cancer (Zhang et al. 2009). However, at this concentration, the compound did not appreciably inhibit the activity of any of the 82 human kinases in the panel (Table 6), suggesting that Compound X does not target this class of proteins. Thereafter we undertook a more rigorous program to define the compound's molecular target and mechanism of action and, given the plethora of potential molecular targets, our primary approach was to attempt unbiased affinity purification.

*3.4.1. Affinity purification of proteins that interact with Compound X*

To unambiguously identify the target of Compound X, we sought to develop an affinity probe, which could be linked to a solid substrate and used to screen cell lysate for proteins that physically interact with the pharmacophore of the compound. To learn whether we could modify the structure of Compound X without affecting its activity, we extended the findings of our initial structure activity relationship (SAR) analysis using additional Compound X analogues (Table 7) (Todorovic et al. 2010). This exercise illustrated that derivatives containing a 4-carbon alkyl or 6-carbon acyl chain modification at the para-position on the aromatic ring retained potent activity, suggesting that a linker might be tolerated at this position. Replacing these groups with an amide-linked 8-chain polyethyleneglycol-carboxylic acid (PEG8-COOH) moiety resulted in a compound which, although less potent than the acylated derivative, still retained activity (Figure 12A). This ligand (Compound X-PEG8-COOH) was then coupled to amine coated

magnetic beads by amide bond formation catalyzed by 1-ethyl-3-(3-dimethylaminopropyl) carbodiimide (EDAC) and *N*-hydroxysuccinimide (NHS) (manufacturers protocol) (Figure 12B). The remaining free amines present on the beads were then capped using excess sodium acetate in a second EDAC/NHS-catalyzed reaction to create the final affinity resin.

Tumor lysates were prepared by homogenizing freshly-isolated ~1g N#202 tumor chunks under mild detergent and hypotonic salt conditions in the presence of protease and phosphatase inhibitors (Chen et al. 2007). Following a one hour lysis on ice, the suspensions were centrifuged and supernatants collected as cytoplasmic fractions. When indicated, nuclear extracts were prepared by resuspending the pellet in hypertonic lysis buffer containing 400 mM sodium chloride and incubating for a further 20 minutes on ice prior to centrifugation and supernatant collection. In the latter cases, the two fractions were mixed to generate whole cell lysates. Protein concentration in the lysates was quantified using a Bradford assay (typically 25-50 mg/mL) and aliquots were frozen at -20$^{o}$C. Prior to the affinity experiments, lysates were thawed and diluted to 2 mg/mL in binding buffer (Chen et al. 2007) then incubated with the affinity resin (~2 x $10^{8}$ beads) in the presence or absence of 100 µM competing Compound X for 1 hour at 4$^{o}$C. Beads were then collected by magnet and washed 3 times with excess phosphate-buffered saline (PBS) to eliminate proteins that were non-specifically bound to the resin. Material that remained on the beads after washing was eluted by boiling in reducing SDS buffer and run on a 4-12% Bis-Tris polyacrylamide gel. Gels were then silver stained to visualize proteins present in the various lanes.

Using this strategy, we reproducibly observed a small number of bands in the lanes containing eluate from the non-competition assay (when excess soluble Compound X was

omitted from the binding buffer), but not the competition assay (when Compound X was included) (Figure 12C-D). These bands as well as control blank bands from each gel were excised and subjected to proteolytic digestion and mass spectrometry. The resulting peptide fingerprints were then used to search online databases (SwissProt, NCB, and Mascot) to identify the proteins present in the bands. Unfortunately, these first analyses yielded no significant results, presumably because the concentration of protein in the bands was below the detection limit of the mass spectrometer. We therefore attempt to scale up the affinity purification step, combined several lanes from two gels, and resubmitted these as a single sample (Figure 12E). In so doing, we obtained the identity of a small number of mouse proteins that were not found in the blank band; namely cytokeratin 5 (CK5), cytokeratin 79 (CK79), and murine serum albumin. We attempted to directly assess whether these proteins were responsible for the band of interest by repeating the binding assay and performing a Western blot (Figure 13A-C). In the case of CK5 and CK79, the banding patterns produced by antibodies against these two proteins did not indicate that they represented the band in the silver stained gel. Furthermore, these two proteins were not detected in tumor lysate, although as expected, CK5 was detected in mouse hide lysate. Unfortunately the antibody against CK79, which was raised in mice against human CK79, proved to be incompatible with our system. This may have been because the protein was simply not expressed in the tumor, or because the primary antibody was unable to recognize the mouse variant of CK79. Alternatively, the AlexaFluor-coupled anti-mouse IgG secondary antibody, which reacted with abundant mouse immunoglobulin heavy chain (50 kDa) present in the lysate, may have obscured detection of the 58 kDa keratin.

Unlike the anti-keratin antibodies, the antibody against murine serum albumin did produce a band of the same molecular weight as the band identified in the silver stained gel, as is clearly illustrated by a juxtaposition of scanned images of these materials (Figure 13C). In addition, the apparent molecular weight and/or the intensity of this band was altered when excess Compound X was included in the binding assay, though it is difficult to assess the latter quantitatively because these experiments are inherently not conducive to inclusion of loading controls. Nonetheless, these observations strongly suggest that the protein identified in the silver stain was in fact albumin. It should be noted that the anti-albumin antibody also reacts with bovine serum albumin (BSA) (data not shown) and that this protein is a component of the bead storage buffer, as suggested by the bead manufacturer. Therefore, we cannot exclude the possibility that the albumin in both the silver stain and the Western blot was of bovine origin. Nevertheless, it is interesting to note that whatever the source of the albumin, addition of Compound X to the binding assay altered its ability to bind to the affinity resin and thus, Compound X likely directly physically interacts with this protein. This may not be surprising since albumin is known to bind a wide range of small molecules (Martinez-Gomez et al. 2006), and although such an interaction does not offer an attractive explanation for the activity of this compound against tumor cells, this finding is nonetheless interesting in light of the observation that serum, which contains albumin in abundance, can render Compound X less effective.

*3.4.2. Serum protects cells from Compound X*

We noted a profound difference in the potency of Compound X when we compared N#202 tumor cells propagated adherently in serum-containing medium to matched samples of TMS propagated in serum-free medium using proliferation assays (Figure 14A). Because fetal

bovine serum (FBS) is present in adherent tumor cell cultures, but not in sphere cultures, we investigated the relationship between serum and the activity of Compound X using combination assays.

In order to assay two agents simultaneously, the individual components are first serially diluted and then combined in a matrix, such that all pair-wise combinations are produced (Greco et al. 1995; Borisy et al. 2003; Lehar et al. 2007). Cells were subjected to the combination matrix in an alamarBlue assay under sphere-forming conditions and the response at each combination dose was compared to the response predicted at that dose by mathematical models, which are built based on the activity of the single agents. In this way, the interaction between compounds can be classified as masked, additive, synergistic, or antagonistic, and the degree of synergy or antagonism can be quantified (Loewe and Muischenek 1926; Chou and Talalay 1984; Greco et al. 1995; Borisy et al. 2003; Lehar et al. 2007).

Using this experimental protocol, we determined that FBS decreased both the potency and efficacy of Compound X in a dose-dependent manner, and exerted its protective effects at concentrations as low as 0.16% (Figure 14B). Because serum causes tumor cells to adhere and loose tumorigenic capacity (Cariati et al. 2008; Kurpios et al. 2011), it is conceivable that FBS might reduce the compound's apparent effectiveness by inducing a program of differentiation and eliminating sensitive cells from the population. Indeed, in these experiments, addition of FBS to chemically-defined medium caused sphere-derived MCF7 cells to adhere to the plastic. To address this possibility, we subjected MCF7 cells propagated as either spheres (enriched in TICs (Cariati et al. 2008)) or adherent cells (depleted of TICs (Cariati et al. 2008)) to Compound X in either their standard growth media or in serum-free, growth factor-free media. To accomplish

this task we seeded adherent and sphere-derived cells (passaged greater than 5 times) into wells of a 384-well plate and incubated these for 24 hours. We then removed the media, added serum-free/growth factor-free DMEM, and incubated for 1 hour to wash out the serum. The wash media was then removed and replaced with either fresh serum-free/growth factor-free media, or cell-specific standard growth media (DMEM with 10% FBS for adherent cells or human stem cell medium for sphere-derived cells). Compound X was then added and plates and cells were incubated for 24 hours. alamarBlue was then added and fluorescence was read 24 hours thereafter.

As expected, the adherent cells were resistant to Compound X's anti-proliferative effects when treated in the presence of serum. However, when these same cells were treated in the absence of serum, they were as sensitive to the compound as their sphere-derived counterparts (Figure 14C). This demonstrates that serum's ability to induce an adherent phenotype in tumor cells is unrelated to its ability to protect them from Compound X, and suggests that both tumorigenic and non-tumorigenic cells are sensitive to the effects of the compound when treated in the absence of serum. Moreover, the cells propagated in serum-free growth factor-free medium were slightly more sensitive to the compound than cells growing in chemically-defined medium containing EGF, bFGF, and B27, suggesting that these components may also provide some protection from Compound X. In support of this conclusion, B27 is capable of shifting the $IC_{50}$ of this compound in a dose-dependent manner (Figure 15A).

To determine whether albumin, the most abundant protein species in both serum- (3.5-5.0 mg/mL) (Shen et al. 2004) and B27-containing medium (1.25-2.5 mg/mL) (Fedoroff and Richardson 2001) might be responsible for the protective action of these agents, we subjected

MCF7 cells to Compound X in the presence of varying doses of BSA. Although BSA alone inhibited proliferation at doses higher than 1.25 mg/mL, at this dose it provided modest protection from Compound X, shifting the $IC_{50}$ but not the maximal effect of the compound (Figure 15B). This suggests that although BSA may bind and sequester the compound, other factors are required to achieve the levels of protection provided by serum or B27.

*3.4.3. Compound X produces reactive oxygen species*

Along with other biologically active molecules, serum and B27 contain anti-oxidants. Because toxoflavin has been shown to generate hydrogen peroxide ($H_2O_2$) (Latuasan and Berends 1961), we inquired whether Compound X might do the same, and if so, whether anti-oxidants were capable of abrogating its anti-proliferative effects. To address the first question, we performed a reactive oxygen species (ROS) detection assay using oxidized difluorofluorescein diacetate (DFF-dA) as a readout. DFF-dA is a cell-permeable fluorescein-based molecule, which in its reduced form is non-fluorescent, but when oxidized by $H_2O_2$ or other ROS, fluoresces with spectral characteristics similar to fluorescein (Diehn et al. 2009). Using this probe in a microplate-based assay, we determined that Compound X and $H_2O_2$ induced a dose-dependent increase in the oxidized DFF-dA signal relative to DMSO treated controls (Figure 16A). After 24 hours incubation, fluorescence measurements indicated that 5-20 µM Compound X generated a signal comparable to 1-7 mM $H_2O_2$, suggesting that the compound acted as a catalyst. It is notable that the dose of Compound X required to generate large quantities of $H_2O_2$ was ~50-fold higher than than the $IC_{50}$ in proliferation assays in spheres. However, the dose-response curves elicited by Compound X in these and many other assays were generally very shallow (Hill slope <

0.5) and the maximal effect was often only achieved at doses of 1-10 µM. Therefore, although not conclusive, it is possible that production of ROS can account for the toxicity of Compound X.

The mechanism of $H_2O_2$ production by Compound X may proceed by transient reduction of the flavin ring to a non-aromatic, high-energy species that is stabilized by up to 6 resonance structures, which may subsequently reduce molecular oxygen to $H_2O_2$ in a manner that regenerates the aromatic parent compound (Figure 16C-D). Alternatively, Compound X may simply oxidize the DFF-dA probe. Interestingly, the non-toxic fervenulin derivative of Compound X (Fervenulin X) did not cause oxidation of the DFF-dA probe and therefore likely did not produce ROS (Figure 16B). This may be because reduced Fervenulin X can only exist in two energetically-unfavorable, non-aromatic resonance forms (Figure 16E). Of note, the addition of 10 mM reduced glutathione (GSH), a ubiquitous intracellular peptide, which acts a key mediator of redox balance, diminished the oxidized DFF-dA signal induced by 10 µM Compound X (Figure 16B).

In light of this latter finding, we next questioned whether GSH could provide protection from the anti-proliferative activity of Compound X in serum-free medium. When we incubated MCF7 sphere-derived cells with various concentrations of GSH for 2 hours and then subjected them to various concentrations of Compound X, we found that both agents acted as anti-proliferatives but that each agent protected cells from the other (Figure 17). Interestingly, in these experiments, the $IC_{50}$ of Compound X alone was higher than in previous proliferation assays using MCF7 sphere-derived cells. This may have been because in these experiments, cells were seeded into 384-well plates 2 hours prior to the addition of compound whereas in other experiments compound was added immediately after cells were seeded.

The observation that Compound X and GSH act as an antagonistic pair is interesting for a number of reasons. First, glutathione can be converted from its reduced (GSH) to oxidized (GSSG) forms by glutathione peroxidases (GPX) in the presence of $H_2O_2$, and from GSSG to GSH by glutathione reductases in the presence of NADPH (Ng et al. 2007). Thus, this peptide can act as a reservoir of oxidized or reduced substrate to consume reactive molecules with one or the other propensity. Second, GSH can be conjugated to electrophilic groups by glutathione s-transferases (GST), and can thus detoxify a variety of reactive compounds (Dourado et al. 2008). Therefore, two explanations, which are not necessarily mutually exclusive, might explain these antagonistic effects. First, GSH might allow cells to cope with excess $H_2O_2$ produced by Compound X through the action of GPX, and second, conjugation of GSH to Compound X by GST may prevent it from acting as an oxidizing agent. Both explanations are also consistent with the antagonistic effect of Compound X on GSH-induced toxicity.

While it is unclear whether Compound X differentially induces ROS production in TMS and MMS, global gene expression profiling of these cells suggests that enzymes responsible for metabolizing ROS are collectively expressed at lower levels in TMS than in MMS (Table 8), and gene set enrichment analysis (Subramanian et al. 2005) suggests that this difference is significant ($p$ = 0.002 ). Thus, the hypothesis that Compound X induces oxidative cell death might offer an explanation for its selectivity, as well as its reduced potency in serum-containing media.

Hydrogen peroxide typically exerts cytotoxic effects by generating oxygen radicals in the so-called Fenton reaction:

$$(1)\ Fe^{2+} + H_2O_2 \rightarrow Fe^{3+} + OH\cdot + OH^-$$

(2) $Fe^{3+} + H_2O_2 \rightarrow Fe^{2+} + OOH\cdot + H^+$

These radicals can then oxidize protein, DNA, and lipids – altering their chemical structure and biological function. Previous work has shown that compounds which chelate iron can reduce the toxicity of $H_2O_2$ as well as the toxicity of compounds that produce $H_2O_2$ (Nakagawa et al. 2004). We therefore sought to determine whether such a compound would protect cells from Compound X. Indeed, in combination assays, *O*-phenanthroline provided modest protection from both Compound X and $H_2O_2$, shifting the $IC_{50}$ of Compound X by twofold and maximal effect level by 10-20% when used at a concentration of 10 μM (Figure 18A-B), a result consistent with the hypothesis that Compound X exerts its toxic effects through a peroxide intermediate.

One of the primary mechanisms by which cells protect themselves from peroxide damage is through expression of catalase, which converts $H_2O_2$ to water and molecular oxygen (Thorpe et al. 2004). To determine whether overexpression of catalase might protect cells from Compound X we transfected adherent MCF7 cells with a DNA construct encoding the human cDNA for catalase, expressed under control of the CMV promoter (Origene pCMV-XL5). Twenty-four hours after transfection, the cells were trypsinized, plated in 384-well plates at 20,000 cell/well in either DMEM supplemented with 10% FBS or serum-free/growth factor-free DMEM, and treated with either Compound X or $H_2O_2$. At the time of trypsinization and resuspension, crude estimates of catalase activity were taken by administering a high concentration of $H_2O_2$ to each cell suspension. Although catalase-transfected cells generated substantially more oxygen bubbles than did non-transfected or salmon sperm DNA-transfected controls when $H_2O_2$ was added, all cells were about equally sensitive to both $H_2O_2$ and Compound X as determined by alamarBlue fluorescence assays (Figure 19A). Interestingly, in these experiments, the raw

alamarBlue signals produced from cells plated in the absence of serum and growth factors (~1 x $10^8$ relative fluorescence units) indicated that they were indeed viable, although they did not proliferate to the same extent as those plated in serum-containing medium (~2 x $10^8$ RFU).

It is unclear why catalase overexpression does not render toxic concentrations of $H_2O_2$ non-toxic, however it may be the result of incomplete transfection of the target population. Alternatively, the toxic effects of $H_2O_2$ might be mediated extracellularly through lipid or cell surface protein peroxidation, and because in this system catalase was confined to the cytosol, we may not have observed any effect. To rule out the latter possibility, we attempted to supplement the growth medium with catalase by adding lysate derived from either catalase- or salmon sperm DNA-transfected cells to MCF7 cells grown as spheres. Interestingly, in these experiments, cell lysate from catalse-transfected cells provided modest protection from both Compound X and $H_2O_2$ as compared to lysate from salmon sperm DNA-transfected cells (Figure 19B) (Compound X: $IC_{50\text{-SS DNA}}$ = 210 nM (CI = 150-300 nM) and $IC_{50\text{-Catalase}}$ = 520 nM (CI = 410-680 nM), $H_2O_2$: $IC_{50\text{-SS DNA}}$ = 3.7 mM (CI = 3.3-4.2 mM) and $IC_{50\text{-Catalase}}$ = 7.4 nM (CI = 6.0-9.1 mM)). This suggests that addition of extracellular catalase can reduce the toxicity of both Compound X and $H_2O_2$. It is possible that increasing the amount of extracellular catalase beyond that used in these assays may have provided a greater degree of protection from Compound X- or $H_2O_2$-induced cell death, however, it was not possible to increase the concentration of lysate beyond 2.5 µg protein/mL as this led to unacceptable toxicity. Thus although we cannot formally conclude that the toxicity of Compound X is mediated by an ability to generate $H_2O_2$, the collection of experiments described above strongly suggest that the activity of this molecule against breast cancer cells is likely related to its chemical reactivity as an oxidizing agent.

*3.5. Compound X and the Wnt/β-catenin pathway*

In addition to the affinity purification/silver stain and ROS assays, we carried out a separate series of experiments to determine whether another published activity of toxoflavin – namely its ability to disrupt the physical interaction between the sequence-specific transcription factor, T-cell factor 4 (TCF4) and the co-activator, β-catenin (Lepourcelet et al. 2004) – might explain the activity of Compound X. Together, these proteins form a complex that activates the transcription of gene-targets of the canonical Wnt signaling pathway – a pathway which is thought to play an important role in embryonic stem cells (Ying et al. 2008), mammary stem cells (Shackleton et al. 2006; Zeng and Nusse 2010), and cancer stem cells (Zhao et al. 2007; Malanchi et al. 2008; Barker et al. 2009; Vermeulen et al. 2010). Notably, a number of components of the Wnt/β-catenin pathway and its transcriptional targets are overexpressed in TMS compared to MMS and MMS induced to differentiate *in vitro*, suggesting that canonical Wnt signaling may play an important role in Her2/Neu-induced mammary tumorigenesis (R. M. Hallett, D. Ilieva and J. A. Hassell, unpublished data). Collectively, these findings led us to speculate that Compound X's selectivity might be explained if it were a Wnt pathway inhibitor, acting by a mechanism that involves disruption of the TCF4/β-catenin complex.

To assess whether Compound X physically interacts with TCF4 or β-catenin, we opted to use the affinity resin/Western blot protocol described above. Disappointingly, we were unable to detect TCF4 in tumor lysates even when up to 40 μg of protein was loaded, and were furthermore unable to enrich for the protein using the affinity resin (data not shown). By contrast, we detected β-catenin and another of its protein partners, E-cadherin, in abundance in tumor lysate (Figure 20). These two proteins form a complex at adherens junctions and

constitute the major pool of β-catenin within epithelial cells (Huber and Weis 2001). Interestingly, both of these proteins bound to the affinity resin at approximately the same ratio as they were present in the lysate, suggesting that they bound as a complex. However, an equal amount of protein was eluted from the resin, whether or not Compound X was included as a competitor in the binding assay. This suggests that the binding of this complex is not specific to the pharmacophore of Compound X and is either due to interaction with the PEG linkers, the acetate caps, or the beads themselves. As an alternative explanation, we may not have included a sufficient amount of soluble Compound X to overcome binding to the affinity resin, and thus we cannot rule out the possibility that the interaction between the resin and the β-catenin/E-cadherin complex may have indeed been specific to the pharmacophore of Compound X. Unfortunately, for these experiments, as for the previous set of affinity purification experiments, it is not a simple task to include loading controls, as one cannot readily predict which proteins might bind to the column in an unchanging manner.

*Wnt reporter assays*

We also inquired whether Compound X could in fact inhibit TCF4/β-catenin-dependent transactivation in human cancer cells. To this end, we generated stable populations of MCF7 breast cancer cells and HCT116 colon carcinoma cells by infecting with a 7xTOP-FLASH reporter vector containing a puromycin resistance cassette, and selecting with puromycin. We validated that the stable reporter lines accurately read out Wnt/β-catenin signaling using BIO ((2'Z,3'E)-6-Bromoindirubin-3'-oxime) and CHIR99021 (Figure 21 A-D). These small molecules are inhibitors of GSK3β, a key catalytic component of the destruction box, which also comprises Axin, APC, LRP5/6 and CKIα (Behrens et al. 1998; Tseng et al. 2006; Ying et al. 2008). Among many other

substrates, GSK3β phosphorylates β-catenin, which targets it for poly-ubiquitination and subsequent proteasomal degradation. Accordingly, inhibition of GSK3β allows free β-catenin to accumulate in the cytosol, enter the nucleus and activate transcription of Wnt target genes.

Importantly, in both cell lines, both BIO and CHIR99021 led to a robust induction of luciferase activity, demonstrating that the integrated reporter was responsive to increases in free β-catenin levels. Interestingly, in these assays the basal level of Wnt activity was nearly undetectable in MCF7 cells (~2 luminescence units/well), although it was 15- to 20-fold higher in HCT116 cells, which harbor an activating mutation in β-catenin (Taketo 2004). Thus, although both MCF7 and HCT116 cells contained an integrated and transcriptionally active reporter construct, we were unable to determine whether Compound X was capable of abrogating Wnt signaling in the stably-infected MCF7 cells, as there was no detectable Wnt signaling to inhibit. However, using the HCT116 cells, we showed that Compound X reduced luminescence values in a dose-dependent manner, although the magnitude of the decrease was nearly identical to the reduction in cell viability as judged by alamarBlue (Figure 21E). This suggested that the reduction in reporter activity induced by Compound X was merely a consequence of toxicity, not specific activity against β-catenin-dependent transcription. However, we cannot exclude the possibility that HCT116 cells require β-catenin-dependent transcription to remain viable and that it may therefore be impossible to inhibit Wnt-signaling in these cells without inducing cell death.

## 4. DISCUSSION

In an attempt to identify small molecular weight compounds that target breast TICs, but not normal stem cells, we developed a high-throughput proliferation screen and employed mouse mammary TMS and MMS as the respective model systems. Whereas the ultimate goal of

the research program was to identify agents that target human breast TICs, we opted to use the murine systems primarily because they offered a much richer and more renewable source of stem cells than are available from human tissue sources. Supporting this decision are several lines of evidence which suggest that the chosen model of murine mammary cancer provides an accurate representation of a subset of human breast cancers (Guy et al. 1992; Herschkowitz et al. 2007). However, it bears mention that there are several important differences between human and murine breast tumors.

First, the genetic alterations in human Her2-positive tumors are distinctly different than those in the N#202 model. In human tumors, Her2 is more often overexpressed due to amplifications at the genomic level (Slamon et al. 1987), whereas in the mouse model, Neu is overexpressed under the control of a strong, hormonally-responsive viral promoter (Stewart et al. 1984). Moreover, whereas mutations in the *Neu* transgene are commonplace in the N#202 model (Siegel et al. 1994), mutations in the *Her2* locus are not typically observed in human Her-2 positive tumors (Lemoine et al. 1990). Thus, although activation of this EGFR family member likely plays a causal role in some human and mouse mammary cancers, the mechanism of its activation is likely quite different between naturally occurring human Her2-positive tumors and tumors arising in N#202 transgenic mice.

Second, human breast tumors are often found to comprise a very small fraction of functional TICs (Al-Hajj et al. 2003; Ishizawa et al. 2011), whereas in transgenic mouse models the frequency of TICs is orders of magnitude higher (Kurpios et al. 2011) – an incongruency which has also been raised in tumors of the hematopoietic system, and has called into question the validity of the cancer stem cell hypothesis. Whereas the first group to prospectively isolate

human leukemia-initiating cells reported that they were rare among bulk tumor cells, estimating their frequency to be about 1 in 250,000 (Lapidot et al. 1994), a report presented in *Science* in 2007 showed, using a syngeneic transplantation assay, that hematopoietic malignancies arising in certain strains of transgenic mice contain a high fraction of TICs, at least as high as 1 in 10, and likely much higher (Kelly et al. 2007). The authors of the latter study suggest that the apparent paucity of TICs in human malignancies is due to inadequacies in the xenotransplantation assays used to detect them – citing the occurrence of residual immune response in some strains of immune-compromised mice, as well as the inability of some mouse growth factors to act upon their human growth factor receptor counterparts (Kelly et al. 2007). Detracting from the definitiveness of this claim, however, are observations that tumors arising in other transgenic mouse models of cancer, including hematopoietic (Jaiswal et al. 2003; So et al. 2003), mammary (Cho et al. 2008), intestinal (Barker et al. 2009) and brain (Read et al. 2009) cancers, do in fact contain rare tumorigenic cells. Hence, it appears as though many tumors do follow a cancer stem cell model, since transplantation deficiencies alone cannot explain the rarity of TICs in these mouse-in-mouse studies. Furthermore, different investigators have obtained vastly different frequencies of TICs even within a single model (Liu et al. 2007; Vaillant et al. 2008; Kurpios et al. 2011), suggesting that transplantation technique plays a key role estimates on TIC frequency. Moreover, even in tumor models which comprise rich populations of TICs, and thus might be assumed not to follow a cancer stem cell model, propagating tumor cells in serum-containing medium can dramatically reduce the frequency of TICs despite the continued proliferation of tumor cells in culture (Kurpios et al. 2011). This implies that TICs in these models are in fact capable of differentiation and loss of tumorigenicity, and hence follow the central tenets of the cancer stem cell hypothesis. Still, the fact that the frequency of TICs

within human breast tumors is so different than those in the N#202 model might raise some concerns about using these tumors to identify compounds to treat human breast cancer patients, yet ultimately, we felt that this increased frequency of TICs would be advantageous to our drug discovery efforts.

Another caveat to using the experimental system we set forth relates to the issue of selectivity. The rationale for using mouse MMS in our counter-screen was founded upon several key assumptions. First, we assumed that MMS comprise a normal population of stem cells that are most similar to breast TICs in the N#202 model. Second, we hypothesized that a common set of signaling pathways govern the survival and self-renewal of most normal somatic stem cells, whereas this machinery may be different in TICs. Third, we hypothesized that compounds that exhibited low toxicity in MMS would be well tolerated *in vivo*. In retrospect, this last assumption may have been slightly off-the-mark, given that the MTD of Compound X in mice was a mere 4 mg/kg. Indeed, for the purpose of future drug discovery screens, it may be wiser to use cells that are more directly responsible for adverse toxic events in patients, such as cardiomyocytes (Sawyer et al. 2010), hepatocytes (Martinez et al. 2010), or hematopoietic cells (Crivori et al. 2011) to attempt to predict whole-organism toxicity. Furthermore, as judged by gene set enrichment analysis, MMS represent a more mesenchymal cell type than TMS (Gene set: Jechlinger EMT down in TMS, $p < 0.001$), and given that normal mammary epithelial cells induced to undergo an EMT have been employed to identify compounds which target breast TICs (Gupta et al. 2009), compound which target MMS may also be useful anti-breast TIC agents. Hence, by focusing our search on compounds that selectively target TMS, we may have missed other interesting compounds.

Nevertheless, using our high-throughput screening strategy, we identified a selective compound that showed activity in both mouse and human breast TMS *in vitro* and mouse mammary tumors *in vivo*. We demonstrated that the activity of this compound required a central toxoflavin moiety and that its selectivity was dependent on the presence of an aromatic ring substitution at position 3 on the azapteridine ring. The observation that toxoflavin itself is active, but not selective, begs for a comparison to be made between this molecule and the more decorated and selective derivatives. It is notable that although MMS are relatively resistant to Compound X, these cells are in fact targeted at doses above 5 µM, suggesting that even in resistant cells, Compound X exhibits some toxicity. Moreover, this toxicity is likely not due to general high-dose toxicity since Fervenulin X, which is identical to Compound X, but for the position of a single methyl group, is non-toxic at does up to 100 µM.

One of the most notable changes induced in toxoflavin by the addition of an aromatic ring is a change in the molecule's hydrophobicity. As evidenced by the estimated $\log P_{(octanol/water)}$ values of toxoflavin (logP = -1.5) and Compound X (logP = 0.82) (logP calculator available online at: http://intro.bio.umb.edu/111-112/OLLM/111F98/jlogp/test.html), toxoflavin is preferentially soluble in aqueous solvents whereas Compound X is preferentially soluble in hydrophobic solvents. Indeed, Compound X and other aromatic ring-substituted analogues have a tendency to precipitate out of solution when the 10 mM stocks (dissolved in 100% DMSO) are diluted in water at too high a concentration (i.e. 1 mM in 10% DMSO). This physical feature may in of itself explain the difference in activity of these two classes of compounds. For example, if TMS contain greater amount of lipid per cell than MMS, Compound X might preferentially accumulate to higher local concentration in TMS and therein exert a more toxic effect. Toxoflavin, by contrast,

might be equally distributed in the media and intracellular aqueous compartments in both TMS and MMS preparations and thus exert toxic effects that are equivalent in both cell types.

Another possible explanation for the selectivity of Compound X may be related to the relative ability of MMS or TMS to metabolize the compound or eliminate it from the cell interior. If MMS degrade or efflux Compound X more readily than do TMS, this might explain the compound's selective toxicity. Such an explanation would also imply that both cell populations metabolize or eliminate toxoflavin with equal efficiency.

Finally, the difference in selectivity between toxoflavin and Compound X might reflect a difference in their protein interaction specificities. Unfortunately, our affinity experiments did not yield any conclusive results with respect to the molecular target of Compound X in mammary tumors cells, therefore it becomes difficult to make comparisons between these two molecules with respect to the proteins they may target.

The results of the DFF-dA assay demonstrate that Compound X generates ROS, an activity which has previously been ascribed to toxoflavin. Whereas the ROS generated by toxoflavin is thought to be $H_2O_2$ (Latuasan and Berends 1961), in the case of Compound X, the nature of the ROS produced is unclear. Given that catalase overexpression did not protect cells from Compound X, the hypothesis that this molecule is $H_2O_2$ may not be fully supported. Yet in these experiments catalase was also unable to protect cells from $H_2O_2$. Therefore, it is likely that the set up of this assay was not optimized, and it is remains a distinct possibility that $H_2O_2$ is the toxic species produced by Compound X. In addition, it is worth mentioning that different reactive oxygen species are metabolized by different families of enzymes (Thorpe et al. 2004), and thus even if an optimized catalase expression system failed to protect cells from Compound

X, the hypothesis that Compound X is toxic due to production of ROS would not be fully negated – indeed the observations that serum, GSH, B27, and *o*-phenanthroline provide protection from Compound X are fully consistent with a role of ROS in the activity of this compound.

Because toxoflavin has previously been shown to interrupt the interaction between TCF4 and β-catenin *in vitro* and because of the putatively important role of the Wnt pathway in N#202 tumors, we sought to determine whether Compound X might act as a Wnt inhibitor. Although we were able to pull down β-catenin using the affinity resin, the interaction between the resin and this protein seemed to be unrelated to the chemical moiety representing the pharmacophore of Compound X. The results of our TOP-FLASH reporter assays offered some evidence that this compound inhibits Wnt signaling, but whether the observed decrease in luminescence is due to specific activity on β-catenin-dependent transcription, or is rather a result of reduced cell viability is unclear.

**5. CONCLUSION**

Through our screening campaign, we identified more than 200 compounds which potently inhibited the proliferation of mouse mammary TMS-derived cells, suggesting that they may target breast TICs in the N#202 model. Structural and mechanistic analyses of these hit compounds allowed us to infer proteins and processes that likely are important for the viability and/or proliferation of these cells, including several proteins which have not previously been shown to play a role in breast cancer. Among our hits, we identified a number of drugs that are approved for indications unrelated to cancer, but that may in fact show efficacy in breast cancer patients. It may therefore be interesting to learn whether these drugs have additive or greater than additive effects when used in combination with currently approved breast cancer therapies

*in vitro* or *in vivo*. If such combinations prove efficacious, it may provide a rationale to fast-track these drugs into clinical breast cancer trials.

Unique among the nearly 32,000 compounds in the screen was Compound X, as it was more potent in TMS-derived cells than in normal MMS-derived cells. We later showed that this compound shrank mouse mammary tumors and induced tumor cell death, though whether this treatment strategy reduced the TIC-burden in these tumors was not entirely clear. Nonetheless, the interesting biological activities exhibited by this compound prompted us to define its molecular target and mechanism of action. Through this exercise, we hoped to gain insight into a pertinent biological difference that exists between normal stem cells and their transformed counterparts.

Because of its structural similarity to toxoflavin, we questioned whether Compound X displays some of the same properties as have been published for this less decorated flavin. Unfortunately, the results of the molecular target identification study identified albumin as the primary binding partner of Compound X, and this offered little explanation for the compound's mechanism of action. Interestingly though, several experiments suggested that the potency of Compound X in breast tumor cells was related to its chemical reactivity as an oxidizing agent.

Finally, because this compound exhibited a very low MTD in mice and activated cytochrome P450 enzymes (data not shown) it will likely never become a drug. Despite the unfavorable properties exhibited by Compound X, this study illustrates how serum-free culture systems that promote stem cell self-renewal can be used to discover compounds that may show activity against breast TICs *in vivo*.

**6. REFERENCES**


1. Al-Hajj, M., Wicha, M.S., Benito-Hernandez, A., Morrison, S.J., and Clarke, M.F. 2003. Prospective identification of tumorigenic breast cancer cells. Proc Natl Acad Sci U S A. 100, 3983-3988.
2. Barker, N., Ridgway, R.A., van Es, J.H., van de Wetering, M., Begthel, H., van den Born, M., Danenberg, E., Clarke, A.R., Sansom, O.J., and Clevers, H. 2009. Crypt stem cells as the cells-of-origin of intestinal cancer. Nature. 457, 608-611.
3. Behrens, J., Jerchow, B.A., Wurtele, M., Grimm, J., Asbrand, C., Wirtz, R., Kuhl, M., Wedlich, D., and Birchmeier, W. 1998. Functional interaction of an axin homolog, conductin, with beta-catenin, APC, and GSK3beta. Science. 280, 596-599.
4. Borisy, A.A., Elliott, P.J., Hurst, N.W., Lee, M.S., Lehar, J., Price, E.R., Serbedzija, G., Zimmermann, G.R., Foley, M.A., Stockwell, B.R*., et al.* 2003. Systematic discovery of multicomponent therapeutics. Proc Natl Acad Sci U S A. 100, 7977-7982.
5. Cariati, M., Naderi, A., Brown, J.P., Smalley, M.J., Pinder, S.E., Caldas, C., and Purushotham, A.D. 2008. Alpha-6 integrin is necessary for the tumourigenicity of a stem cell-like subpopulation within the MCF7 breast cancer cell line. Int J Cancer. 122, 298-304.
6. Chaffer, C.L., Brueckmann, I., Scheel, C., Kaestli, A.J., Wiggins, P.A., Rodrigues, L.O., Brooks, M., Reinhardt, F., Su, Y., Polyak, K*., et al.* 2011. Normal and neoplastic nonstem cells can spontaneously convert to a stem-like state. Proc Natl Acad Sci U S A. 108, 7950-7955.
7. Chen, D., Cui, Q.C., Yang, H., and Dou, Q.P. 2006. Disulfiram, a clinically used anti-alcoholism drug and copper-binding agent, induces apoptotic cell death in breast cancer cultures and xenografts via inhibition of the proteasome activity. Cancer Res. 66, 10425-10433.
8. Chen, S., Takanashi, S., Zhang, Q., Xiong, W., Zhu, S., Peters, E.C., Ding, S., and Schultz, P.G. 2007. Reversine increases the plasticity of lineage-committed mammalian cells. Proc Natl Acad Sci U S A. 104, 10482-10487.
9. Cho, R.W., Wang, X., Diehn, M., Shedden, K., Chen, G.Y., Sherlock, G., Gurney, A., Lewicki, J., and Clarke, M.F. 2008. Isolation and molecular characterization of cancer stem cells in MMTV-Wnt-1 murine breast tumors. Stem Cells. 26, 364-371.
10. Chong, C.R., and Sullivan, D.J., Jr. 2007. New uses for old drugs. Nature. 448, 645-646.
11. Chou, T.C., and Talalay, P. 1984. Quantitative analysis of dose-effect relationships: the combined effects of multiple drugs or enzyme inhibitors. Adv Enzyme Regul. 22, 27-55.
12. Cicalese, A., Bonizzi, G., Pasi, C.E., Faretta, M., Ronzoni, S., Giulini, B., Brisken, C., Minucci, S., Di Fiore, P.P., and Pelicci, P.G. 2009. The tumor suppressor p53 regulates polarity of self-renewing divisions in mammary stem cells. Cell. 138, 1083-1095.
13. Collins, A.T., Berry, P.A., Hyde, C., Stower, M.J., and Maitland, N.J. 2005. Prospective identification of tumorigenic prostate cancer stem cells. Cancer Res. 65, 10946-10951.
14. Creighton, C.J., Li, X., Landis, M., Dixon, J.M., Neumeister, V.M., Sjolund, A., Rimm, D.L., Wong, H., Rodriguez, A., Herschkowitz, J.I*., et al.* 2009. Residual breast cancers after conventional therapy display mesenchymal as well as tumor-initiating features. Proc Natl Acad Sci U S A. 106, 13820-13825.

15. Crivori, P., Pennella, G., Magistrelli, M., Grossi, P., and Giusti, A.M. 2011. Predicting myelosuppression of drugs from in silico models. J Chem Inf Model. 51, 434-445.
16. Dick, J.E. 2008. Stem cell concepts renew cancer research. Blood. 112, 4793-4807.
17. Diehn, M., Cho, R.W., Lobo, N.A., Kalisky, T., Dorie, M.J., Kulp, A.N., Qian, D., Lam, J.S., Ailles, L.E., Wong, M.*, et al.* 2009. Association of reactive oxygen species levels and radioresistance in cancer stem cells. Nature. 458, 780-783.
18. Dontu, G., Abdallah, W.M., Foley, J.M., Jackson, K.W., Clarke, M.F., Kawamura, M.J., and Wicha, M.S. 2003. In vitro propagation and transcriptional profiling of human mammary stem/progenitor cells. Genes Dev. 17, 1253-1270.
19. Dourado, D.F., Fernandes, P.A., and Ramos, M.J. 2008. Mammalian cytosolic glutathione transferases. Curr Protein Pept Sci. 9, 325-337.
20. Fedoroff, S., and Richardson, A. (2001). Protocols for neural cell culture, 3rd edn (Totowa, N.J., Humana Press).
21. Fillmore, C.M., and Kuperwasser, C. 2008. Human breast cancer cell lines contain stem-like cells that self-renew, give rise to phenotypically diverse progeny and survive chemotherapy. Breast Cancer Res. 10, R25.
22. Frank, D. 2008. Patent # WO 2008/156644 A2.
23. Garcia, R.A., Hotchkiss, J.H., and Steinkraus, K.H. 1999. The effect of lipids on bongkrekic (Bongkrek) acid toxin production by Burkholderia cocovenenans in coconut media. Food Addit Contam. 16, 63-69.
24. Ginestier, C., Hur, M.H., Charafe-Jauffret, E., Monville, F., Dutcher, J., Brown, M., Jacquemier, J., Viens, P., Kleer, C.G., Liu, S.*, et al.* 2007. ALDH1 is a marker of normal and malignant human mammary stem cells and a predictor of poor clinical outcome. Cell Stem Cell. 1, 555-567.
25. Goh, K.C., Wang, H., Yu, N., Zhou, Y., Zheng, Y., Lim, Z., Sangthongpitag, K., Fang, L., Du, M., Wang, X.*, et al.* 2004. PLK1 as a Potential Drug Target in Cancer Therapy. Drug Development Research. 62, 13.
26. Greco, W.R., Bravo, G., and Parsons, J.C. 1995. The search for synergy: a critical review from a response surface perspective. Pharmacol Rev. 47, 331-385.
27. Gupta, P.B., Onder, T.T., Jiang, G., Tao, K., Kuperwasser, C., Weinberg, R.A., and Lander, E.S. 2009. Identification of selective inhibitors of cancer stem cells by high-throughput screening. Cell. 138, 645-659.
28. Guy, C.T., Webster, M.A., Schaller, M., Parsons, T.J., Cardiff, R.D., and Muller, W.J. 1992. Expression of the neu protooncogene in the mammary epithelium of transgenic mice induces metastatic disease. Proc Natl Acad Sci U S A. 89, 10578-10582.
29. Hansford, L.M., McKee, A.E., Zhang, L., George, R.E., Gerstle, J.T., Thorner, P.S., Smith, K.M., Look, A.T., Yeger, H., Miller, F.D.*, et al.* 2007. Neuroblastoma cells isolated from bone marrow metastases contain a naturally enriched tumor-initiating cell. Cancer Res. 67, 11234-11243.
30. Harris, C.A., Ward, R.L., Dobbins, T.A., Drew, A.K., and Pearson, S. 2011. The efficacy of HER2-targeted agents in metastatic breast cancer: a meta-analysis. Ann Oncol. 22, 1308-1317.
31. Herschkowitz, J.I., Simin, K., Weigman, V.J., Mikaelian, I., Usary, J., Hu, Z., Rasmussen, K.E., Jones, L.P., Assefnia, S., Chandrasekharan, S.*, et al.* 2007. Identification of

conserved gene expression features between murine mammary carcinoma models and human breast tumors. Genome Biol. 8, R76.
32. Hortobagyi, G.N. 2001. Overview of treatment results with trastuzumab (Herceptin) in metastatic breast cancer. Semin Oncol. 28, 43-47.
33. Huber, A.H., and Weis, W.I. 2001. The structure of the beta-catenin/E-cadherin complex and the molecular basis of diverse ligand recognition by beta-catenin. Cell. 105, 391-402.
34. Iliopoulos, D., Hirsch, H.A., Wang, G., and Struhl, K. 2011. Inducible formation of breast cancer stem cells and their dynamic equilibrium with non-stem cancer cells via IL6 secretion. Proc Natl Acad Sci U S A. 108, 1397-1402.
35. Ishizawa, K., Rasheed, Z.A., Karisch, R., Wang, Q., Kowalski, J., Susky, E., Pereira, K., Karamboulas, C., Moghal, N., Rajeshkumar, N.V.*, et al.* 2011. Tumor-initiating cells are rare in many human tumors. Cell Stem Cell. 7, 279-282.
36. Jaiswal, S., Traver, D., Miyamoto, T., Akashi, K., Lagasse, E., and Weissman, I.L. 2003. Expression of BCR/ABL and BCL-2 in myeloid progenitors leads to myeloid leukemias. Proc Natl Acad Sci U S A. 100, 10002-10007.
37. Kelly, P.N., Dakic, A., Adams, J.M., Nutt, S.L., and Strasser, A. 2007. Tumor growth need not be driven by rare cancer stem cells. Science. 317, 337.
38. Kondratyev, M., Kreso, A., Hallett, R.M., Girgis-Gabardo, A., Barcelon, M.E., Ilieva, D., Ware, C., Majumder, P.K., and Hassell, J.A. 2011. Gamma-secretase inhibitors target tumor-initiating cells in a mouse model of ERBB2 breast cancer. Oncogene.
39. Kurpios, N.A., Girgis-Gabardo, A., Hallett, R.M., Rogers, S., Gludish, D.W., Kockeritz, L., Woodgett, J., Cardiff, R., and Hassell, J.A. 2011. Single Unpurified Tumor-Initiating Cells Elicit Tumors after Transplantation Demonstrating their High Frequency in Breast Tumors of Multiple Mouse Models. Oncogene (Submitted).
40. Lapidot, T., Sirard, C., Vormoor, J., Murdoch, B., Hoang, T., Caceres-Cortes, J., Minden, M., Paterson, B., Caligiuri, M.A., and Dick, J.E. 1994. A cell initiating human acute myeloid leukaemia after transplantation into SCID mice. Nature. 367, 645-648.
41. Latuasan, H.E., and Berends, W. 1961. On the origin of the toxicity of toxoflavin. Biochim Biophys Acta. 52, 502-508.
42. Lee, H.E., Kim, J.H., Kim, Y.J., Choi, S.Y., Kim, S.W., Kang, E., Chung, I.Y., Kim, I.A., Kim, E.J., Choi, Y.*, et al.* 2011. An increase in cancer stem cell population after primary systemic therapy is a poor prognostic factor in breast cancer. Br J Cancer. 104, 1730-1738.
43. Lehar, J., Zimmermann, G.R., Krueger, A.S., Molnar, R.A., Ledell, J.T., Heilbut, A.M., Short, G.F., 3rd, Giusti, L.C., Nolan, G.P., Magid, O.A.*, et al.* 2007. Chemical combination effects predict connectivity in biological systems. Mol Syst Biol. 3, 80.
44. Lemoine, N.R., Staddon, S., Dickson, C., Barnes, D.M., and Gullick, W.J. 1990. Absence of activating transmembrane mutations in the c-erbB-2 proto-oncogene in human breast cancer. Oncogene. 5, 237-239.
45. Lepourcelet, M., Chen, Y.N., France, D.S., Wang, H., Crews, P., Petersen, F., Bruseo, C., Wood, A.W., and Shivdasani, R.A. 2004. Small-molecule antagonists of the oncogenic Tcf/beta-catenin protein complex. Cancer Cell. 5, 91-102.
46. Levenberg, B., and Linton, S.N. 1966. On the biosynthesis of toxoflavin, an azapteridine antibiotic produced by Pseudomonas cocovenenans. J Biol Chem. 241, 846-852.

47. Li, X., Lewis, M.T., Huang, J., Gutierrez, C., Osborne, C.K., Wu, M.F., Hilsenbeck, S.G., Pavlick, A., Zhang, X., Chamness, G.C.*, et al.* 2008. Intrinsic resistance of tumorigenic breast cancer cells to chemotherapy. J Natl Cancer Inst. 100, 672-679.
48. Liao, M.J., Zhang, C.C., Zhou, B., Zimonjic, D.B., Mani, S.A., Kaba, M., Gifford, A., Reinhardt, F., Popescu, N.C., Guo, W.*, et al.* 2007. Enrichment of a population of mammary gland cells that form mammospheres and have in vivo repopulating activity. Cancer Res. 67, 8131-8138.
49. Liu, J.C., Deng, T., Lehal, R.S., Kim, J., and Zacksenhaus, E. 2007. Identification of tumorsphere- and tumor-initiating cells in HER2/Neu-induced mammary tumors. Cancer Res. 67, 8671-8681.
50. Loewe, S., and Muischenek, H. 1926. Effect of combinations: mathematical basis of problem. Arch Exp Pharmakol. 37, 140.
51. Malanchi, I., Peinado, H., Kassen, D., Hussenet, T., Metzger, D., Chambon, P., Huber, M., Hohl, D., Cano, A., Birchmeier, W.*, et al.* 2008. Cutaneous cancer stem cell maintenance is dependent on beta-catenin signalling. Nature. 452, 650-653.
52. Mani, S.A., Guo, W., Liao, M.J., Eaton, E.N., Ayyanan, A., Zhou, A.Y., Brooks, M., Reinhard, F., Zhang, C.C., Shipitsin, M.*, et al.* 2008. The epithelial-mesenchymal transition generates cells with properties of stem cells. Cell. 133, 704-715.
53. Martinez-Gomez, M.A., Sagrado, S., Villanueva-Camanas, R.M., and Medina-Hernandez, M.J. 2006. Characterization of basic drug-human serum protein interactions by capillary electrophoresis. Electrophoresis. 27, 3410-3419.
54. Martinez, S.M., Bradford, B.U., Soldatow, V.Y., Kosyk, O., Sandot, A., Witek, R., Kaiser, R., Stewart, T., Amaral, K., Freeman, K.*, et al.* 2010. Evaluation of an in vitro toxicogenetic mouse model for hepatotoxicity. Toxicol Appl Pharmacol. 249, 208-216.
55. Middleton, T., Lim, H.B., Montgomery, D., Rockway, T., Liu, D., Klein, L., Qin, W., Harlan, J.E., Kati, W.M., and Molla, A. 2007. Azapteridine Inhibitors of Hepatitis C Virus RNA-Dependent RNA Polymerase. Letters in Drug Design & Discovery. 4.
56. Muller, W.J., Sinn, E., Pattengale, P.K., Wallace, R., and Leder, P. 1988. Single-step induction of mammary adenocarcinoma in transgenic mice bearing the activated c-neu oncogene. Cell. 54, 105-115.
57. Nakagawa, H., Hasumi, K., Woo, J.T., Nagai, K., and Wachi, M. 2004. Generation of hydrogen peroxide primarily contributes to the induction of Fe(II)-dependent apoptosis in Jurkat cells by (-)-epigallocatechin gallate. Carcinogenesis. 25, 1567-1574.
58. Neve, R.M., Chin, K., Fridlyand, J., Yeh, J., Baehner, F.L., Fevr, T., Clark, L., Bayani, N., Coppe, J.P., Tong, F.*, et al.* 2006. A collection of breast cancer cell lines for the study of functionally distinct cancer subtypes. Cancer Cell. 10, 515-527.
59. Ng, C.F., Schafer, F.Q., Buettner, G.R., and Rodgers, V.G. 2007. The rate of cellular hydrogen peroxide removal shows dependency on GSH: mathematical insight into in vivo H2O2 and GPx concentrations. Free Radic Res. 41, 1201-1211.
60. O'Brien, C.A., Pollett, A., Gallinger, S., and Dick, J.E. 2007. A human colon cancer cell capable of initiating tumour growth in immunodeficient mice. Nature. 445, 106-110.
61. Pharmaceutica, J. 2004a. Patent # WO2004/007498 A3.
62. Pharmaceutica, J. 2004b. Patent # WO2004/007499 A1.
63. Prince, M.E., Sivanandan, R., Kaczorowski, A., Wolf, G.T., Kaplan, M.J., Dalerba, P., Weissman, I.L., Clarke, M.F., and Ailles, L.E. 2007. Identification of a subpopulation of

cells with cancer stem cell properties in head and neck squamous cell carcinoma. Proc Natl Acad Sci U S A. 104, 973-978.

64. Quintana, E., Shackleton, M., Sabel, M.S., Fullen, D.R., Johnson, T.M., and Morrison, S.J. 2008. Efficient tumour formation by single human melanoma cells. Nature. 456, 593-598.
65. Read, T.A., Fogarty, M.P., Markant, S.L., McLendon, R.E., Wei, Z., Ellison, D.W., Febbo, P.G., and Wechsler-Reya, R.J. 2009. Identification of CD15 as a marker for tumor-propagating cells in a mouse model of medulloblastoma. Cancer Cell. 15, 135-147.
66. Regenthal, R., Krueger, M., Koeppel, C., and Preiss, R. 1999. Drug levels: therapeutic and toxic serum/plasma concentrations of common drugs. J Clin Monit Comput. 15, 529-544.
67. Reya, T., Morrison, S.J., Clarke, M.F., and Weissman, I.L. 2001. Stem cells, cancer, and cancer stem cells. Nature. 414, 105-111.
68. Reynolds, B.A., and Weiss, S. 1992. Generation of neurons and astrocytes from isolated cells of the adult mammalian central nervous system. Science. 255, 1707-1710.
69. Roesch, A., Fukunaga-Kalabis, M., Schmidt, E.C., Zabierowski, S.E., Brafford, P.A., Vultur, A., Basu, D., Gimotty, P., Vogt, T., and Herlyn, M. 2010. A temporarily distinct subpopulation of slow-cycling melanoma cells is required for continuous tumor growth. Cell. 141, 583-594.
70. Sawyer, D.B., Peng, X., Chen, B., Pentassuglia, L., and Lim, C.C. 2010. Mechanisms of anthracycline cardiac injury: can we identify strategies for cardioprotection? Prog Cardiovasc Dis. 53, 105-113.
71. Schatton, T., Murphy, G.F., Frank, N.Y., Yamaura, K., Waaga-Gasser, A.M., Gasser, M., Zhan, Q., Jordan, S., Duncan, L.M., Weishaupt, C.*, et al.* 2008. Identification of cells initiating human melanomas. Nature. 451, 345-349.
72. Shackleton, M., Vaillant, F., Simpson, K.J., Stingl, J., Smyth, G.K., Asselin-Labat, M.L., Wu, L., Lindeman, G.J., and Visvader, J.E. 2006. Generation of a functional mammary gland from a single stem cell. Nature. 439, 84-88.
73. Sharkawi, M. 1980. Inhibition of alcohol dehydrogenase by disulfiram; possible relation to the disulfiram-ethanol reaction. Life Sci. 27, 1939-1945.
74. Shen, Y., Jacobs, J.M., Camp, D.G., 2nd, Fang, R., Moore, R.J., Smith, R.D., Xiao, W., Davis, R.W., and Tompkins, R.G. 2004. Ultra-high-efficiency strong cation exchange LC/RPLC/MS/MS for high dynamic range characterization of the human plasma proteome. Anal Chem. 76, 1134-1144.
75. Siegel, P.M., Dankort, D.L., Hardy, W.R., and Muller, W.J. 1994. Novel activating mutations in the neu proto-oncogene involved in induction of mammary tumors. Mol Cell Biol. 14, 7068-7077.
76. Singh, S.K., Clarke, I.D., Terasaki, M., Bonn, V.E., Hawkins, C., Squire, J., and Dirks, P.B. 2003. Identification of a cancer stem cell in human brain tumors. Cancer Res. 63, 5821-5828.
77. Slamon, D.J., Clark, G.M., Wong, S.G., Levin, W.J., Ullrich, A., and McGuire, W.L. 1987. Human breast cancer: correlation of relapse and survival with amplification of the HER-2/neu oncogene. Science. 235, 177-182.
78. So, C.W., Karsunky, H., Passegue, E., Cozzio, A., Weissman, I.L., and Cleary, M.L. 2003. MLL-GAS7 transforms multipotent hematopoietic progenitors and induces mixed lineage leukemias in mice. Cancer Cell. 3, 161-171.

79. Stewart, T.A., Pattengale, P.K., and Leder, P. 1984. Spontaneous mammary adenocarcinomas in transgenic mice that carry and express MTV/myc fusion genes. Cell. 38, 627-637.
80. Strecker, T.E., Shen, Q., Zhang, Y., Hill, J.L., Li, Y., Wang, C., Kim, H.T., Gilmer, T.M., Sexton, K.R., Hilsenbeck, S.G*., et al.* 2009. Effect of lapatinib on the development of estrogen receptor-negative mammary tumors in mice. J Natl Cancer Inst. 101, 107-113.
81. Subramanian, A., Tamayo, P., Mootha, V.K., Mukherjee, S., Ebert, B.L., Gillette, M.A., Paulovich, A., Pomeroy, S.L., Golub, T.R., Lander, E.S*., et al.* 2005. Gene set enrichment analysis: a knowledge-based approach for interpreting genome-wide expression profiles. Proc Natl Acad Sci U S A. 102, 15545-15550.
82. Taketo, M.M. 2004. Shutting down Wnt signal-activated cancer. Nat Genet. 36, 320-322.
83. Thorpe, G.W., Fong, C.S., Alic, N., Higgins, V.J., and Dawes, I.W. 2004. Cells have distinct mechanisms to maintain protection against different reactive oxygen species: oxidative-stress-response genes. Proc Natl Acad Sci U S A. 101, 6564-6569.
84. Todorovic, N., Giacomelli, A., Hassell, J.A., Frampton, C.S., and Capretta, A. 2010. Microwave-assisted synthesis of 3-aryl-pyrimido[5,4-e][1,2,4]triazine-5,7-(1H,6H)-dione libraries: derivatives of toxoflavin. Tetrahedron Letters. 51, 4.
85. Tseng, A.S., Engel, F.B., and Keating, M.T. 2006. The GSK-3 inhibitor BIO promotes proliferation in mammalian cardiomyocytes. Chem Biol. 13, 957-963.
86. Ursini-Siegel, J., Schade, B., Cardiff, R.D., and Muller, W.J. 2007. Insights from transgenic mouse models of ERBB2-induced breast cancer. Nat Rev Cancer. 7, 389-397.
87. Vaillant, F., Asselin-Labat, M.L., Shackleton, M., Forrest, N.C., Lindeman, G.J., and Visvader, J.E. 2008. The mammary progenitor marker CD61/beta3 integrin identifies cancer stem cells in mouse models of mammary tumorigenesis. Cancer Res. 68, 7711-7717.
88. Vermeulen, L., De Sousa, E.M.F., van der Heijden, M., Cameron, K., de Jong, J.H., Borovski, T., Tuynman, J.B., Todaro, M., Merz, C., Rodermond, H*., et al.* 2010. Wnt activity defines colon cancer stem cells and is regulated by the microenvironment. Nat Cell Biol. 12, 468-476.
89. Ying, Q.L., Wray, J., Nichols, J., Batlle-Morera, L., Doble, B., Woodgett, J., Cohen, P., and Smith, A. 2008. The ground state of embryonic stem cell self-renewal. Nature. 453, 519-523.
90. Youn, B.S., Sen, A., Kallos, M.S., Behie, L.A., Girgis-Gabardo, A., Kurpios, N., Barcelon, M., and Hassell, J.A. 2005. Large-scale expansion of mammary epithelial stem cell aggregates in suspension bioreactors. Biotechnol Prog. 21, 984-993.
91. Yu, F., Yao, H., Zhu, P., Zhang, X., Pan, Q., Gong, C., Huang, Y., Hu, X., Su, F., Lieberman, J*., et al.* 2007. let-7 regulates self renewal and tumorigenicity of breast cancer cells. Cell. 131, 1109-1123.
92. Zeng, Y.A., and Nusse, R. 2010. Wnt proteins are self-renewal factors for mammary stem cells and promote their long-term expansion in culture. Cell Stem Cell. 6, 568-577.
93. Zhang, J., Yang, P.L., and Gray, N.S. 2009. Targeting cancer with small molecule kinase inhibitors. Nat Rev Cancer. 9, 28-39.
94. Zhang, J.H., Chung, T.D., and Oldenburg, K.R. 1999. A Simple Statistical Parameter for Use in Evaluation and Validation of High Throughput Screening Assays. J Biomol Screen. 4, 67-73.

95. Zhao, C., Blum, J., Chen, A., Kwon, H.Y., Jung, S.H., Cook, J.M., Lagoo, A., and Reya, T. 2007. Loss of beta-catenin impairs the renewal of normal and CML stem cells in vivo. Cancer Cell. 12, 528-541.

**7. FIGURES**

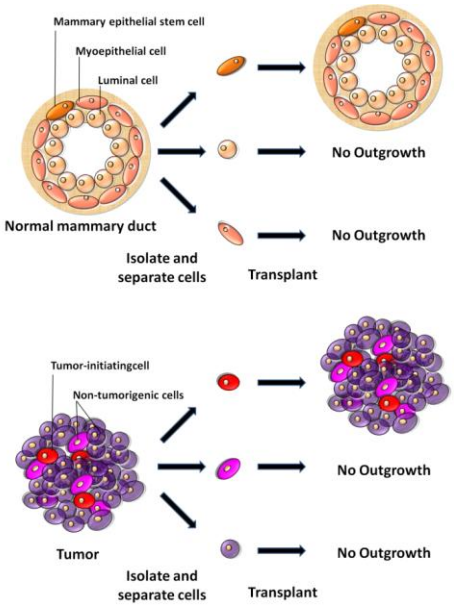


Figure 1. *Normal and tumor tissues are organized as cellular hierarchies.* In normal tissues, exemplified here by the mammary gland, only somatic stem cells are capable of re-growing a complete organ following transplant into a recipient animal. Of the cells in a tumor, only TICs possess true tumor reconstitution potential. FACS analysis can be used to prospectively isolate stem and non-stem, as well as tumorigenic and non-tumorigenic cell populations.

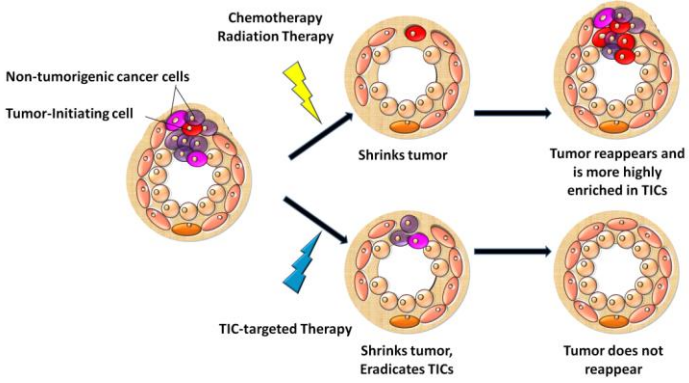


Figure 2. *Targeting TICs may lead to more durable cancer cures*. Although current front-line therapies effectively shrink tumors, the minority TICs may be refractory. These residual cells have the capacity to regenerate a tumor that is more highly enriched in TICs. By contrast, agents that target TICs would be expected to shrink tumors and prevent relapse, even if some non-tumorigenic cells were spared. In addition, if normal stem cells are spared, tissue homeostasis can be maintained. Depicted in the figure is a mammary tumor before and after standard or TIC-targeted treatment.

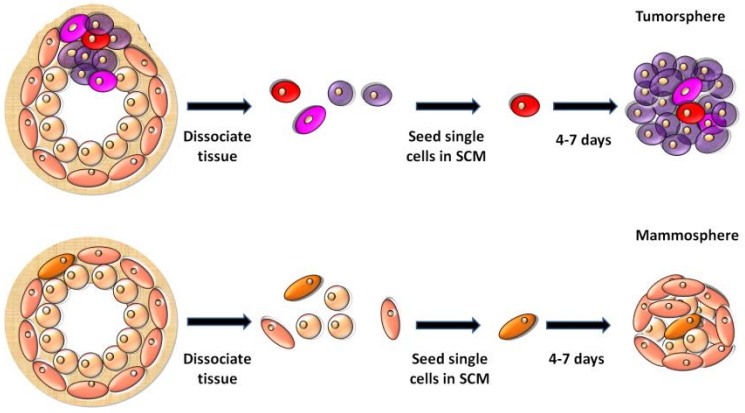


Figure 3. *Mammosphere and tumorsphere formation.* Following tissue resection, dissociation, and seeding in chemically-defined medium containing EGF, bFGF, and B27 (SCM), differentiated cells rapidly perish within 6 hours. Thereafter, stem and/or progenitor cells proliferate to form spheres.

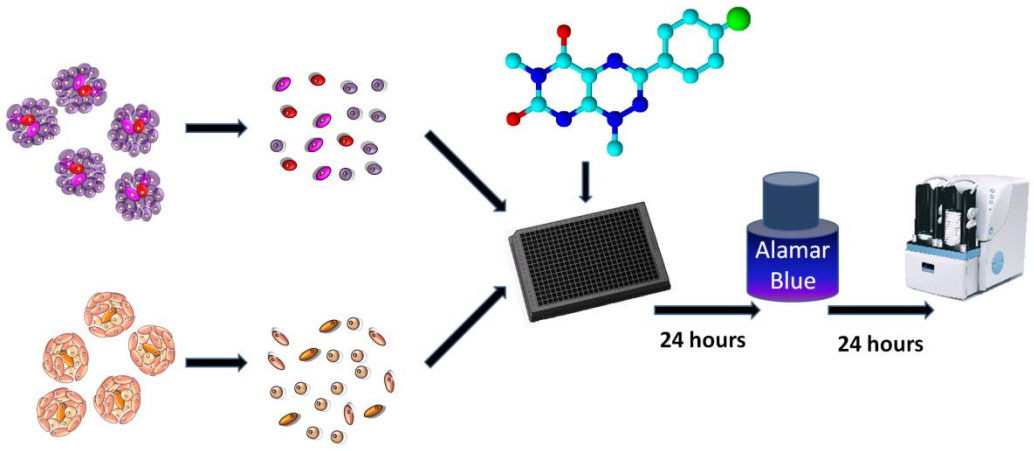


Figure 4. *A high-throughput chemical screen to identify selective inhibitors of TMS-derived cells.* Prior to screening, established TMS and MMS preparations are dissociated to single cells and seeded in 384-well plates in the presence of compound. Twenty-four hours thereafter, alamarBlue is added, and following a further 24 hours, fluorescence is read.

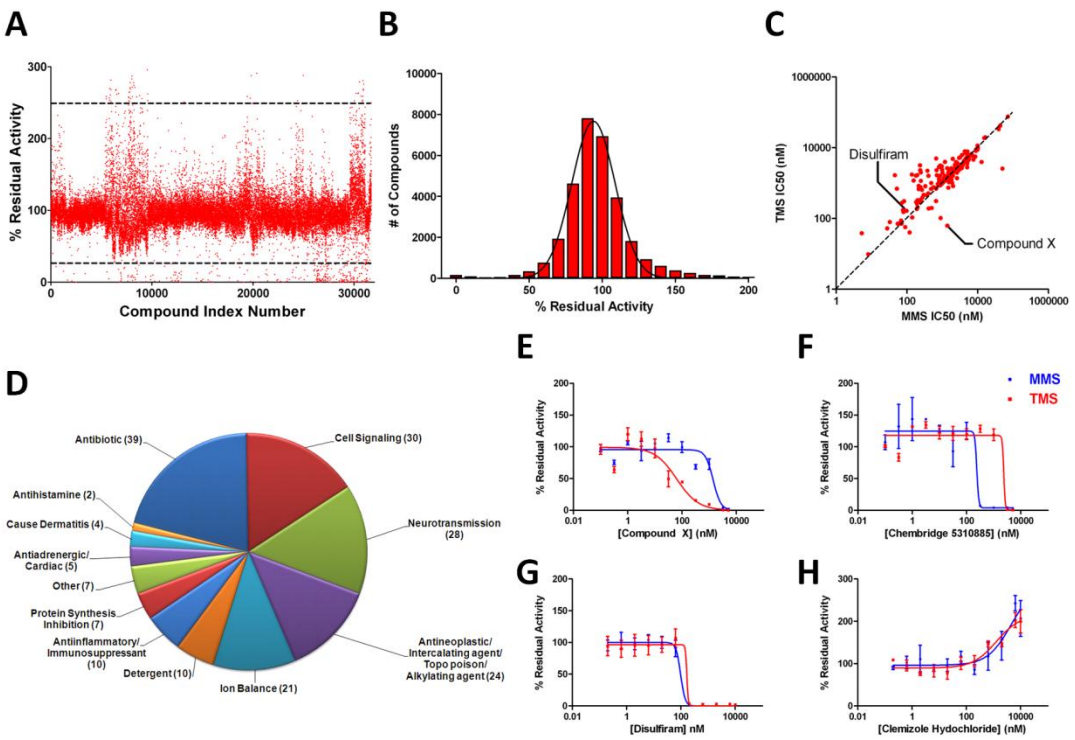


Figure 5. *High throughput screen analysis and identification of Compound X.* (A) A scatterplot of compound activities in the primary screen reveals that most compounds have no appreciable effect on TMS-derived cells. (B) A histogram demonstrates that these conform to a Gaussian distribution. (C) Plotting the $IC_{50}$ of inhibitory compounds in TMS- and MMS-derived cells helps identify potent and selective compounds. (D) Literature searches were carried out to discover common biological indications among hit compounds. (E-H) Selected dose-response curves illustrate TMS- and MMS-selective compounds, as well as non-selective, and agonistic compounds.

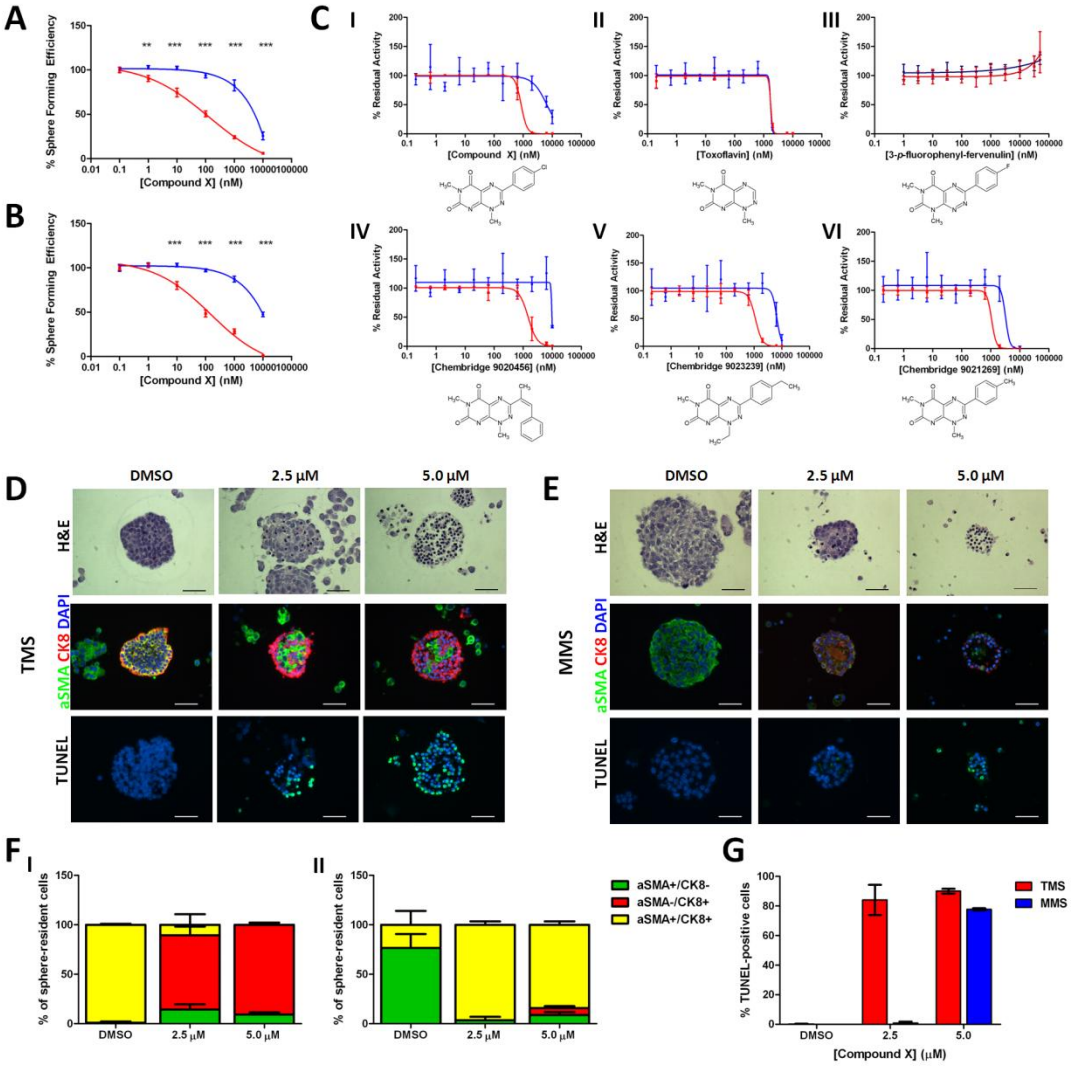


Figure 6. In vitro *characterization of Compound X.* Sphere-forming assays carried out using established sphere preparations (A) or primary cells (B) demonstrate that Compound X significantly preferentially inhibits the formation of TMS (red) compared to MMS (blue) (** $p < 0.005$, *** $p < 0.0001$, data shown is average of 3 biological replicates). (C) Preliminary SAR analyses were carried out using Compound X analogues in dose-response proliferation assays in TMS and MMS. (D-E) Compound X induces morphological and maker expression changes in intact TMS and MMS, and preferentially induces cell death in TMS (Images captured at 400x magnification, scale bars = 50 µm). (F) Quantification of mammary epithelial lineage marker expression in TMS (i) and MMS (ii) in the absence or presence of Compound X. (G) Quantification of apoptotic nuclei in TMS and MMS in the absence or presence of Compound X.

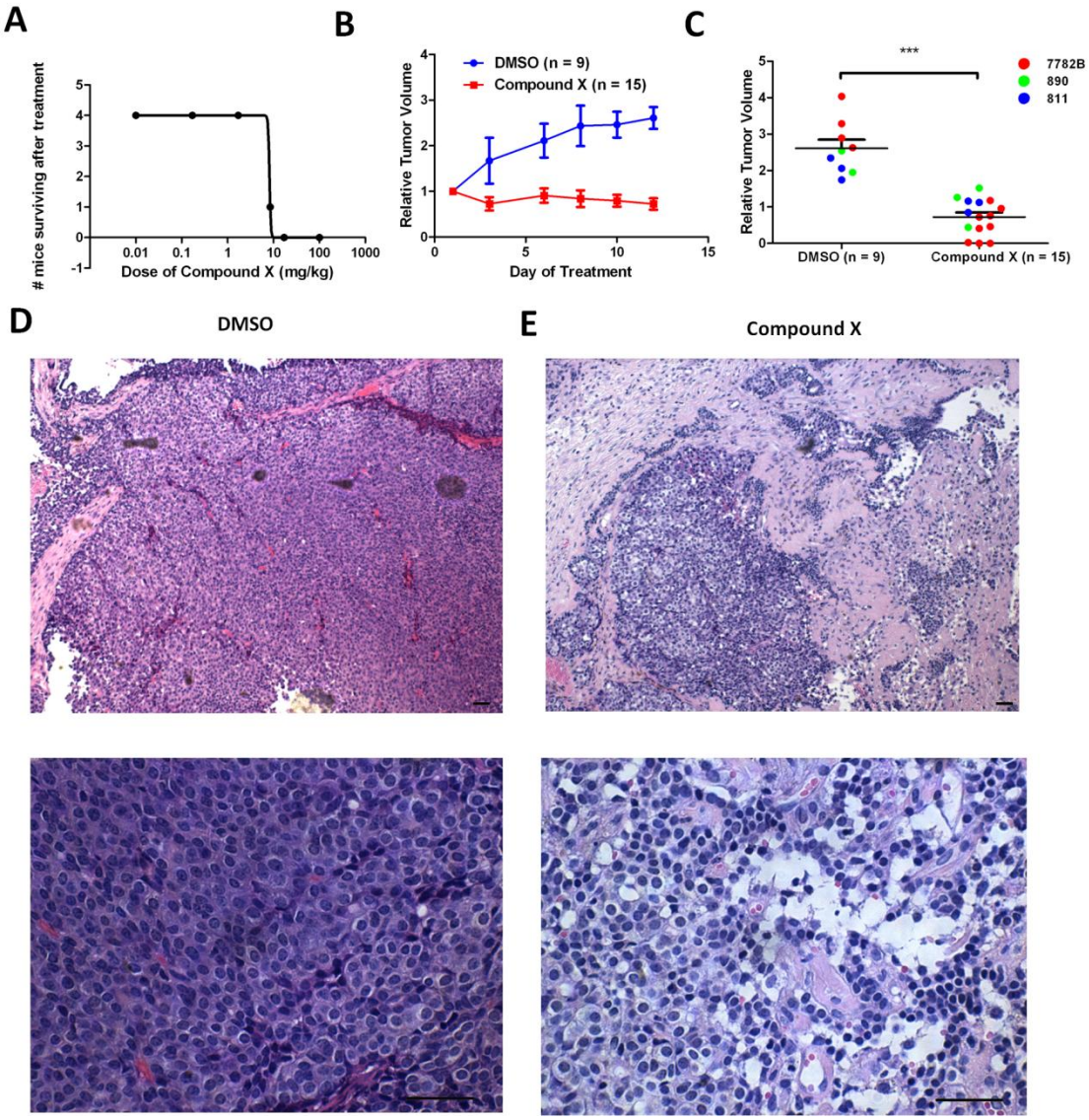


Figure 7. *Compound X significantly inhibits N#202 tumor growth in mice*. (A) The maximum tolerated dose was established by one time intraperitoneal injection of FVB/N mice. (B) FVB/N mice bearing mammary tumors established by subcutaneous injection of N#202 tumor cells were treated with Compound X at 4 mg/kg/day. Tumor size was measured and normalized to the size before treatment began. (C) A pooled analysis reveals that the effect on N#202 tumors is significant (*** $p < 0.0001$). (D-E) Hematoxylin and eosin staining reveals differences in tumor morphologies among Compound X and DMSO-treated cohorts (top – low power (100x), bottom – high power (400x), scale bars = 50 µm).

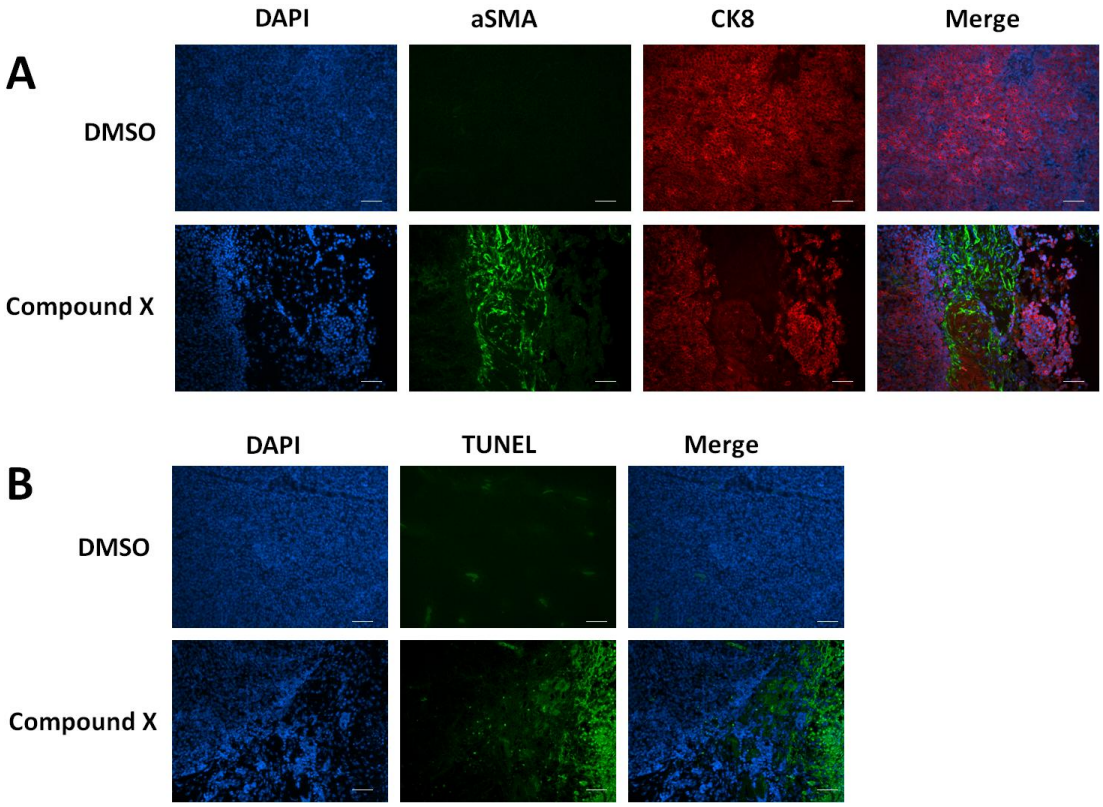


Figure 8. *Compound X alters lineage marker expression and induces cell death in N#202 tumor cells.* (A) aSMA and CK8 differentially stain treated versus control tumors. (B) Groups of TUNEL-positive cells were found only in Compound X-treated tumors (Images captured at 200x magnification, scale bars = 50 µm).

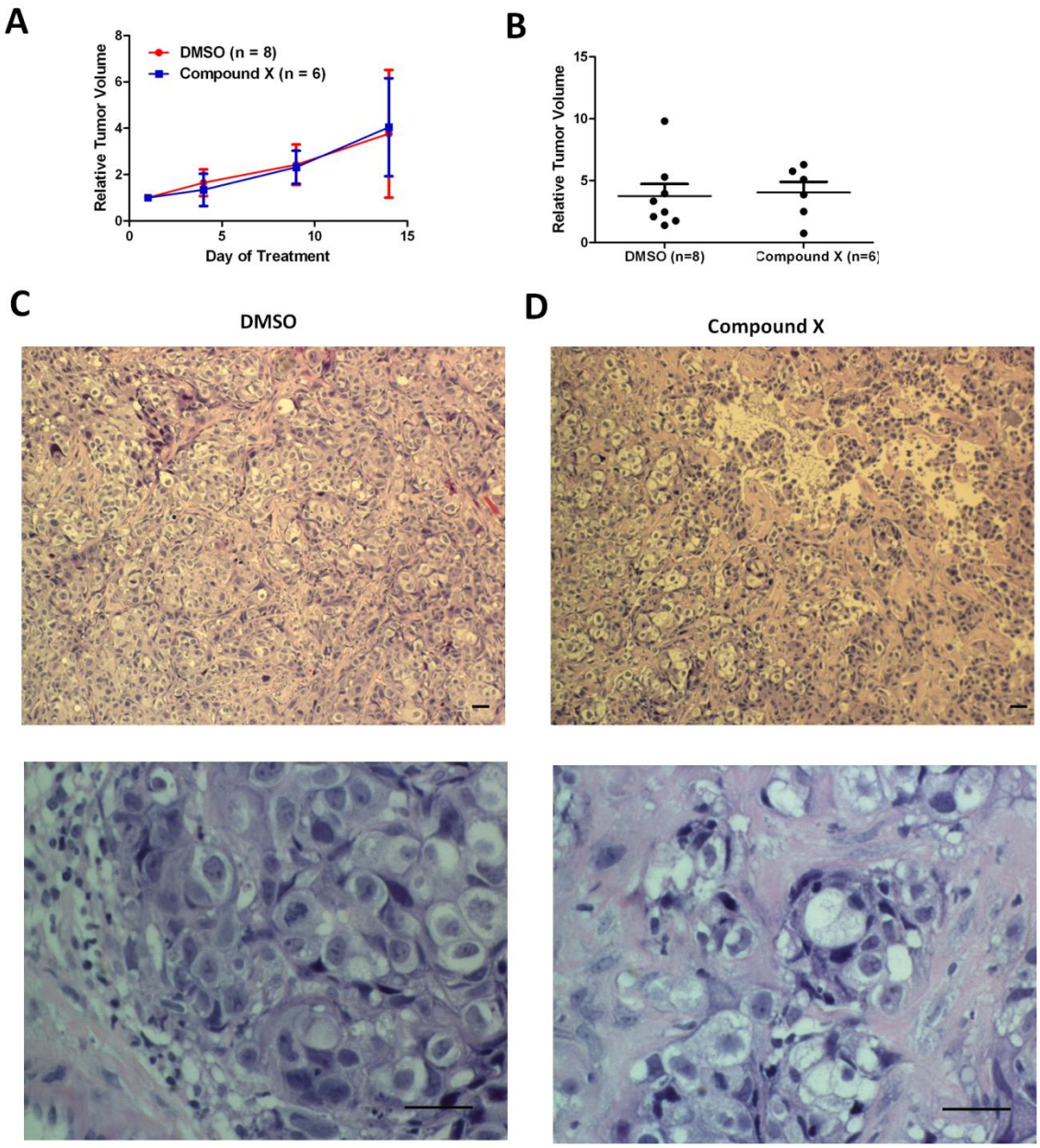


Figure 9. *Compound X does not significantly inhibit HCC1954 tumor growth in mice*. (A-B) NSG mice bearing mammary tumors established by subcutaneous injection of HCC1954 tumor cells were treated with Compound X at 2 mg/kg/day. Tumor size was measured and normalized to the size before treatment began. (C-D) Hematoxylin and eosin staining revealed no obvious differences in tumor morphologies among Compound X and DMSO-treated cohorts (top – low power (100x), bottom – high power (400x), scale bars = 50 µm).

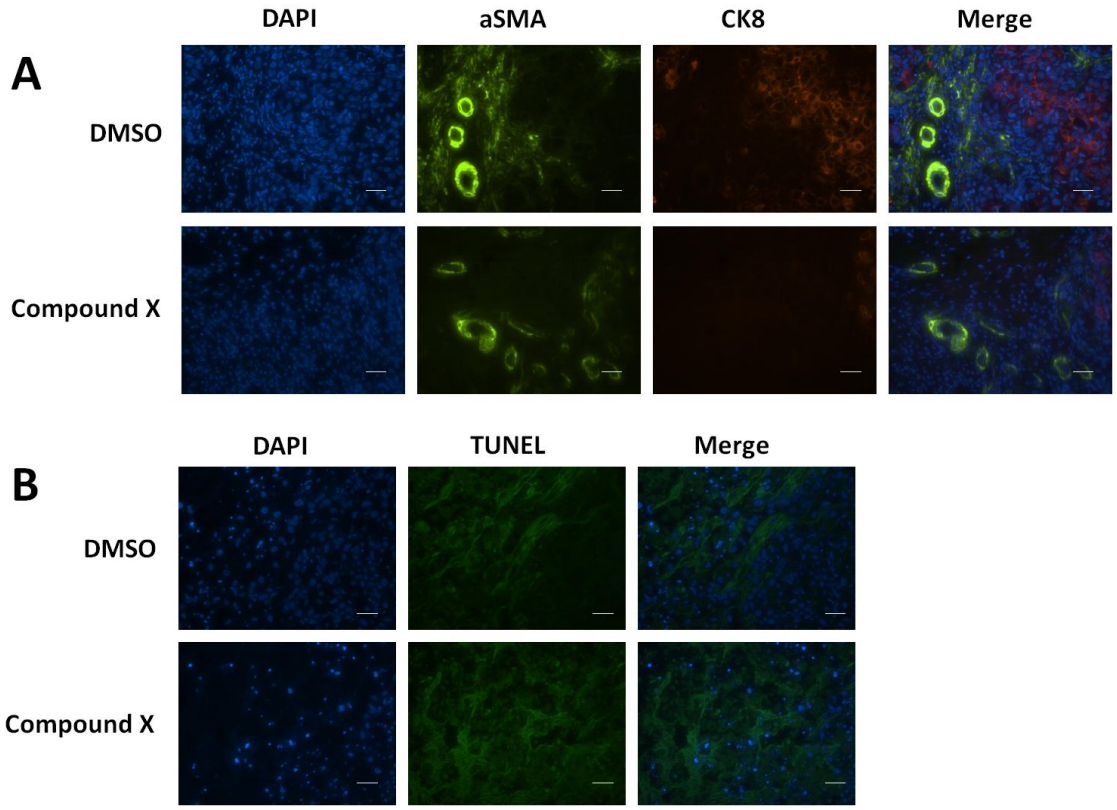


Figure 10. *Compound X does not alter the expression of lineage markers or induce cell death in HCC1954 tumors.* (A) aSMA and CK8 do not differentially stain treated versus control tumors. (D) TUNEL-positive debris was present in both treated and control tumors (Images captured at 200x magnification, scale bars = 50 µm).

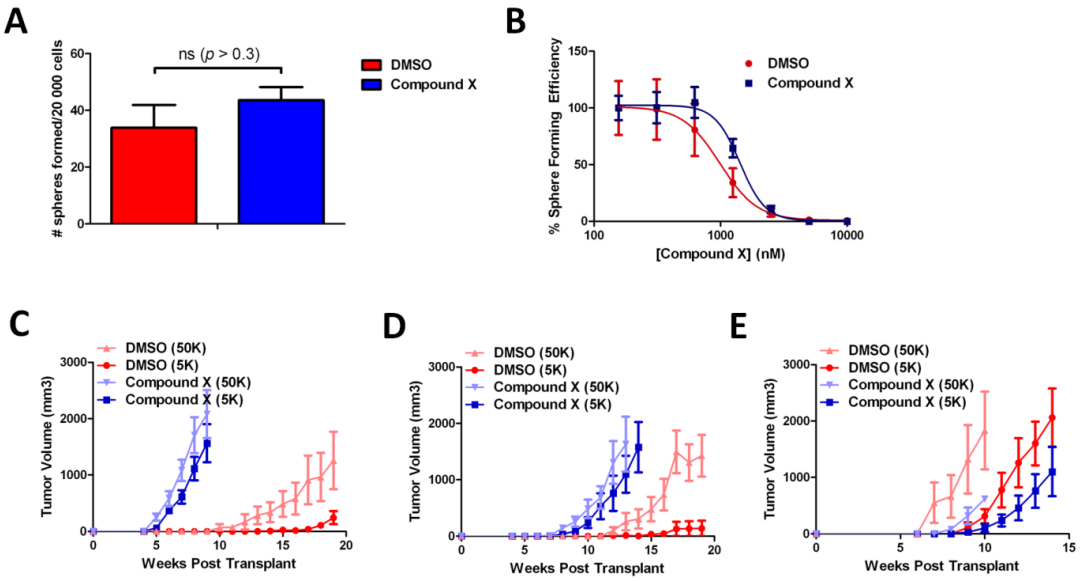


Figure 11. *Compound X does not affect the sphere-forming cells present in treated tumors, but alters the latency to tumor formation in serial transplants.* Tumors from treated N#202 mice were dissociated and seeded in chemically-defined medium using no treatment (A) or various doses of Compound X (B), and spheres were counted following a 7-day incubation. (C-E) Tumor cells from these cohorts were also transplanted subcutaneously into recipient FVB/N mice at 50,000 (50K) or 5000 (5K) cells per dose and tumor size was monitored (C – cohort 7782B, D – cohort 811a, E – cohort 811b).

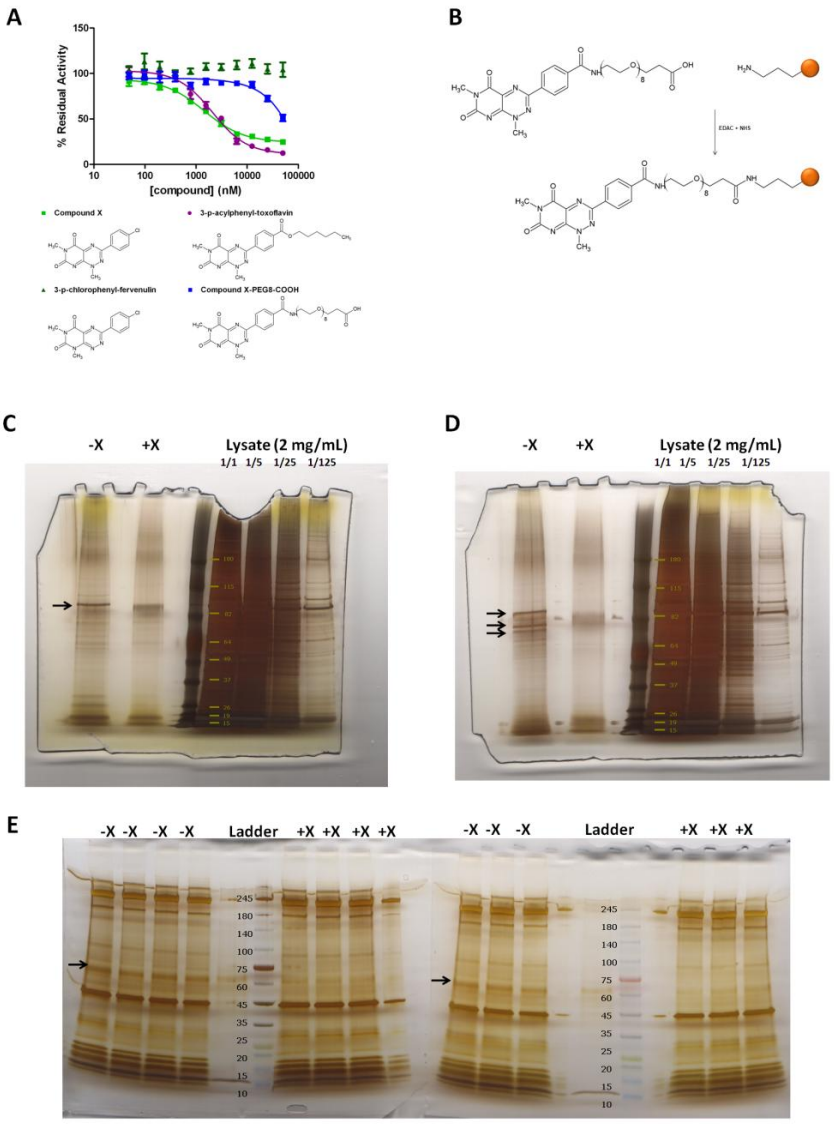


Figure 12. *Development and application of an active Compound X affinity probe.* (A) Single MCF7 cells were seeded in 384-well plates in the presence of the compounds indicated. The plates were incubated for 24 hours prior to addition of alamarBlue. Following a further 24 hours of incubation fluorescence was read and normalized. (B) The carboxylic acid group of Compund X-PEG8-COOH was activated using *N*-hydroxysuccinimide (NHS) and 1-ethyl-3-(3-dimethylaminopropyl) carbodiimide (EDAC) and coupled to amine-coated magnetic beads. Tumor lysate was incubated with this affinity resin in the presence or absence of soluble competing Compound X. After washing and eluting bound protein by boiling in SDS buffer, the eluate was run on a denaturing gel and silver stained (C-E). Bands present in the absence but not in the presence of Compound X (arrows) were excised and submitted for mass spectrometric analysis.

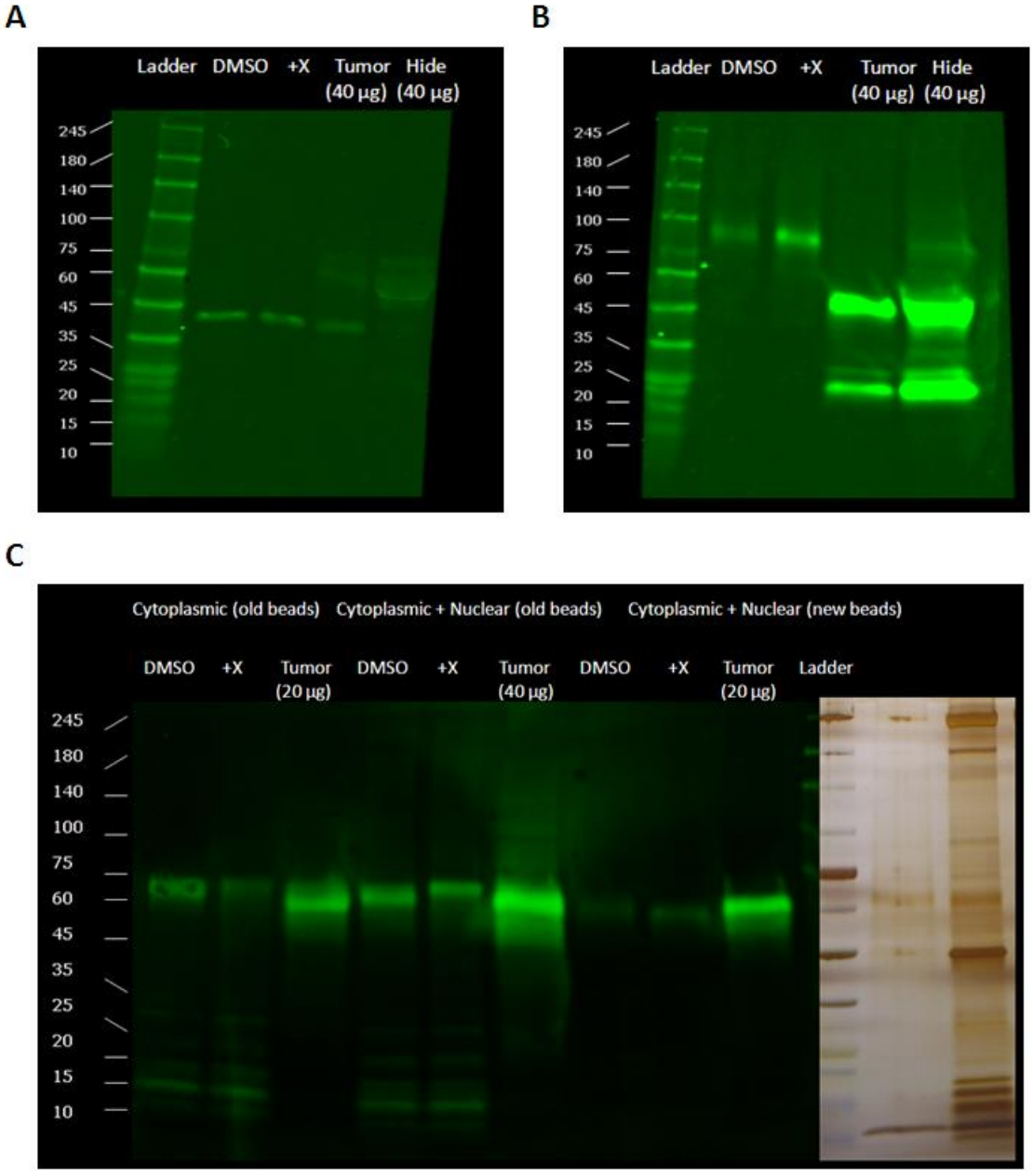


Figure 13. *Western blots reveal that albumin likely physically interacts with Compound X*. Following affinity experiments, Western blots were carried out using antibodies against CK5 (~55kDa) (A), CK79 (~58 kDa) (B), and serum albumin (~60 kDa) (C). Multiple preparations of beads and lysates were used in these experiments, as indicated. The right hand side of panel C is a cropped image of a non-competition lane in the silver stain, note the band at ~60 kDa.

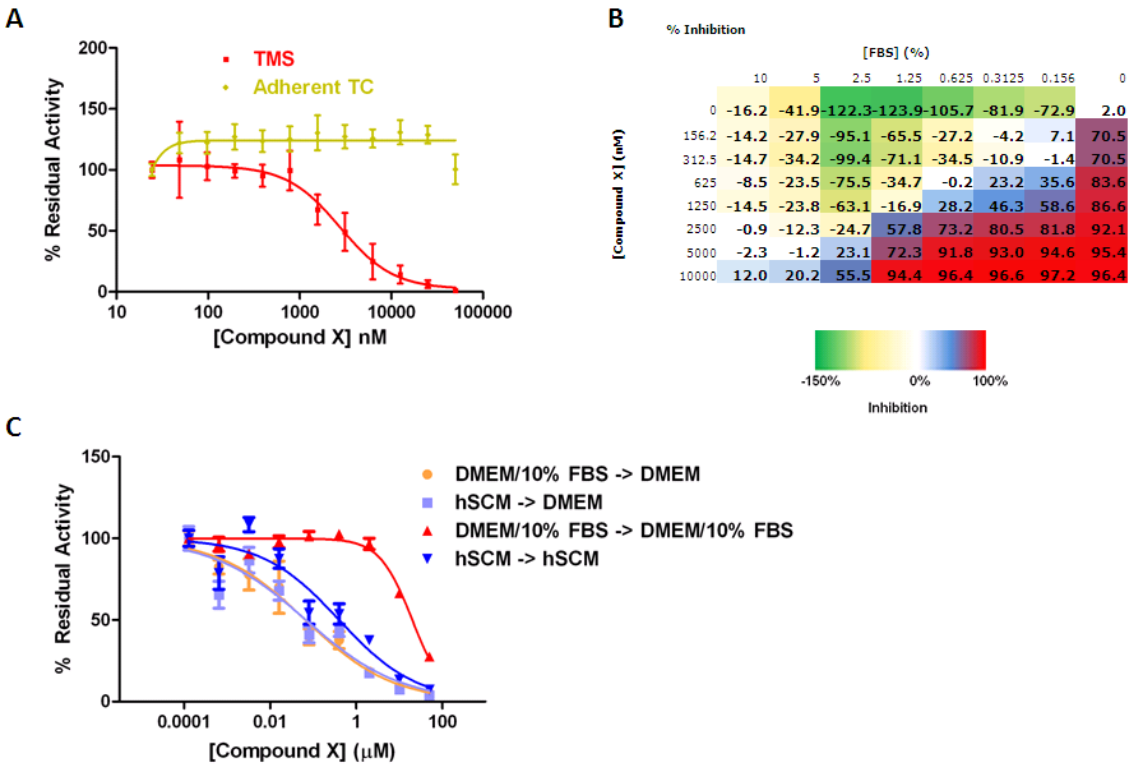


Figure 14. *Serum antagonizes Compound X*. (A) Compound X has no effect on adherent N#202 tumor cells up to 25 µM as judged by an alamarBlue proliferation assay. (B) FBS shifts the IC50 and maximal effect of Compound X in a dose dependent manner in MCF7 sphere-derived cells. (C) Adherent and sphere-derived MCF7 cells were seeded in wells of a 384-well plate and incubated for 24 hours. Media was then removed and serum-free/growth factor-free DMEM was added for 1 hour. This media was then removed and replaced with either serum-free/growth factor-free media (DMEM), or standard growth media (DMEM with 10% FBS or human stem cell medium (hSCM)). Compound X was then added and plates were incubated for 24 hours. alamarBlue was then added and fluorescence was read 24 hours thereafter.

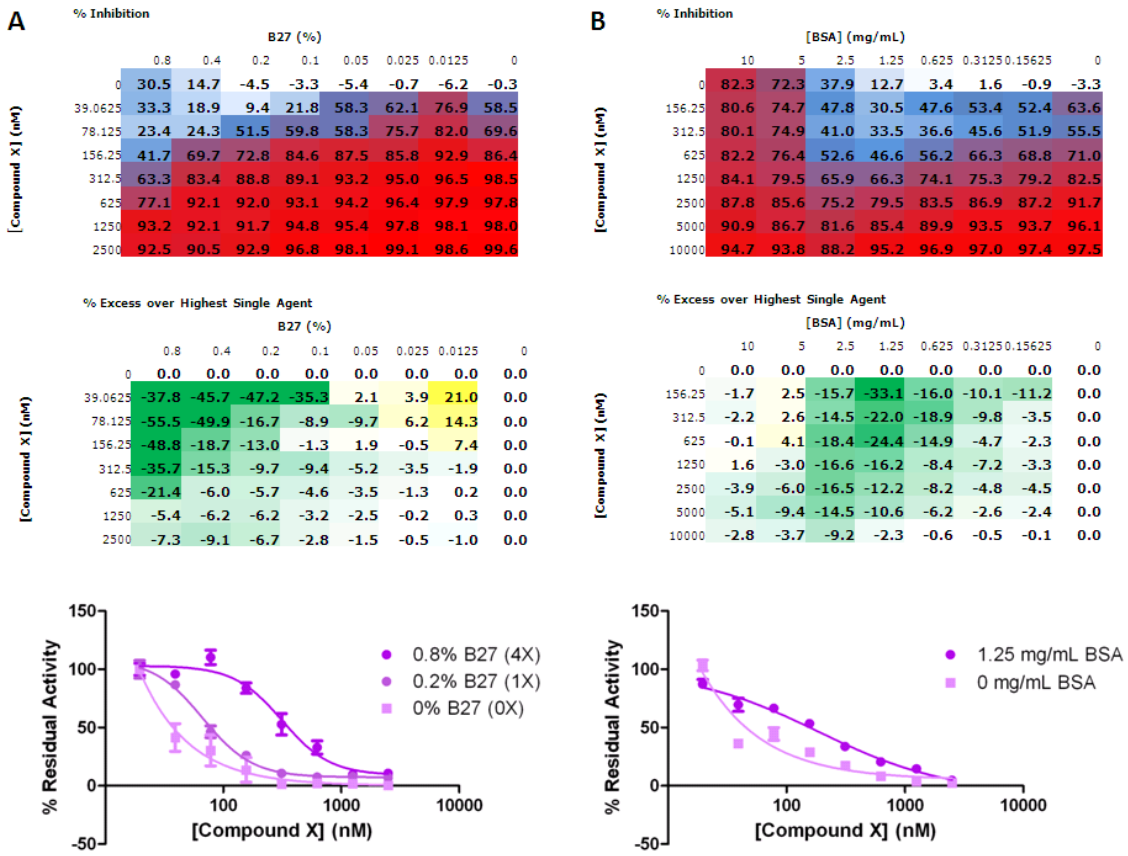


Figure 15. *B27 and BSA reduce the potency of Compound X*. B27 (A) and BSA (B) were serially diluted and combined with serially-diluted Compound X in a matrix. MCF7 sphere-derived cells were then subjected to the matrix in an alamarBlue assay.

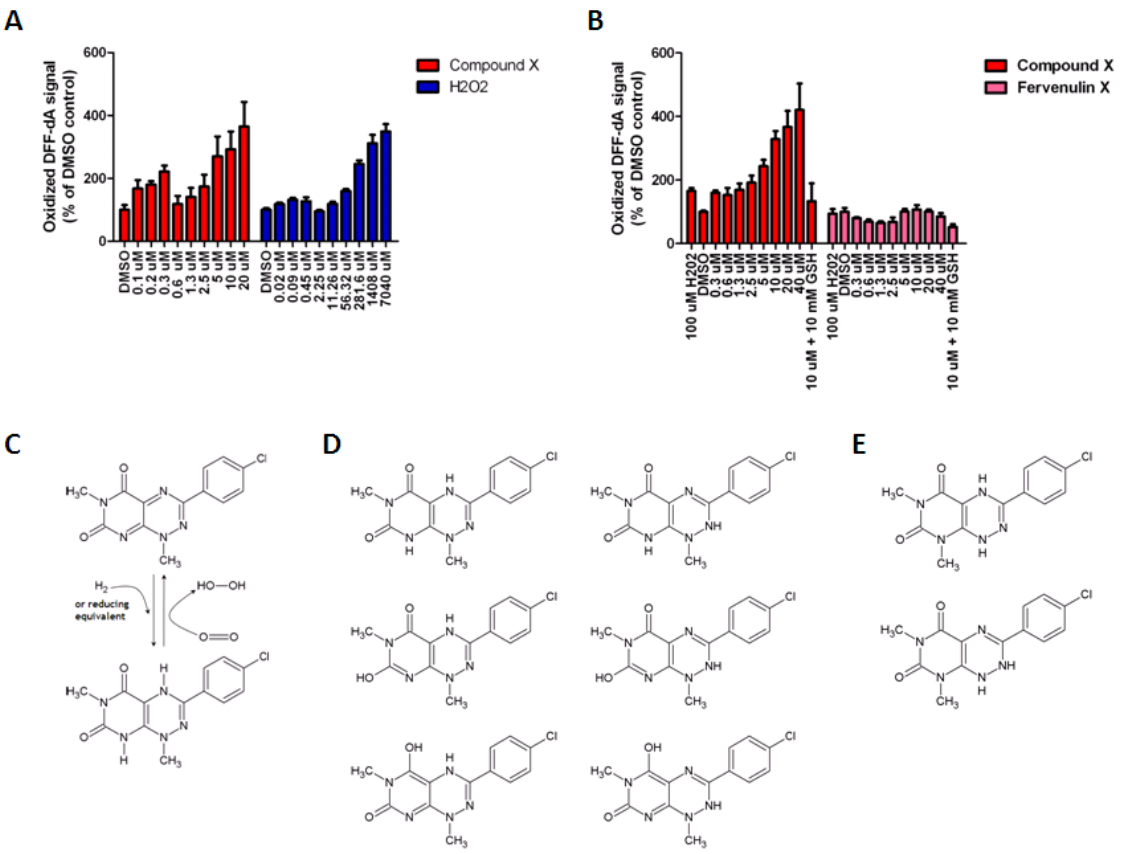


Figure 16. *Compound X, but not Fervenulin X, produces reactive oxygen species*. (A-B) Adherent MCF7 were subjected to ROS detection assays using DFF-dA. (C) Compound X might be reduced by molecular hydrogen or some reducing equivalent to yield a high-energy, but moderately stable intermediate, which then can reduce molecular oxygen to produce hydrogen peroxide. The reason that Compound X, but not Fervenulin X, produces $H_2O_2$ may be because the reduced Compound X intermediate is stabilized by up to 6 resonance forms (D), whereas the Fervenulin X intermediate can only exist in two resonance forms (E) and therefore may be so energetically unfavorable as to never exist.

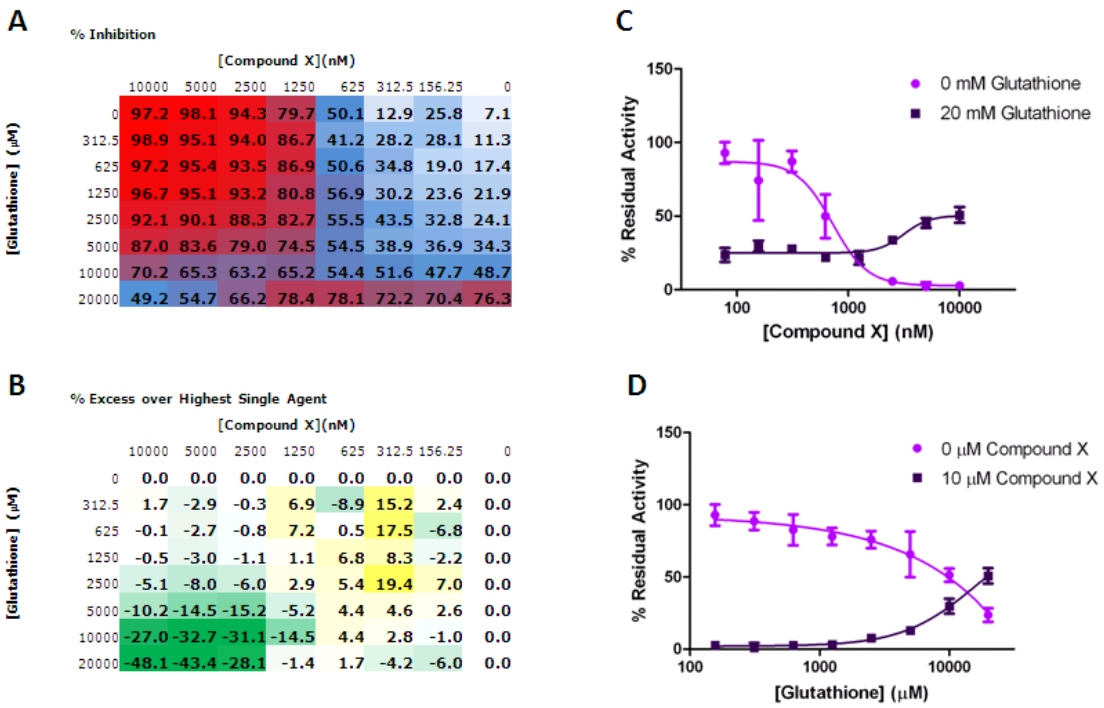


Figure 17. *Compound X and reduced glutathione partially antagonize one another.* GSH decreases the maximal inhibitory effect achieved by Compound X in MCF7 sphere-derived cells, and vice versa.

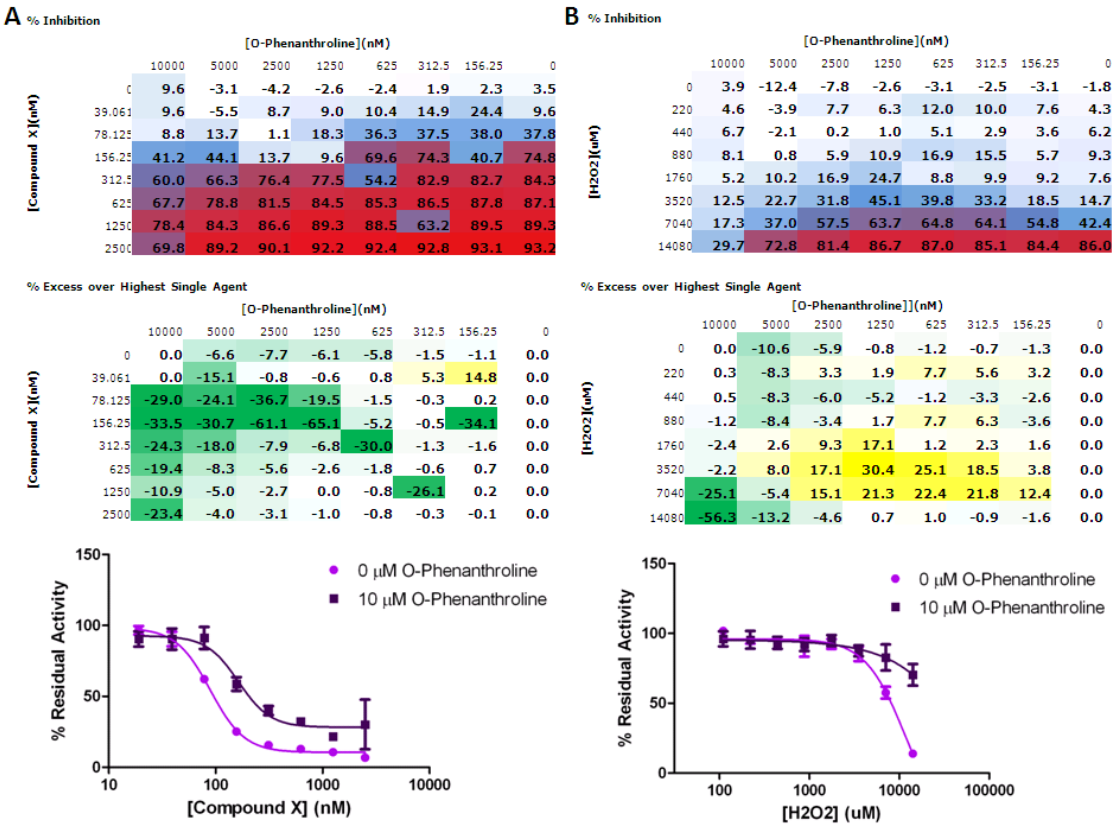


Figure 18. O-*Phenanthroline protects cells from Compound X and hydrogen peroxide*. *O*-phenanthroline, a compound which chelates iron, shifts the $IC_{50}$ and maximal effect levels of Compound X and $H_2O_2$ to higher doses in MCF7 sphere-derived cells.

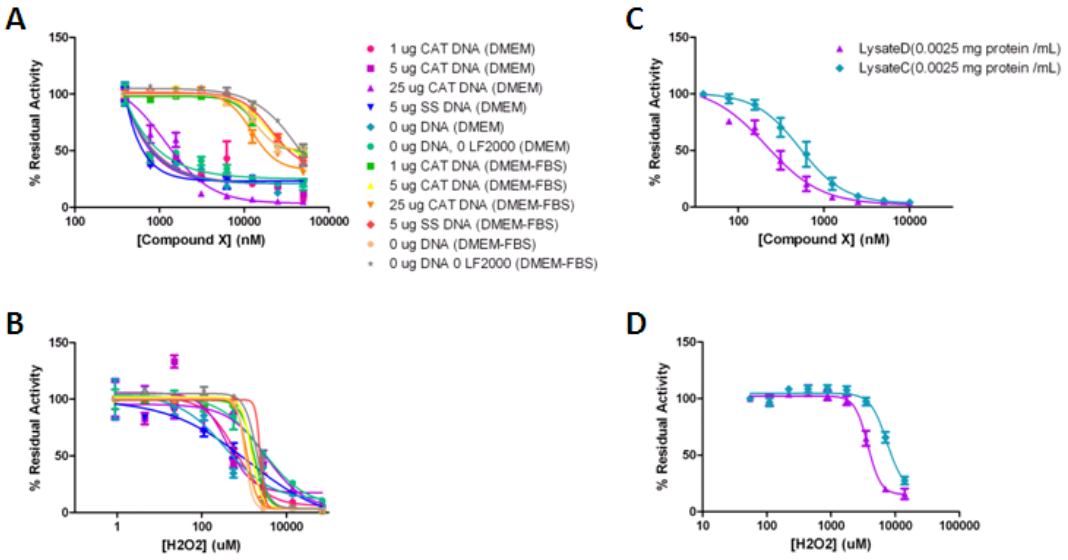


Figure 19. *Cells transfected with a catalase expression plasmid are not resistant to hydrogen peroxide or Compound X.* Adherent cells were transiently transfected with pCMV-XL5 plasmid (Origene) and 24 hours later were trypsinized, reseeded in DMEM/10% FBS or DMEM lacking serum and subjected to treatment with varying doses of Compound X (A) or $H_2O_2$ (B). alamarBlue was added 12 hours after compound addition and the plates were read following another 12 hours incubation (assay was completed 48 hours post transfection). (C) MCF7 sphere-derived cells were grown in the presence of lysate from salmon sperm-transfected (lysate D) or catalase-transfected (lysate C) cells (average of 3 biological experiments).

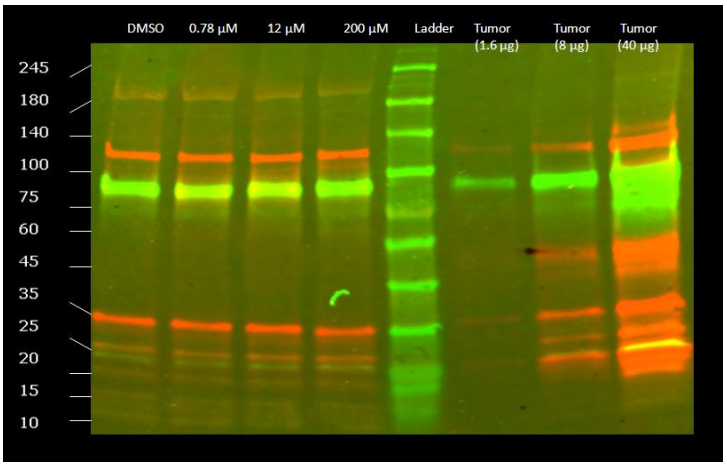


Figure 20. *Affinity-Western for β-catenin and E-cadherin*. Following affinity purification experiments carried out in the absence (DMSO) or presence of various concentrations of Compound X. We performed a Western blot using antibodies against β-catenin (~90 kDa) (green) and E-cadherin (~120 kDa) (red).

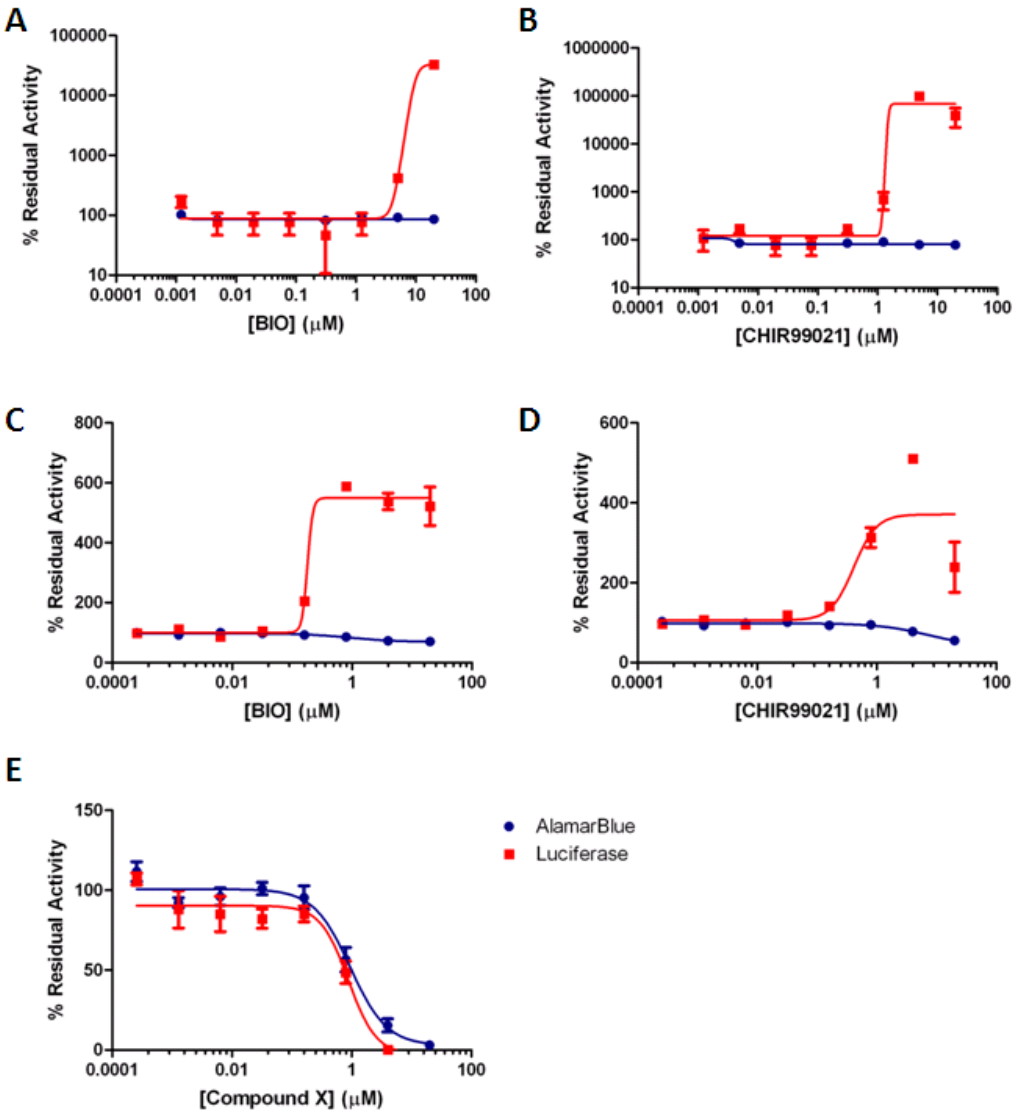


Figure 21. *Wnt reporter assays.* Adherent MCF7 cells (A-B) or adherent HCT116 cells (C-E) harboring an integrated Wnt reporter were treated with inhibitors of GSK3β or Compound X and subjected to a multiplexed alamarBlue/firefly luciferase assay.

## 8. TABLES

Table 1. *$IC_{50}$ values for all compounds tested in proliferation assays in TMS- and MMS-derived cells.*

| Supplier | Compound Name | MMS IC50 (nM) | TMS IC50 (nM) |
|---|---|---|---|
| Maybridge | BTB 02467 | 6.8E+02 | 2.3E+03 |
| Maybridge | BTB 07373 | 7.2E+01 | 2.8E+02 |
| Maybridge | BTB 10303 | >1.0E+03 | 1.3E+03 |
| Maybridge | BTB 14417 | 1.8E+02 | 1.6E+03 |
| Maybridge | BTB 14447 | 1.4E+02 | 1.8E+03 |
| Maybridge | CD 00793 | 3.8E+02 | 2.2E+03 |
| Maybridge | AW 00934 | 8.7E+02 | >3.2E+02 |
| Maybridge | CD 11507 | 1.3E+03 | >1.0E+03 |
| Maybridge | HTS 06488 | 4.6E+01 | 1.7E+03 |
| Maybridge | HTS 07592 | 1.6E+03 | 1.9E+03 |
| Maybridge | HTS 12742 | 1.5E+03 | 1.6E+03 |
| Maybridge | JFD 00035 | 1.0E+03 | 1.2E+03 |
| Maybridge | JFD 00597 | 1.7E+03 | 1.6E+03 |
| Maybridge | JFD 00742 | 1.3E+04 | 4.0E+03 |
| Maybridge | JFD 00787 | 1.1E+03 | >1.0E+03 |
| Maybridge | JFD 00972 | 1.4E+03 | 2.7E+03 |
| Maybridge | JFD 00979 | 5.3E+00 | 3.8E+01 |
| Maybridge | JFD 01136 | 2.3E+03 | 3.3E+03 |
| Maybridge | JFD 02816 | 1.3E+03 | 1.5E+03 |
| Maybridge | KM 00713 | 1.9E+03 | 1.0E+03 |
| Maybridge | KM 00767 | 1.2E+03 | 1.2E+03 |
| Maybridge | KM 00794 | 1.2E+03 | 1.4E+03 |
| Maybridge | KM 00909 | 1.8E+03 | >1.0E+03 |
| Maybridge | KM 02595 | 2.5E+03 | 2.6E+03 |
| Maybridge | KM 03341 | >1.0E+03 | >1.0E+03 |
| Maybridge | KM 03684 | 2.5E+02 | 1.2E+03 |
| Maybridge | KM 03776 | 2.1E+02 | 6.8E+02 |
| Maybridge | KM 04416 | 2.5E+02 | 2.0E+03 |
| Maybridge | KM 05413 | 2.3E+02 | 3.2E+03 |
| Maybridge | KM 05590 | >1.0E+03 | 1.4E+03 |
| Maybridge | KM 05882 | >3.2E+03 | 5.7E+03 |
| Maybridge | KM 06346 | 1.5E+02 | 1.2E+03 |
| Maybridge | KM 06874 | 1.2E+03 | 1.6E+03 |

| | | | |
|---|---|---|---|
| Maybridge | KM 07965 | 1.3E+03 | 1.4E+03 |
| Maybridge | KM 08041 | >3.2E+03 | 6.6E+03 |
| Maybridge | MWP 00602 | >3.2E+03 | 9.6E+02 |
| Maybridge | MWP 01055 | 9.0E+02 | >3.2E+03 |
| Maybridge | NRB 04094 | 5.7E+02 | 7.7E+02 |
| Maybridge | NRB 04162 | 3.0E+02 | 4.6E+02 |
| Maybridge | PD 00433 | >3.2E+03 | 4.8E+03 |
| Maybridge | PHG 00966 | 1.1E+03 | 1.4E+03 |
| Maybridge | PHG 00967 | 1.5E+03 | 1.4E+03 |
| Maybridge | RB 00158 | 2.5E+03 | 2.3E+03 |
| Maybridge | RF 01687 | 2.1E+03 | >1.0E+03 |
| Maybridge | RH 01403 | 1.6E+03 | 1.2E+03 |
| Maybridge | RH 02211 | 1.6E+03 | 1.3E+03 |
| Maybridge | RJC 02988 | 8.0E+02 | 1.3E+03 |
| Maybridge | RJC 02997 | 2.5E+03 | 2.4E+03 |
| Maybridge | RJC 03760 | 2.6E+03 | 3.7E+03 |
| Maybridge | RJF 00706 | 5.4E+03 | 4.8E+03 |
| Maybridge | RJF 01666 | 2.4E+03 | 2.4E+03 |
| Maybridge | S 01369 | 1.2E+03 | >1.0E+03 |
| Maybridge | S 02829 | 5.1E+03 | >3.2E+03 |
| Maybridge | S 03980 | 1.0E+03 | 1.0E+03 |
| Maybridge | S 04055 | 1.8E+02 | 2.9E+02 |
| Maybridge | S 05237 | 2.1E+02 | 8.4E+02 |
| Maybridge | S 05384 | 4.0E+02 | 5.1E+02 |
| Maybridge | S 07429 | 9.2E+02 | 1.1E+03 |
| Maybridge | S 07624 | 2.4E+03 | 3.2E+03 |
| Maybridge | S 10252 | 1.0E+03 | 1.1E+03 |
| Maybridge | S 11423 | 2.2E+03 | >1.0E+03 |
| Maybridge | S 11897 | 8.3E+01 | 3.1E+02 |
| Maybridge | S 12950 | 9.1E+02 | 1.0E+03 |
| Maybridge | S 14295 | >1.0E+03 | 1.4E+03 |
| Maybridge | S 14683 | 3.6E+03 | 3.3E+03 |
| Maybridge | S 14685 | 2.9E+03 | 2.3E+03 |
| Maybridge | SEW 06256 | >3.2E+03 | >3.2E+03 |
| Maybridge | SJC 00391 | 5.0E+03 | 5.0E+03 |
| Maybridge | SPB 01621 | 1.8E+03 | 1.1E+03 |
| Maybridge | SPB 01622 | >1.0E+03 | 1.6E+03 |
| Maybridge | SPB 01986 | 1.1E+03 | 1.3E+03 |
| Maybridge | SPB 02669 | 1.0E+03 | >1.0E+03 |

| | | | |
|---|---|---|---|
| Maybridge | SPB 06553 | 2.6E+03 | 1.4E+03 |
| Maybridge | SPB 07215 | 7.9E+02 | 8.8E+02 |
| Maybridge | SPB 07445 | 1.4E+03 | >1.0E+03 |
| Maybridge | SPB 07895 | 1.8E+03 | 1.3E+03 |
| Maybridge | TL 00165 | 2.8E+03 | 2.9E+03 |
| Maybridge | XBX 00150 | >1.0E+03 | 1.3E+03 |
| Maybridge | XBX 00315 | N/A | N/A |
| Maybridge | XBX 00316 | N/A | N/A |
| Chembridge | 5108260.0 | 1.8E+03 | 1.6E+03 |
| Chembridge | 5124607.0 | >1.0E+03 | >1.0E+03 |
| Chembridge | 5169083.0 | 1.2E+03 | 1.2E+03 |
| Chembridge | 5175150.0 | 1.2E+03 | 1.3E+03 |
| Chembridge | 5217336.0 | 3.2E+03 | >3.2E+03 |
| Chembridge | 5234104.0 | 1.4E+03 | 6.3E+01 |
| Chembridge | 5267003.0 | 5.2E+01 | 7.0E+02 |
| Chembridge | 5272685.0 | >1.0E+03 | 1.7E+03 |
| Chembridge | 5279631.0 | 1.7E+03 | 1.8E+03 |
| Chembridge | 5282288.0 | >1.0E+03 | >1.0E+03 |
| Chembridge | 5310885.0 | 2.4E+02 | 2.3E+03 |
| Chembridge | 5352494.0 | 1.8E+03 | 2.6E+03 |
| Chembridge | 5354204.0 | >3.2E+03 | 5.0E+03 |
| Chembridge | 5355207.0 | 3.1E+03 | >3.2E+03 |
| Chembridge | 5457220.0 | 3.5E+03 | 3.4E+03 |
| Chembridge | 5454910.0 | >1.0E+03 | 2.4E+03 |
| Chembridge | 5456843.0 | 2.7E+03 | 3.4E+03 |
| Chembridge | 5537491.0 | >3.2E+03 | 5.0E+03 |
| Chembridge | 5543164.0 | 8.7E+02 | 3.2E+03 |
| Chembridge | 5540635.0 | >3.2E+03 | 4.7E+03 |
| Chembridge | 5557823.0 | 2.5E+03 | 3.2E+03 |
| Chembridge | 5565451.0 | 6.7E+02 | >3.2E+03 |
| Chembridge | 5611138.0 | 9.9E+02 | 2.4E+03 |
| Chembridge | 5603579.0 | 8.1E+02 | 2.9E+03 |
| Chembridge | 5672102.0 | 1.6E+03 | 1.6E+03 |
| Chembridge | 5653447.0 | 1.5E+03 | 2.4E+03 |
| Chembridge | 5670412.0 | 2.6E+03 | 2.0E+03 |
| Chembridge | 5664149.0 | 1.6E+03 | 2.5E+03 |
| Chembridge | 5685331.0 | 2.6E+03 | >1.0E+03 |
| Chembridge | 5781441.0 | 1.1E+03 | >1.0E+03 |
| Chembridge | 5712612.0 | 1.3E+03 | >1.0E+03 |

| | | | |
|---|---|---|---|
| Chembridge | 5670522.0 | 1.6E+03 | 1.2E+03 |
| Chembridge | 5749131.0 | >1.0E+03 | 1.2E+03 |
| Chembridge | 6627149.0 | 1.5E+03 | 1.7E+03 |
| Maybridge | HTS 07931 | 5.1E+03 | >3.2E+03 |
| Maybridge | HTS 08181 | 5.7E+03 | 4.9E+03 |
| Maybridge | HTS 08797 | 5.5E+03 | 4.5E+03 |
| Maybridge | HTS 09779 | 5.0E+03 | 5.6E+03 |
| Maybridge | HTS 12431 | 5.0E+03 | 6.8E+03 |
| Maybridge | JFD 03101 | 7.6E+03 | 4.7E+03 |
| Maybridge | KM 01952 | 4.3E+03 | 4.3E+03 |
| Maybridge | KM 04625 | 4.3E+03 | >3.2E+03 |
| Maybridge | KM 04736 | >3.2E+03 | >3.2E+03 |
| Chembridge | 5230315.0 | 4.1E+03 | 4.3E+03 |
| Chembridge | 5256886.0 | >3.2E+03 | >3.2E+03 |
| Chembridge | 5265303.0 | >3.2E+03 | >3.2E+03 |
| Chembridge | 5306189.0 | >3.2E+03 | >3.2E+03 |
| Chembridge | 6615462.0 | >3.2E+03 | >3.2E+03 |
| BIOMOL | Hypocrellin A | 5.7E+03 | >3.2E+03 |
| Prestwick | Monensin Sodium Salt | 8.9E+02 | 1.0E+02 |
| BIOMOL | Mitomycin C | 2.5E+03 | 2.9E+03 |
| Prestwick | Acacetin | 5.2E+03 | N/A |
| Prestwick | Azaguanine-8 | >2.0E+02 | 2.0E+02 |
| Prestwick | Mitoxantrone | 2.0E+03 | 2.5E+03 |
| MicroSource | Dactinomycin | 1.2E+02 | 4.1E+01 |
| Prestwick | Doxorubicin HCl | 8.9E+01 | 5.7E+01 |
| BIOMOL | Lapachone, b- | 1.7E+03 | 1.7E+03 |
| MicroSource | Amsacrine | 9.7E+02 | 3.0E+03 |
| BIOMOL | Mycophenolic Acid | N/A | N/A |
| Prestwick | Anisomycin | 7.0E+01 | 7.2E+01 |
| Prestwick | Lycorine HCl | 5.1E+03 | 3.6E+03 |
| MicroSource | Allodeoxycholic Acid | 3.2E+03 | 5.3E+03 |
| BIOMOL | Rifamycin SV-Na | 6.7E+02 | 7.2E+02 |
| Sigma | Dequalinium Analog C-14 linker | 2.5E+02 | 3.5E+02 |
| BIOMOL | Phorbol 12-myristate 13-acetate, 4a- | 8.6E+02 | 1.6E+03 |
| MicroSource | Sanguinarine Sulfate | 8.9E+02 | 1.1E+03 |
| MicroSource | Tetrachloroisopthalonitrile | 3.3E+01 | 8.0E+01 |
| MicroSource | Pristimerin | 2.7E+02 | 6.5E+02 |
| MicroSource | Pristimerol | 1.9E+02 | 2.6E+02 |
| Prestwick | Terconazole | >2.0E+03 | 4.4E+03 |

| | | | |
|---|---|---|---|
| MicroSource | Obtusaquinone | 3.3E+02 | 8.2E+02 |
| Prestwick | Amodiaquin diHCl diH2O | >6.3E+02 | 1.6E+03 |
| MicroSource | Oxyquinoline hemisulfate | N/A | N/A |
| Prestwick | Chrysene-1,4-quinone | 1.5E+03 | 2.0E+03 |
| Prestwick | Cantharidin | 2.3E+03 | 2.3E+03 |
| MicroSource | Tyrothricin | 6.7E+02 | 7.0E+02 |
| MicroSource | Lasalocid Sodium | 1.1E+03 | 1.2E+03 |
| MicroSource | Benzalkonium chloride | 1.9E+03 | 1.9E+03 |
| MicroSource | Cetylpyridinium chloride | 1.0E+03 | 1.0E+03 |
| MicroSource | Helenine | 2.4E+03 | 4.0E+03 |
| Prestwick | Metergoline | 2.0E+03 | 2.4E+03 |
| Prestwick | R(-) Apomorphine HCl | 4.8E+02 | 1.0E+03 |
| MicroSource | Thiothixene | 1.9E+02 | 1.7E+03 |
| Prestwick | Thioridazine | 2.4E+02 | 7.7E+02 |
| MicroSource | Rosolic Acid | 2.0E+03 | 8.3E+02 |
| Prestwick | Clomiphene Citrate (Z,E) | 4.1E+02 | 1.9E+02 |
| Prestwick | Suloctidil | 4.0E+02 | 1.6E+03 |
| MicroSource | Niloticin | 2.4E+03 | >2.0E+03 |
| Novartis | PKF118-310 | 7.4E+02 | 9.5E+02 |
| Novartis | PKF115-584 | 4.6E+03 | 4.9E+03 |
| Novartis | CGP049090 | 4.3E+03 | 7.9E+03 |
| Prestwick | Sulconazole nitrate | 5.0E+03 | 5.0E+03 |
| Prestwick | Miconazole | 5.0E+03 | 5.0E+03 |
| Prestwick | Clemizole Hcl | N/A | N/A |
| Prestwick | Sertaconazole | N/A | N/A |
| Sigma | Sandoz 58-035 | N/A | N/A |
| BIOMOL | Gambogic Acid | 2.8E+01 | 5.3E+01 |
| MicroSource | Dihydrogambogic Acid | 5.5E+01 | 7.2E+01 |
| MicroSource | Tetrahydrogambogic Acid | 1.2E+03 | 4.0E+03 |
| MicroSource | Decahydrogambogic Acid | 8.4E+02 | 1.6E+03 |
| MicroSource | Gambogic Acid Amide | 7.7E+01 | 1.7E+02 |
| MicroSource | Acetyl Isogambogic Acid | 6.8E+01 | 8.7E+01 |
| | Rapamycin | >6.3E+03 | >6.3E+03 |
| | LY294002 | 1.6E+04 | 2.0E+04 |
| BIOMOL | E6 Berbamine | 2.5E+03 | 3.0E+03 |
| BIOMOL | Brefeldin A | >1.0E+04 | >1.0E+04 |
| BIOMOL | Cape | 1.8E+03 | 1.3E+03 |
| BIOMOL | Chaconine, a - | 1.6E+03 | 1.6E+03 |
| BIOMOL | Geldanamycin | 8.0E+00 | 9.8E+00 |

| | | | |
|---|---|---|---|
| BIOMOL | Gliotoxin | 6.2E+01 | 7.2E+01 |
| BIOMOL | Ochratoxin A | N/A | N/A |
| BIOMOL | Patulin | 3.5E+03 | 2.7E+03 |
| BIOMOL | Radicicol | 8.0E+01 | 1.5E+02 |
| BIOMOL | Shikonin | 2.0E+02 | 2.1E+02 |
| BIOMOL | Tubercidin | 8.3E+02 | 2.9E+03 |
| BIOMOL | Tunicamycin B | 2.0E+02 | 3.3E+02 |
| BIOMOL | Vineomycin A1 | 1.9E+02 | 1.9E+02 |
| Prestwick | (-)-Eseroline fumarate salt | N/A | N/A |
| Prestwick | Alexidine dihydrochloride | 1.5E+03 | 1.7E+03 |
| Prestwick | Astemizole | 7.0E+02 | 1.7E+03 |
| Prestwick | Ciclopirox ethanolamine | >1.0E+04 | >1.0E+04 |
| Prestwick | Disulfiram | 9.7E+01 | 1.7E+02 |
| Prestwick | Fendiline hydrochloride | 7.4E+03 | 5.9E+03 |
| Prestwick | GBR 12909 dihydrochloride | 5.7E+03 | 6.1E+03 |
| Prestwick | Hycanthone | 8.5E+03 | 5.6E+03 |
| Prestwick | Ivermectin | 2.0E+03 | 4.9E+03 |
| Prestwick | Mefloquine hydrochloride | 3.3E+03 | 2.6E+03 |
| Prestwick | Methiothepin maleate | 5.0E+03 | 2.8E+03 |
| Prestwick | Oxyphenbutazone | N/A | N/A |
| Prestwick | Parthenolide | 3.6E+03 | 6.2E+03 |
| Prestwick | Perhexiline maleate | 1.2E+03 | 1.3E+03 |
| Prestwick | Perphenazine | 3.8E+03 | 3.3E+03 |
| Prestwick | Piperacetazine | 8.9E+03 | 8.2E+03 |
| Prestwick | Prazosin hydrochloride | 4.8E+03 | 5.1E+03 |
| Prestwick | Sertraline | 3.8E+03 | 3.3E+03 |
| Prestwick | Terfenadine | 1.1E+03 | 1.2E+03 |
| Prestwick | Tetrandrine | 1.6E+03 | 1.8E+03 |
| Prestwick | Tomatine | 2.8E+02 | 4.0E+02 |
| Prestwick | Trifluoperazine dihydrochloride | 5.0E+03 | 4.2E+03 |
| Sigma | ( R)-(+)-WIN 55,212-2 mesylate | N/A | N/A |
| Sigma | Bay 11-7085 | 8.8E+02 | 1.0E+03 |
| Sigma | Calmidazolium chloride | 1.6E+03 | 1.7E+03 |
| Sigma | CGP-74514A hydrochloride | 1.6E+03 | 1.7E+03 |
| Sigma | DL-erythro-Dihydrosphingosine | 5.1E+03 | 7.8E+03 |
| Sigma | GR 127935 hydrochloride | 1.9E+03 | 1.9E+03 |
| Sigma | SB 224289 hydrochloride | 5.0E+03 | 5.0E+03 |
| MicroSource | AMLODIPINE BESYLATE | 1.7E+03 | 1.8E+03 |
| MicroSource | ANTHOTHECOL | 8.1E+02 | 1.1E+03 |

| | | | |
|---|---|---|---|
| MicroSource | ERYSOLIN | N/A | N/A |
| MicroSource | N,N-HEXAMETHYLENEAMILORIDE | N/A | N/A |
| MicroSource | NONOXYNOL-9 | 9.9E+03 | 1.2E+04 |
| MicroSource | PHENYLMERCURIC ACETATE | 1.4E+02 | 1.1E+02 |
| MicroSource | THIMEROSAL | 2.4E+02 | 2.9E+02 |
| MicroSource | THIRAM | N/A | N/A |
| MicroSource | TRIFLUOPERAZINE HYDROCHLORIDE | 3.2E+03 | 3.1E+03 |
| Sigma | Metrazoline oxalate | 4.3E+04 | 4.2E+04 |
| Sigma | Na-p-Tosyl-L-lysine chloromethyl ketone hydrochloride | 4.4E+03 | 7.2E+03 |
| BIOMOL | Cyclopamine | 7.1E+04 | 7.6E+04 |
| MicroSource | 3,4-DIDESMETHYL-5-DESHYDROXY-3'-ETHOXYSCLEROIN | N/A | N/A |
| MicroSource | VIOLASTYRENE | 3.9E+04 | 3.4E+04 |
| Prestwick | Cephalothin sodium salt | N/A | N/A |
| Prestwick | Chlorambucil | N/A | N/A |
| Prestwick | Salmeterol | 1.5E+04 | 1.9E+04 |
| Prestwick | Trioxsalen | N/A | N/A |
| Sigma | Betaine hydrochloride | N/A | N/A |
| OICR | Cyclopamine | N/A | N/A |
| OICR | AM0019-051-001 (p-fluorophenyl-fervenulin | N/A | N/A |
| OICR | OICR00254A | 1.0E+04 | 1.0E+04 |
| OICR | JM0010-058-08 | 2.8E+03 | 3.2E+03 |
| OICR | FK-506 | N/A | N/A |
| OICR | Cerosporine | 5.2E+03 | 4.5E+03 |
| Capretta | p-fluorophenyl-toxoflavin | 6.6E+02 | 3.1E+02 |
| Capretta | Compound X | 1.5E+03 | 7.5E+02 |
| MicroSource | Lasalocid Sodium | 1.6E+03 | 1.8E+03 |
| Prestwick | Clomiphene Citrate (Z,E) | 1.9E+03 | 1.9E+03 |
| Prestwick | Disulfiram | 3.2E+03 | 7.0E+01 |
| Prestwick | Ivermectin | 4.9E+03 | 4.0E+03 |
| Cayman | PI-103 | 9.0E+03 | 9.0E+03 |
| Prestwick | Thioridazine | 2.7E+03 | 2.6E+03 |
| Prestwick | Parthenolide | 3.0E+03 | 2.9E+03 |
| Prestwick | Mefloquine hydrochloride | 3.0E+03 | 5.2E+03 |
| Maybridge | KM 08041 | >2.0E+03 | 2.6E+03 |
| Maybridge | NRB 04094 | 2.0E+03 | 1.6E+03 |
| Maybridge | PD 00433 | 9.9E+03 | 8.9E+03 |
| Maybridge | SPB 06553 | 1.5E+03 | 1.1E+03 |

| | | | |
|---|---|---|---|
| Prestwick | Disulfiram | 2.1E+03 | 2.2E+03 |
| BIOMOL | Gambogic Acid | 3.7E+02 | 4.6E+02 |
| Capretta | p-fluorophenyl-toxoflavin | 4.8E+02 | 6.9E+02 |
| OICR | AM0019-051-001 (p-fluorophenyl-fervenulin | N/A | N/A |
| Schimmer | Bortezomib | <2.0E+01 | <2.0E+01 |
| Schimmer | Fingolimod | N/A | N/A |
| Schimmer | Hydroxychloroquine | N/A | N/A |
| Schimmer | Imatinib | >6.3E+02 | >2.0E+03 |
| Schimmer | Masitinib | 6.8E+03 | 6.6E+03 |
| Schimmer | Rifapentine | N/A | N/A |
| Schimmer | Rifamixin | N/A | N/A |
| Schimmer | Salinomycin | 1.0E+03 | 9.1E+02 |
| Schimmer | Sunitinib | >6.3E+02 | 6.2E+03 |
| Schimmer | Tandutinib | N/A | N/A |
| Schimmer | Vandetanib | >6.3E+03 | >6.3E+03 |
| Schimmer | VX-680/MK-0457 | >6.3E+03 | >6.3E+03 |

Table 2. *Structural analysis of hit compounds identifies classes of structurally related compounds.*

| Category # | Structuralliy Related Compounds |
|---|---|
| 1 | Alpha-Chaconine, Tomatine, Digitonin, Ivermectin, Beta-Escin, |
| 2 | Gentian Violet, Rosolic Acid, Pararosaniline |
| 3 | Tetrandrine, Berberamine, E6 Berberamine, Hernandezine, Cepharanthine, Cephaeline, 7-Oxycanthine, Emetine |
| 4 | Dihydrocelastryl Diacetate, Dihydrocelastrol, Celastrol, Pristimerin, Anthothecol |
| 5 | Sanguinarine, Chelerythrine |
| 6 | Juglone, Plumbagin, Shikonin, Chrysene-1,4-Quinone, Sappanone, JFD 03185, 3,4-Dimethoxydalbergione, 4-Methoxydalbergione, BTB 14417, Aklavine HCl, Pyrromycin, Obtusaquinone, RJC 02988, BTB 14447, JFD 02731, Daunorubicin, Doxorubicin, Idarubicin, Vineomycin |
| 7 | Quinacrine, Primaquine, Amodiaquin, Dequalinium C-14, Mefloquine, Aminacrin, Amsacrine, Acriflavinium HCl, Acrisorcin, Prazosin HCl, XBX 00150 |
| 8 | Chlorhexidine, Alexidine, RJF 00706 |
| 9 | Tegaserod Maleate, 5429924 |
| 10 | Lasalocid Sodium, Monensin, Salinomycin, Narasin, Nigericin |
| 11 | S 07624, S 04055, RB 00158, S 10252, S 03980, S 07429, S 01369 |
| 12 | KM 03341, BTB 02467, KM 05590, KM 06346, Bay 11-7085, KM 03776 |
| 13 | CD 00793, KM 00767, KM 00794, KM 02595, KM 00909, S 05237, JFD 00979, JFD 00972 |
| 14 | SPB 07895, MWP 00602, SPB 01622, SPB 01621, SPB 02669, SPB 01986, RH 01403, KM 05413, HTS 12742, HTS 07592, SPB 07445 |
| 15 | Thiram, Disulfiram, TL 00165 |
| 16 | S 14683, S 14685 |
| 17 | SB 224289, GR 127935, |
| 18 | Cetylpyridinium chloride, Cetrimonium bromide, Benzalkonium chloride, Benzethonium chloride, Methylbenzethonium chloride, Thonzium bromide, DL-erythro-dihydrosphingosine, Dequalinium C-14 |
| 19 | XBX 00315, XBX 00316, S 11897, 5543164 |
| 20 | Antiarol, S 14295 |
| 21 | N,N-Hexamethyleneamiloride, 3’,4’-Dichlorobenzamil |
| 22 | Thimerosal, Phenylmercuric acetate |
| 23 | JFD 00742, JFD 01136, Oxiconazole nitrate, 5352494, SPB 07215 |
| 24 | Thapsigargin, Patulin, Parthenolide, Cantharadin |
| 25 | 5781441, 5279631, 5537491, 5429924, HTS 06488, 5457220, 5169083, 5611138, 5456843, 5603579, 5664149, 5537491, 5272685 |
| 26 | Clomiphene citrate, Tamoxifen citrate |
| 27 | GBR 12909, 5454910 |
| 28 | 5670522, 5672102 |
| 29 | KM 00713, 5661403, S 05384, S 05237, BTB 02101 |
| 30 | 5690102, 5540653 |
| 31 | 5712612, PHG 00966, PHG 00967 |
| 32 | 5670412, 5653447 |
| 33 | JFD 00597, CD 11507, 5282288(keto) |
| 34 | KM 04416, HTS 12959 |
| 35 | KM 06874, KM 06890 |
| 36 | Astemizole, CGP-74514A HCl, 5256229 |
| 37 | (+/-)-Pindobind, Bromoacetyl alprenolol |
| 38 | Chlorpromazine, Chlorprothixene, Flupentixol, Metixene, Perphenazine, Thiothixene, Triflupromazine, Thiethylperazine, Thioridazine, Trifluoperazine, Zuclopenthixol |

Table 3. *Mechanistic information and biological indications related to hit compounds.*

| Compound Name | Mechanistic or Biological Indication |
|---|---|
| | **Alcohol Dehydrogenase** |
| Disulfiram | Alcohol dehydrogenase inhibitor, Proteasome Inhibitor |
| | **Protein Kinase C** |
| Chelerythrine Cl | PKC inhibition |
| Dequalinium analog, C-14 linker | antibacterial, antifungal, PKC inhibition |
| Sanguinarine Sulfate | antineoplastic, antiplaque |
| Sanguinarine | antineoplastic, antiplaque |
| | **Glutathione reductase** |
| Thiram | antifungal, glutathione reductase inhibition, ALDH inhibition? |
| | **Golgi Transport** |
| Brefeldin A | antiviral, protein transport |
| Brefeldin A from Penicillium brefeldianum | antiviral, protein transport |
| | **CDK1** |
| CGP-74514A hydrochloride | cell cycle inhibitor |
| | **Tubulin polymerization/Chaperone** |
| Pristimerin | antineoplastic, antiinflammatory, inhibit tubulin polymerization |
| Dihydrocelastryl Acetate | chaperone stimulant |
| Celastrol | chaperone stimulant, antineoplastic, antiinflammatory, inhibit tubulin polymerization |
| | **Estrogen receptor** |
| Tamoxifen citrate | estrogen receptor inhibition |
| Clomiphene citrate (Z,E) | estrogen receptor inhibition |
| | **HSP90** |
| Geldanamycin | HSP90 inhibition |
| Radicicol | HSP90 inhibition |

| Compound Name | Mechanistic or Biological Indication |
|---|---|
| | **Serotonin** |
| Cephaeline dihydrochloride heptahydrate | emetic, serotonin receptor binding |
| Methiothepin maleate | neurotransmission, serotonin receptor antagonist |
| GR 127935 hydrochloride | neurotransmission, serotonin receptor antagonist |
| SB 224289 hydrochloride | neurotransmission, serotonin receptor antagonist |
| (±)-Pindobind | neurotransmission, serotonin receptor antagonist, adrenoceptor alkylating agent |
| Nortriptyline hydrochloride | neurotransmission, serotonin receptor antagonist, antihistamine, Ach receptor antagonist |
| Sertraline | neurotransmission, SSRI |
| Paroxetine Hydrochloride | neurotransmission, SSRI |
| Tegaserod Maleate | treats IBS, serotonin receptor agonist |
| | **Phenothiazine** |
| Thioridazine hydrochloride | neurotransmission, phenothiazine |
| Perphenazine | neurotransmission, phenothiazine |
| Chlorprothixene hydrochloride | neurotransmission, phenothiazine |
| Zuclopenthixol hydrochloride | neurotransmission, phenothiazine |
| Thiethylperazine malate | neurotransmission, phenothiazine |
| Chlorpromazine | neurotransmission, phenothiazine |
| Chlorpromazine hydrochloride | neurotransmission, phenothiazine |
| Triflupromazine hydrochloride | neurotransmission, phenothiazine |
| Metixene hydrochloride | neurotransmission, phenothiazine |
| Trifluoperazine dihydrochloride | neurotransmission, phenothiazine |
| Thiothixene | neurotransmission, phenothiazine |
| Piperacetazine | neurotransmission, phenothiazine |
| Flupentixol dihydrochloride cis-(Z) | neurotransmission, phenothiazine |

| | |
|---|---|
| | **NFkB** |
| Shikonin | proteasome inhibition |
| Cepharanthine | NFkB inhibition |
| Bay 11-7085 | NFkB inhibition |
| Chaconine, a - | NFkB inhibition, cholinesterase inhibition |
| Parthenolide | NFkB inhibition, oxidative stress |
| Gliotoxin | immunosuppressant, proteasome inhibition |
| | **PP1/PP2A** |
| Cantharidic Acid | phosphatase inhibition |
| Cantharidin | phosphatase inhibition |
| | **PKC/PLC/PLA2/Smase** |
| DL-erythro-Dihydrosphingosine | PKC inhibition, PLC inhibition, PLA2 inhibition |
| Quinacrine dihydrochloride dihydrate | antimalarial, PLA2 inhibition |
| Perhexiline maleate | antianginal, sphingomyelinase inhibition |
| Oxyphenbutazone | antiinflammatory |
| | **Prolyl hydroxylase** |
| Vineomycin A1 | prolyl hydroxylase inhibition |
| | **Glycosylation** |
| Tunicamycin B | protein glycosylation inhibitor, activates unfolded protein response |
| | **Transferrin receptors** |
| Gambogic acid | transferrin receptors, NFkB inhibition |
| Acetyl Isoallogambogic Acid | transferrin receptors, NFkB inhibition |
| Dihydrogambogic Acid | transferrin receptors, NFkB inhibition |
| Acetyl Isogambogic Acid | transferrin receptors, NFkB inhibition |
| Dimethyl Gambogate | transferrin receptors, NFkB inhibition |
| Gambogic Acid Amide | transferrin receptors, NFkB inhibition |
| | **Calcium** |
| Fendiline hydrochloride | antiarrhythmic, antianginal, calcium balance |
| Calmidazolium chloride | calcium balance |
| Amlodipine Besylate | calcium balance |
| Chlorprothixene hydrochloride | neurotransmission, phenothiazine |
| Triflupromazine hydrochloride | neurotransmission, phenothiazine |
| | **Cannabinoid receptor** |
| ( R)-(+)-WIN 55,212-2 mesylate | neurotransmission, cannabinoid receptor agonist |
| | **Dopamine** |
| R(-) Apomorphine hydrochloride hemihydrate | neurotransmission, dopamine receptor agonist |
| GBR 12909 dihydrochloride | neurotransmission, dopamine uptake inhibitor |
| | **Opioid Receptor** |
| (-)-Eseroline fumarate salt | neurotransmission, opioid agonist |
| | **Adrenergic receptor** |
| Prazosin hydrochloride | antiadrenergic |
| Fiduxosin hydrochloride | antiadrenergic |
| Bromoacetyl alprenolol menthane | antiadrenergic |
| | **Angiotensin converting enzyme** |
| Fosinopril Sodium | antihypertensive |
| | **Histamine receptor** |
| Astemizole | antihistamine |
| Terfenadine | antihistamine |
| | **Topoisomerase** |
| Lapachone, b - | RT inhibition, DNA synthesis inhibition, Topo inhibition |
| Dihydrotanshinone | Topo inhibition |
| Hycanthone | antischistosomal agent |
| Amsacrine hydrochloride | antineoplastic (antileukemic), intercalating agent |
| Radicicol | HSP90 inhibition |
| Idarubicin | antineoplastic, intercalating agent, topoisomerase IIa inhibitor |
| Daunorubicin hydrochloride | antineoplastic, intercalating agent, topoisomerase IIa inhibitor |
| Doxorubicin hydrochloride | antineoplastic, intercalating agent, topoisomerase IIa inhibitor |
| | **Oxygen stress** |
| Rubescensin A | oxygen stress, antineoplastic |
| Plumbagin | oxygen stress, antineoplastic, antifertilyaction |

| | |
|---|---|
| Oxyacanthine sulfate | calcium balance |
| Hernandezine | calcium balance |
| Berbamine 2HCl | calcium balance |
| E6 Berbamine | calcium balance |
| Tetrandrine | calcium balance, antifibrogenic |
| Isotetrandrine | calcium balance, antifibrogenic |
| Thapsgargin | calcium balance, induces unfolded protein response |
| | **Cationic Ionophores** |
| Monensin sodium salt | antibacterial, antiprotozoal, ionophore (Na+K+Li+Rb+Tl+Ag+) |
| Monensin Na | antibacterial, antiprotozoal, ionophore (Na+K+Li+Rb+Tl+Ag+) |
| Nigericin Na salt | antibacterial, antiviral, H+/K+ ionophore |
| Narasin | antibacterial, ionophore |
| Salinomycin | antibacterial, ionophore |
| Lasalocid Sodium Salt | ionophore (cationic) |
| Lasalocid sodium salt | antibacterial, ionophore, calcium balance |
| | **Na+/K+ ATPase** |
| Ciclopirox ethanolamine | antifungal, ion balance |
| | **Na+/H+ antiporter** |
| N,N-Hexamethyleneamiloride | H+/Na+ balance, antiviral |
| | **Na+/Ca2+** |
| 3',4'-Dichlorobenzamil | ion balance |
| | **Chloride channel** |
| Ivermectin | antiparasitic, chloride channel |

| | |
|---|---|
| Parthenolide | NFkB inhibition, oxidative stress |
| | **DNA Polymerase** |
| Iodoacetamide | alkylating agent |
| Acriflavinium Hydrochloride | antibacterial, antiviral, intercalating agent |
| Aminacrine | antiinfective, intercalating agent |
| Idarubicin | antineoplastic, intercalating agent, topoisomerase IIa inhibitor |
| Daunorubicin hydrochloride | antineoplastic, intercalating agent, topoisomerase IIa inhibitor |
| Doxorubicin hydrochloride | antineoplastic, intercalating agent, topoisomerase IIa inhibitor |
| Actinomycin D | antineoplastic, intercalating agent, DNA synthesis inhibition, RNA synthesis inhibition |
| Dactinomycin | antineoplastic, intercalating agent, DNA synthesis inhibition, RNA synthesis inhibition |
| Amsacrine hydrochloride | antineoplastic, intercalating agent, immunosuppressant |
| Celastrol | chaperone stimulant, antineoplastic, antiinflammatory, inhibit tubulin polymerization |
| Echinomycin | DNA synthesis inhibition, RNA synthesis inhibition, intercalating agent |
| Chromomycin A3 | DNA synthesis inhibition, RNA synthesis inhibition, intercalating agent |
| Tubercidin | nucleoside analog |
| Anisomycin | protein synthesis inhibition, DNA synthesis inhibition |
| | **Protein Synthesis Inhibition** |
| Anisomycin | protein synthesis inhibition, DNA synthesis inhibition |
| Anisomycin | protein synthesis inhibition, DNA synthesis inhibition |
| Cycloheximide | protein synthesis inhibition |
| Emetine dihydrochloride | protein synthesis inhibition |
| Harringtonine | protein synthesis inhibition |
| Ochratoxin A | protein synthesis inhibition, calcium balance |
| Puromycin dihydrochloride | protein synthesis inhibition |
| | **Glycolysis inhibition** |
| Tubercidin | nucleoside analog, glycolysis inhibition |

Table 4. *Compound X inhibits sphere formation in a panel of human breast cancer cell lines.* The molecular subtypes (Luminal, BasalA, or BasalB), estrogen receptor (ER) status, progesterone receptor (PR) status, and Her2 status, are listed, along with the values of the $IC_{50} \pm SD$.

| Cell Line | Gene Cluster | Estrogen Receptor | Progesterone Receptor | HER2 | IC50 (nM) |
|---|---|---|---|---|---|
| BT474 | Luminal | + | [+] | + | 100 ± 70 |
| HCC202 | Luminal | - | [-] | + | 140 ± 30 |
| MDAMB361 | Luminal | + | [-] | + | 130 ± 50 |
| MDAMB453 | Luminal | - | [-] | | 210 ± 90 |
| MCF7 | Luminal | + | [+] | | 100 ± 10 |
| HCC1569 | Basal A | - | [-] | + | 110 ± 30 |
| HCC1954 | Basal A | - | [-] | + | 160 ± 40 |
| HCC38 | Basal B | - | [-] | | 140 ± 70 |
| MDAMB231 | Basal B | - | [-] | | 190 ± 70 |

Table 5. *Human breast cancer cell lines show differential sensitivity to Compound X*. Fourteen human breast cancer cell lines representing a variety of molecular subtypes and two quasi-normal breast epithelial cell lines (MCF10a, HMLE) were subjected to treatment with Compound X in a 48-hour proliferation assay. Cell lines are arranged with the most sensitive lines at the top of the chart and the most resistant at the bottom (lowest to highest % Residual Activity at 4.4 µM). Information for Relative Fluorescence Units of the DMSO controls, Z' values of the assays, and percent viable cells at the outset of the assay are included.
Definition of Clincial Variables: Lu = luminal, BaA = basal A, BaB = basal B, W = wild type, M = mutant, ER = estrogen receptor, PR = progesterone receptor, P.BR = primary breast tumor, PE = pleural effusion, AC = adenocarcinoma, IDC = intraductal carcinoma, Duc.Ca = ductal carcinoma, MC = medullary carcinoma.

| | Clinical Variables | | | | | | | % Residual Activity | | | | | | | Assay Metrics | | |
|---|---|---|---|---|---|---|---|---|---|---|---|---|---|---|---|---|---|
| Cell line | Gene cluster | ER | PR | HER2 | TP53 | Source | Tumor type | 15 µM | | [Compound X] | | | 3 µM | DMSO | RFU (DMSO ctrl) | Z' | % Viability (t = 0) |
| MDAMB361 | Lu | + | – | + | $-^{WT}$ | P.Br | AC | 3 | 4 | 5 | 6 | 9 | 20 | 100 | 3.44E+08 | 0.74 | 99 |
| BT483 | Lu | + | + | | – | P.Br | IDC, pap | 10 | 8 | 11 | 18 | 11 | 33 | 100 | 4.08E+07 | -0.70 | 55 |
| HS578T | BaB | – | – | | $+^{M}$ | P.Br | IDC | 4 | 4 | 5 | 7 | 15 | 29 | 100 | 2.09E+08 | 0.50 | 99 |
| HCC1500 | BaB | – | – | | – | P.Br | Duc.Ca | 8 | 9 | 11 | 13 | 23 | 47 | 100 | 4.39E+07 | -0.30 | 68 |
| T47D | Lu | + | + | | $++^{M}$ | PE | IDC | 3 | 3 | 3 | 6 | 25 | 70 | 100 | 3.24E+08 | 0.83 | 96 |
| MCF10A | BaB | – | – | | $+/-^{WT}$ | P.Br | F | 4 | 4 | 4 | 8 | 32 | 82 | 100 | 1.35E+08 | 0.67 | 82 |
| HMLE | | | | | | P.Br | Norm. | 4 | 4 | 5 | 16 | 38 | 78 | 100 | 1.12E+08 | 0.47 | 89 |
| MCF7 | Lu | + | + | | $+/-^{WT}$ | PE | IDC | 15 | 20 | 25 | 25 | 41 | 73 | 100 | 3.87E+08 | 0.71 | 96 |
| ZR751 | Lu | + | – | | – | AF | IDC | 4 | 3 | 3 | 12 | 41 | 57 | 100 | 3.56E+08 | 0.77 | 82 |
| MDAMB231 | BaB | – | – | | $++^{M}$ | PE | AC | 3 | 3 | 6 | 23 | 42 | 68 | 100 | 3.19E+08 | 0.71 | 74 |
| MDAMB157 | BaB | – | – | | – | PE | MC | 3 | 3 | 11 | 35 | 51 | 68 | 100 | 4.14E+08 | 0.74 | 90 |
| BT20 | BaA | – | – | | $++^{WT}$ | P.Br | IDC | 15 | 11 | 16 | 33 | 64 | 83 | 100 | 3.80E+08 | 0.78 | 87 |
| MDAMB453 | Lu | – | – | | $-^{WT}$ | PF | AC | 3 | 3 | 10 | 40 | 66 | 86 | 100 | 3.99E+08 | 0.76 | 98 |
| HCC38 | BaB | – | – | | $++^{M}$ | P.Br | Duc.Ca | 8 | 17 | 40 | 57 | 70 | 88 | 100 | 2.87E+08 | 0.76 | 79 |
| BT549 | BaB | – | – | | $++^{M}$ | P.Br | IDC, pap | 4 | 5 | 19 | 49 | 71 | 81 | 100 | 4.00E+08 | 0.74 | 89 |
| HCC1954 | BaA | – | – | + | [+/–] | P.Br | Duc.Ca | 20 | 21 | 34 | 68 | 90 | 92 | 100 | 3.52E+08 | 0.73 | 93 |
| SKBR3 | Lu | – | – | + | + | PE | AC | 5 | 20 | 66 | 85 | 91 | 88 | 100 | 3.90E+08 | 0.76 | 86 |

Cell line information adapted from Neve et al. *Cancer Cell*. 2006

Table 6. *Compound X does not target 82 human kinases*. *In vitro* kinase activity was quantified in the presence of 2 μM Compound X

| Kinase | % | Kinase | % | Kinase | % | Kinase | % |
|---|---|---|---|---|---|---|---|
| Abl(h) | 123 | CSK(h) | 102 | IGF-1R(h) | 125 | PKCμ(h) | 90 |
| Abl(T315I)(h) | 85 | DAPK1(h) | 90 | IKKα(h) | 106 | PKCθ(h) | 111 |
| ALK(h) | 101 | DDR2(h) | 105 | KDR(h) | 110 | PKD2(h) | 118 |
| ARK5(h) | 116 | DYRK2(h) | 99 | LKB1(h) | 115 | Plk1(h) | 108 |
| Aurora-A(h) | 138 | EGFR(h) | 100 | MAPK2(h) | 108 | Plk3(h) | 114 |
| Aurora-B(h) | 119 | EphA2(h) | 106 | MEK1(h) | 109 | Ret(h) | 111 |
| Axl(h) | 107 | EphA7(h) | 106 | MELK(h) | 96 | ROCK-II(h) | 112 |
| Blk(m) | 101 | EphA8(h) | 109 | Met(h) | 118 | Ron(h) | 101 |
| Bmx(h) | 121 | EphB1(h) | 110 | MST3(h) | 114 | Ros(h) | 106 |
| BRK(h) | 103 | EphB4(h) | 116 | NEK2(h) | 103 | Snk(h) | 107 |
| CDK1/cyclinB(h) | 119 | FAK(h) | 113 | NEK3(h) | 101 | TAK1(h) | 105 |
| CDK2/cyclinA(h) | 114 | Fer(h) | 97 | p70S6K(h) | 102 | Tie2(h) | 107 |
| CDK5/p25(h) | 106 | Fes(h) | 112 | PAK4(h) | 104 | TrkA(h) | 100 |
| CDK6/cyclinD3(h) | 97 | FGFR1(h) | 109 | PDGFRα(h) | 100 | Yes(h) | 109 |
| CDK7/cyclinH/MAT1(h) | 98 | FGFR2(h) | 104 | PDK1(h) | 107 | ZAP-70(h) | 105 |
| CDK9/cyclin T1(h) | 106 | FGFR3(h) | 97 | Pim-1(h) | 99 | ZIPK(h) | 101 |
| CHK1(h) | 101 | FGFR4(h) | 96 | PKBα(h) | 91 | | |
| CHK2(h) | 103 | Flt1(h) | 109 | PKCα(h) | 91 | | |
| CK1γ1(h) | 99 | Flt3(h) | 77 | PKCβI(h) | 97 | | |
| CK1γ2(h) | 106 | Flt4(h) | 115 | PKCε(h) | 100 | | |
| CK1γ3(h) | 119 | Hck(h) | 106 | PKCη(h) | 96 | | |
| cKit(h) | 96 | HIPK2(h) | 95 | PKCι(h) | 79 | | |

Table 7. *Relative potency values for Compound X analogues*. Analogues purchased from Chembridge, or synthesized by Nick Todorovic (Fred Capretta's group) were assayed in sphere forming assays using MCF7A cells. The $IC_{50}$ value of each compound was normalized to the $IC_{50}$ value obtained for Compound X in that particular assay.

**IC50 Compound N / IC50 Compound X**

| | Experiment # | | | | | | | | | | | | | | |
|---|---|---|---|---|---|---|---|---|---|---|---|---|---|---|---|
| | 1 | 2 | 3 | 4 | 5 | 6 | 7 | 8 | 9 | 10 | 11 | 12 | 13 | Avg | SD |
| **Compound X – 5234104** 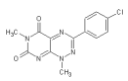 | 1.0 | 1.0 | 1.0 | 1.0 | 1.0 | 1.0 | 1.0 | 1.0 | 1.0 | 1.0 | 1.0 | 1.0 | 1.0 | **1.0** | 0.0 |
| **Toxoflavin**  | | 0.0 | 0.0 | 1.9 | 0.8 | 1.4 | 0.1 | 0.4 | 0.1 | 0.2 | 0.2 | | | **0.5** | 0.7 |
| **5234105** 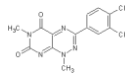 | | | 5.3 | 9.7 | 21 | 35 | 3.9 | 14 | 1.4 | | | | | **13** | 12 |
| **5706059** 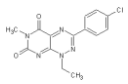 | | 2.1 | 4.6 | 30 | | | | | | | | | | **12** | 16 |
| **5728421** 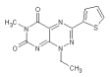 | | | 3.0 | 38 | | | | | | | | | | **20** | 25 |
| **6323599** 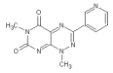 | | | 4.4 | 34 | | | | | | | | | | **19** | 21 |
| **6356172** 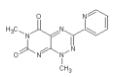 | | | 11 | 37 | | | | | | | | | | **24** | 18 |
| **9019325** 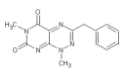 | | | 0.9 | 13 | 1.5 | 1.6 | | | | | | | | **4.2** | 5.8 |
| **9019754** 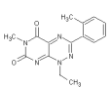 | | 1.2 | 2.1 | 25 | | | | | | | | | | **9.4** | 13 |

| | | | | | | | | | | | | | | | |
|---|---|---|---|---|---|---|---|---|---|---|---|---|---|---|---|
| **9020456** 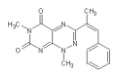 | | 0.0 | 2.4 | 8.7 | | | | | | | | | | **3.7** | 4.5 |
| **9021269** 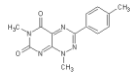 | | 0.0 | 2.6 | 16 | | | | | | | | | | **6.1** | 8.3 |
| **9023239** 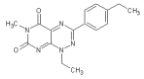 | | 0.3 | 0.9 | 13 | 1.1 | 1.6 | | | | | | | | **3.4** | 5.5 |
| **9023745** 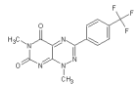 | | | 3.4 | 5.7 | | | | | | | | | | **4.5** | 1.6 |
| **9024894** 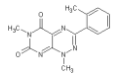 | | | 1.3 | 14 | | | | | | | | | | **7.8** | 9.2 |
| **9028945** 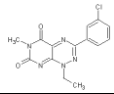 | | | 50 | 670 | | | | | | | | | | **360** | 440 |
| **3-parabromophenyl-toxoflavin** 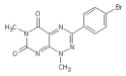 | | | | | 1.7 | 1.8 | | | | | | | | **1.7** | 0.0 |
| **3-parafluorophenyl-toxoflavin** 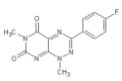 | | | | | 0.8 | 0.8 | 1.7 | 0.2 | 0.1 | | | | | **0.7** | 0.7 |
| **6-butyl-3-parachlorophenyl-toxoflavin** 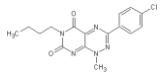 | | | | | 4.9 | 12 | | | | | | | | **8.4** | 5.0 |
| **3-parabutylphenyl-toxoflavin** 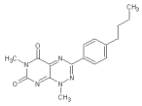 | | | | | | | | | | | | 2.5 | | **2.5** | N/A |
| **3-paracyanophenyl-toxoflavin** 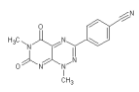 | | | | | | | | | | | | 0.9 | | **0.9** | N/A |

| | | | | | | | | | | | | | | |
|---|---|---|---|---|---|---|---|---|---|---|---|---|---|---|
| **3-paramethylphenyl-toxoflavin** 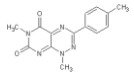 | | | | | | | | | | | 1.1 | | **1.1** | N/A |
| **3-paramethoxyphenyl-toxoflavin** 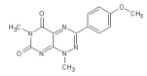 | | | | | | | | | | | 1.0 | | **1.0** | N/A |
| **3-orthochlorophenyl-toxoflavin** 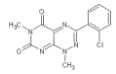 | | | | | | | | | | | 1.9 | | **1.9** | N/A |
| **3-metachlorophenyl-toxoflavin** 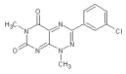 | | | | | | | | | | | 0.8 | | **0.8** | N/A |
| **3-o,p-dichlorophenyl-toxoflavin** 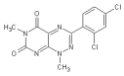 | | | | | | | | | | | 3.0 | | **3.0** | N/A |
| **1-demethyl-Compound X** 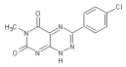 | | | | | | | | | | | | 23 | **23** | N/A |
| **3-p-acylphenyl-toxoflavin** 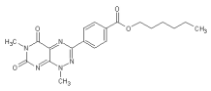 | | | | | | | | | | | | 0.7 | **0.7** | N/A |
| **dag-Tuso3** 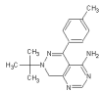 | | | | | | | | | | | | 40 | **40** | N/A |
| **dag-Tuso4** 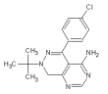 | | | | | | | | | | | | 40 | **40** | N/A |

Table 8. *Genes involved in consumption of ROS are downregulated in TMS*. Collectively, genes that consume oxygen radicals, hydrogen peroxide, and other reactive oxygen species are downregulated in TMS as compared to MMS. Gene set enrichment analysis determined that this gene set is significantly overexpressed in MMS (p = 0.002).

| Gene Name | Symbol | Expn (TMS/ MMS) |
|---|---|---|
| catalase | Cat | 0.85 |
| catalase | Cat | 0.69 |
| glutathione peroxidase 1 | Gpx1 | 0.85 |
| glutathione peroxidase 3 | Gpx3 | 0.97 |
| glutathione peroxidase 4 | Gpx4 | 1.0 |
| glutathione peroxidase 4 | Gpx4 | 1.2 |
| glutathione peroxidase 7 | Gpx7 | 0.61 |
| nucleoredoxin | Nxn | 0.88 |
| nucleoredoxin | Nxn | 0.85 |
| peroxiredoxin 1 | Prdx1 | 0.88 |
| peroxiredoxin 1 | Prdx1 | 0.87 |
| peroxiredoxin 1 | Prdx1 | 0.83 |
| peroxiredoxin 1 | Prdx1 | 0.57 |
| peroxiredoxin 2 | Prdx2 | 0.79 |
| peroxiredoxin 3 | Prdx3 | 0.82 |
| peroxiredoxin 4 | Prdx4 | 0.66 |
| peroxiredoxin 4 | Prdx4 | 0.40 |
| peroxiredoxin 5 | Prdx5 | 0.74 |
| peroxiredoxin 6 | Prdx6 | 1.2 |
| superoxide dismutase 1, soluble | Sod1 | 1.4 |
| superoxide dismutase 1, soluble | Sod1 | 1.2 |
| superoxide dismutase 2, mitochondrial | Sod2 | 1.3 |
| superoxide dismutase 2, mitochondrial | Sod2 | 1.3 |
| superoxide dismutase 2, mitochondrial | Sod2 | 0.97 |
| superoxide dismutase 3, extracellular | Sod3 | 0.94 |
| superoxide dismutase 3, extracellular | Sod3 | 0.91 |


| Gene Name | Symbol | Expn (TMS/ MMS) |
|---|---|---|
| thioredoxin 1 | Txn1 | 0.76 |
| thioredoxin 2 | Txn2 | 0.96 |
| thioredoxin 2 | Txn2 | 0.87 |
| thioredoxin 2 | Txn2 | 0.87 |
| thioredoxin domain containing 1 | Txndc1 | 0.77 |
| thioredoxin domain containing 1 | Txndc1 | 0.67 |
| thioredoxin domain containing 12 (endoplasmic reticulum) | Txndc12 | 0.76 |
| thioredoxin domain containing 14 | Txndc14 | 0.69 |
| thioredoxin domain containing 14 | Txndc14 | 1.0 |
| thioredoxin domain containing 4 (endoplasmic reticulum) | Txndc4 | 0.80 |
| thioredoxin domain containing 4 (endoplasmic reticulum) | Txndc4 | 0.79 |
| thioredoxin domain containing 5 | Txndc5 | 0.65 |
| thioredoxin domain containing 5 | Txndc5 | 0.61 |
| thioredoxin domain containing 9 | Txndc9 | 0.93 |
| thioredoxin domain containing 9 | Txndc9 | 0.79 |
| Thioredoxin peroxidase 2 | LOC545161 | 0.64 |
| thioredoxin-like 1 | Txnl1 | 0.94 |
| thioredoxin-like 1 | Txnl1 | 0.89 |
| thioredoxin-like 1 | Txnl1 | 0.81 |
| thioredoxin-like 1 | Txnl1 | 0.79 |
| thioredoxin-like 1 | Txnl1 | 0.77 |
| thioredoxin-like 2 | Txnl2 | 0.75 |
| thioredoxin-like 2 | Txnl2 | 0.58 |
| thioredoxin-like 4 | Txnl4 | 1.0 |
| thioredoxin-like 5 | Txnl5 | 0.69 |
| thioredoxin-like 5 | Txnl5 | 0.67 |
| thioredoxin-like 5 | Txnl5 | 0.56 |

## 10. APPENDIX

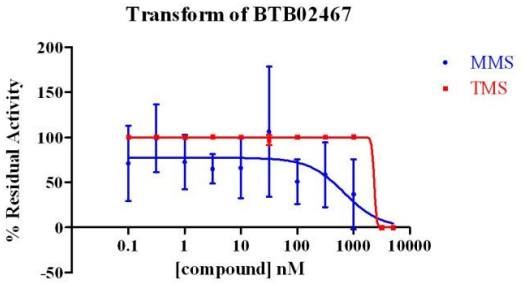
Transform of BTB02467
% Residual Activity
[compound] nM
MMS
TMS

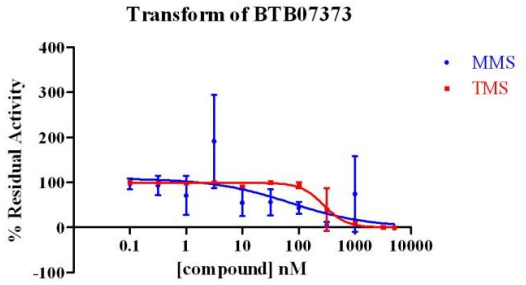
Transform of BTB07373
% Residual Activity
[compound] nM
MMS
TMS

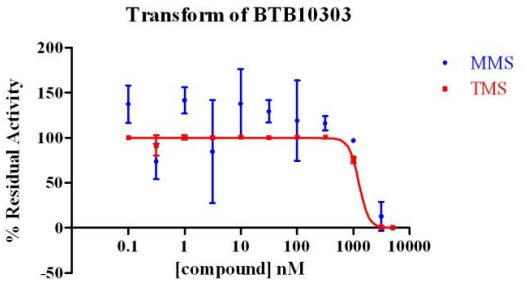
Transform of BTB10303
% Residual Activity
[compound] nM
MMS
TMS

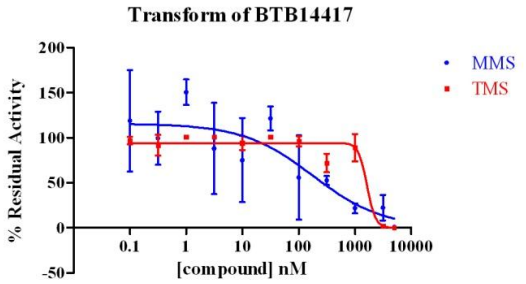
Transform of BTB14417
% Residual Activity
[compound] nM
MMS
TMS

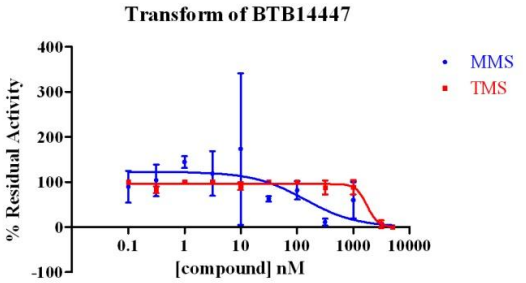
Transform of BTB14447
% Residual Activity
[compound] nM
MMS
TMS

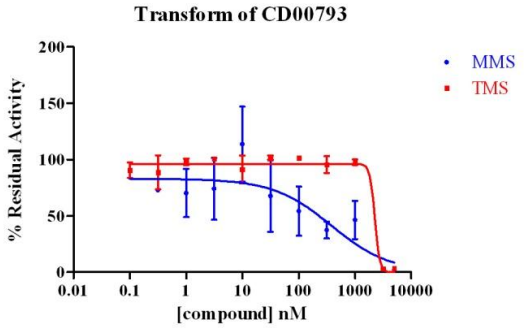
Transform of CD00793
% Residual Activity
[compound] nM
MMS
TMS

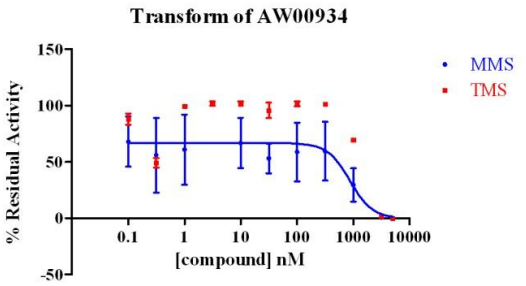
Transform of AW00934
% Residual Activity
[compound] nM
MMS
TMS

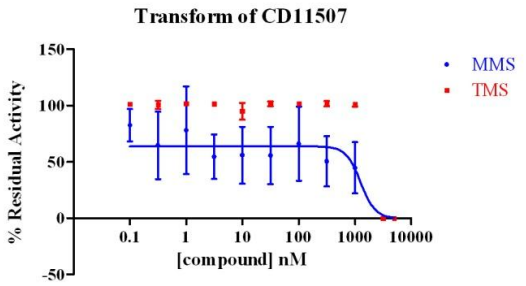
Transform of CD11507
% Residual Activity
[compound] nM
MMS
TMS

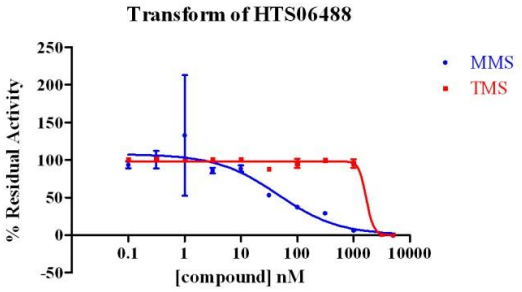
Transform of HTS06488
% Residual Activity
[compound] nM
MMS
TMS

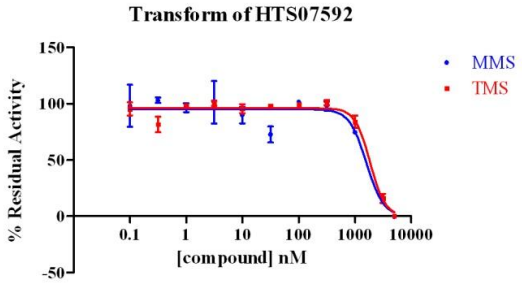
Transform of HTS07592
% Residual Activity
[compound] nM
MMS
TMS

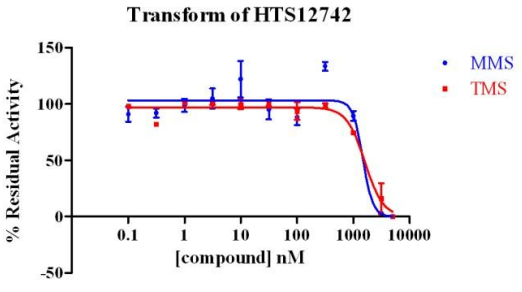
Transform of HTS12742
% Residual Activity
[compound] nM
MMS
TMS

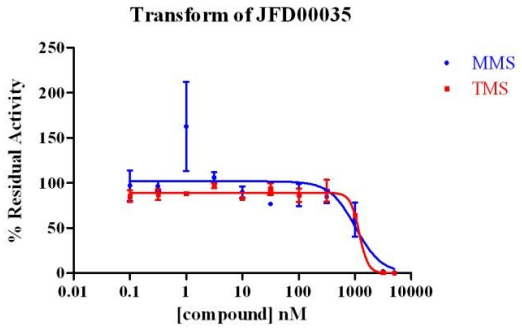
Transform of JFD00035
% Residual Activity
[compound] nM
MMS
TMS

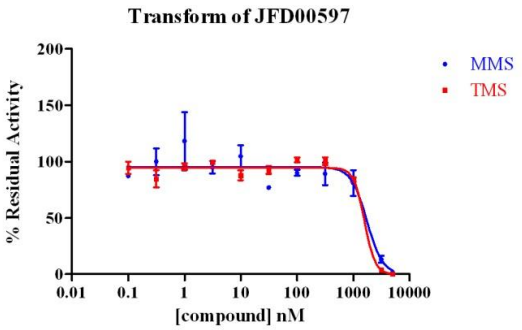
Transform of JFD00597
% Residual Activity
[compound] nM
MMS
TMS

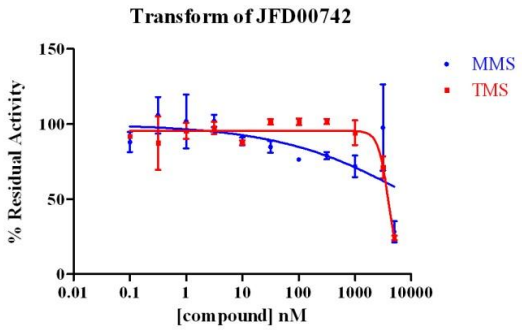
Transform of JFD00742
% Residual Activity
[compound] nM
MMS
TMS

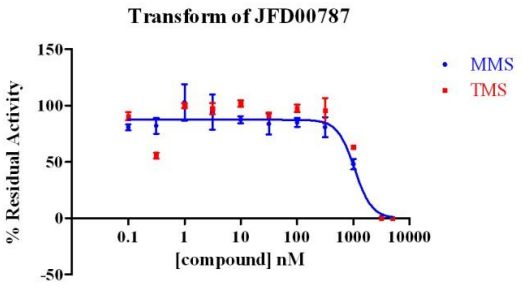
Transform of JFD00787
% Residual Activity
[compound] nM
MMS
TMS

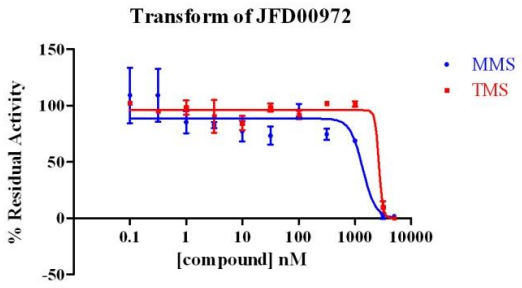
Transform of JFD00972
% Residual Activity
[compound] nM
MMS
TMS

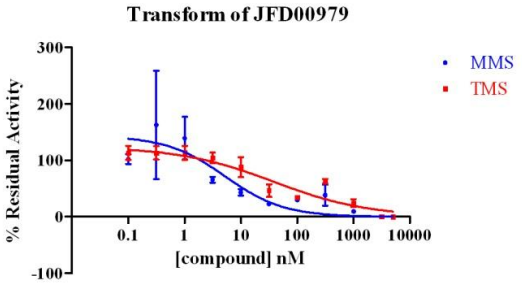
Transform of JFD00979
% Residual Activity
[compound] nM
MMS
TMS

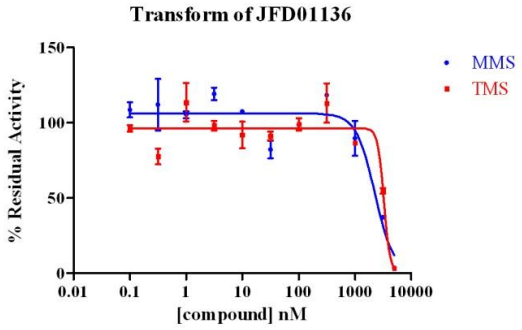
Transform of JFD01136
% Residual Activity
[compound] nM
MMS
TMS

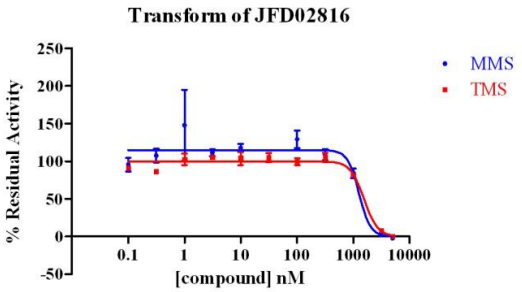
Transform of JFD02816
% Residual Activity
[compound] nM
MMS
TMS

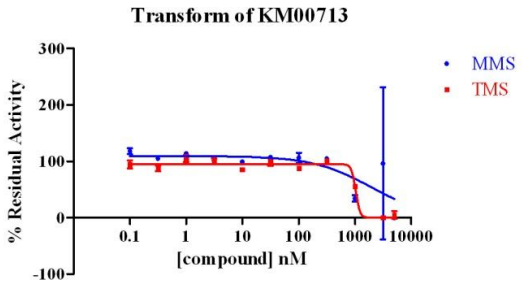
Transform of KM00713
% Residual Activity
[compound] nM
MMS
TMS

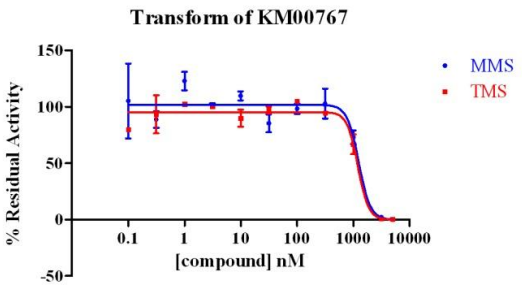
Transform of KM00767
% Residual Activity
[compound] nM
MMS
TMS

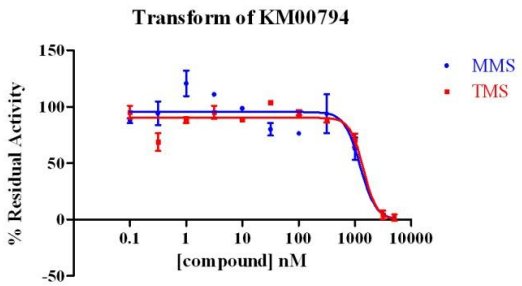
Transform of KM00794
% Residual Activity
[compound] nM
MMS
TMS

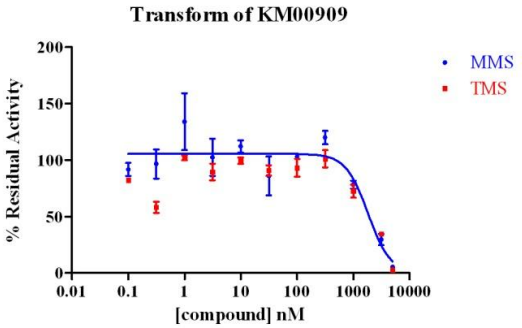
Transform of KM00909
% Residual Activity
[compound] nM
MMS
TMS

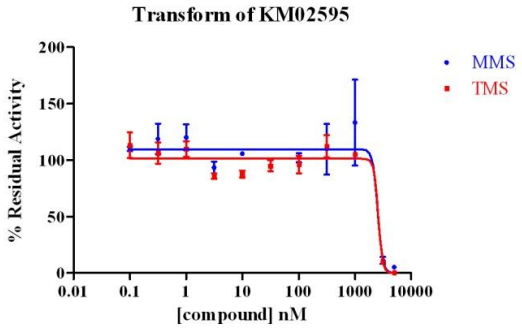
Transform of KM02595
% Residual Activity
[compound] nM
MMS
TMS

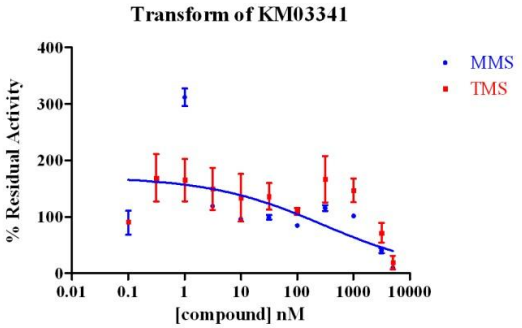
Transform of KM03341
% Residual Activity
[compound] nM
MMS
TMS

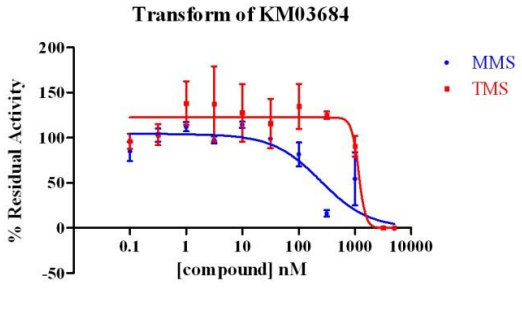
Transform of KM03684
% Residual Activity
[compound] nM
MMS
TMS

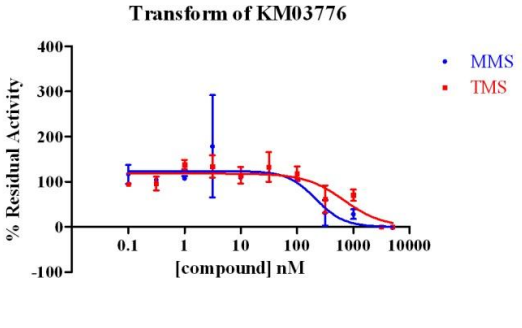
Transform of KM03776
% Residual Activity
[compound] nM
MMS
TMS

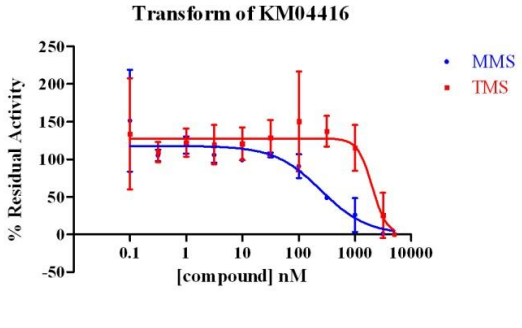
Transform of KM04416
% Residual Activity
[compound] nM
MMS
TMS

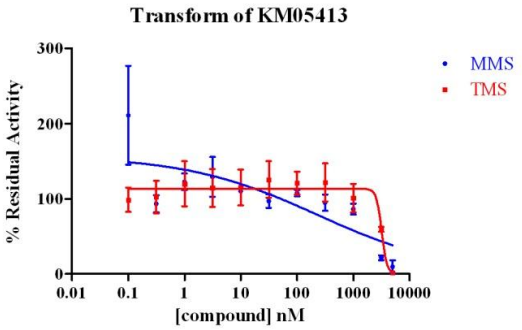
Transform of KM05413
% Residual Activity
[compound] nM
MMS
TMS

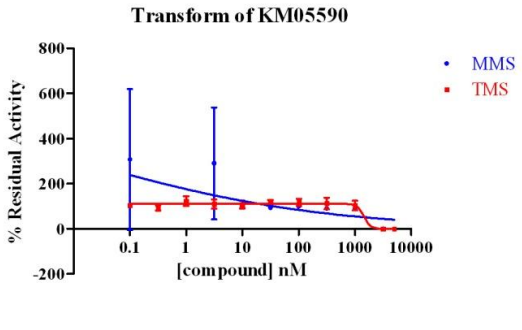
Transform of KM05590
% Residual Activity
[compound] nM
MMS
TMS

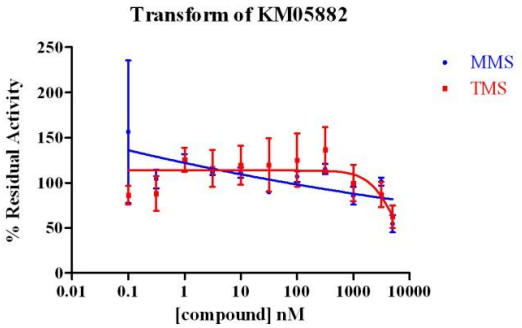
Transform of KM05882
% Residual Activity
[compound] nM
MMS
TMS

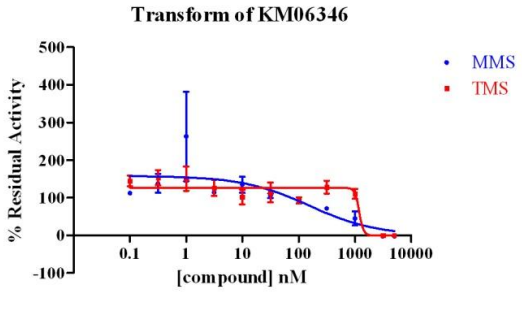
Transform of KM06346
% Residual Activity
[compound] nM
MMS
TMS

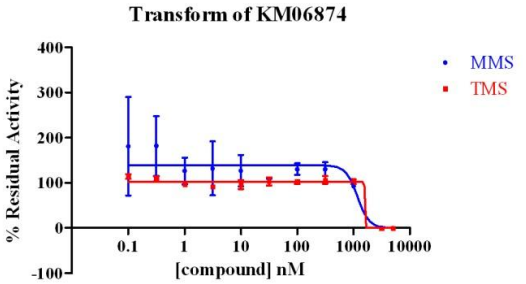
Transform of KM06874
% Residual Activity
[compound] nM
MMS
TMS

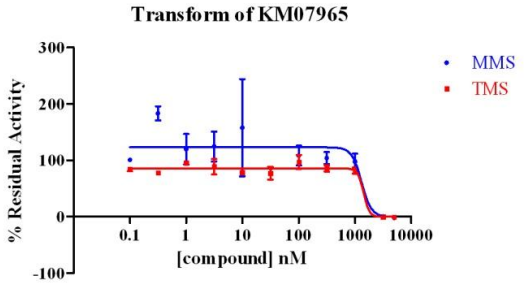
Transform of KM07965
% Residual Activity
[compound] nM
MMS
TMS

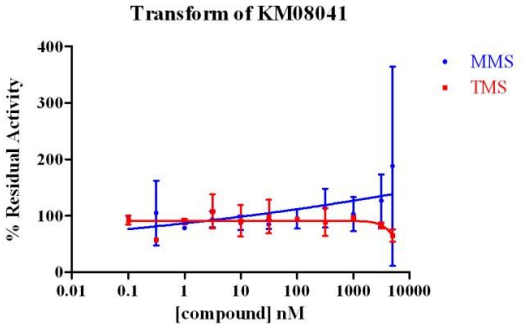
Transform of KM08041
% Residual Activity
[compound] nM
MMS
TMS

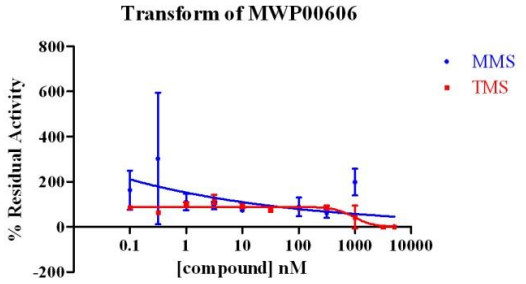
Transform of MWP00606
% Residual Activity
[compound] nM
MMS
TMS

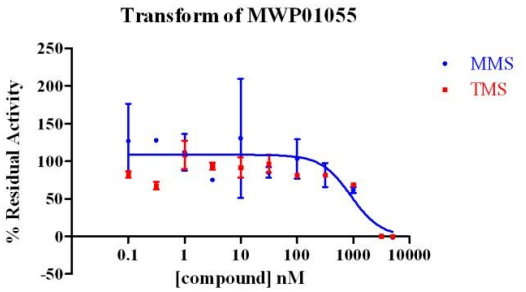
Transform of MWP01055
% Residual Activity
[compound] nM
MMS
TMS

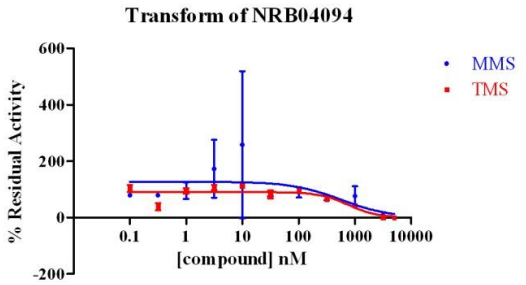
Transform of NRB04094
% Residual Activity
[compound] nM
MMS
TMS

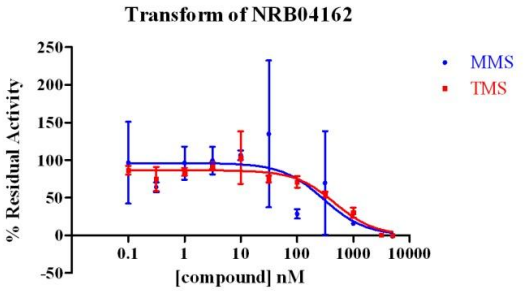
Transform of NRB04162
% Residual Activity
[compound] nM
MMS
TMS

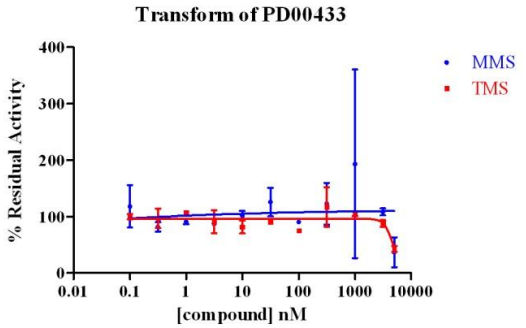
Transform of PD00433
% Residual Activity
[compound] nM
MMS
TMS

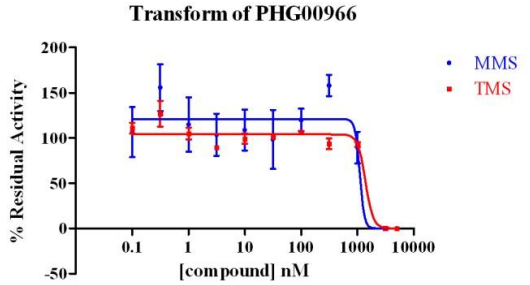
Transform of PHG00966
% Residual Activity
[compound] nM
MMS
TMS

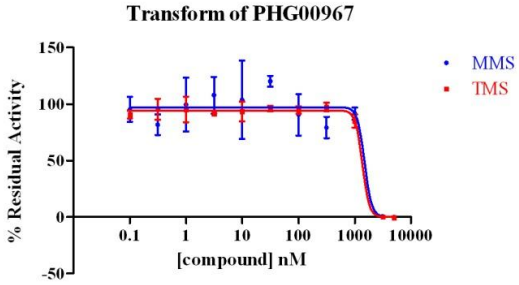
Transform of PHG00967
% Residual Activity
[compound] nM
MMS
TMS

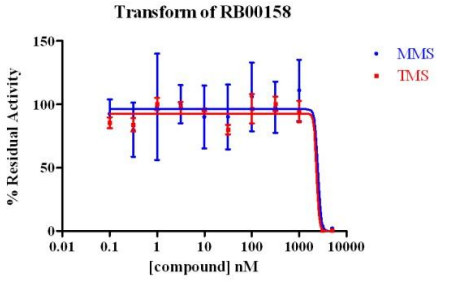
Transform of RB00158
% Residual Activity
[compound] nM
MMS
TMS

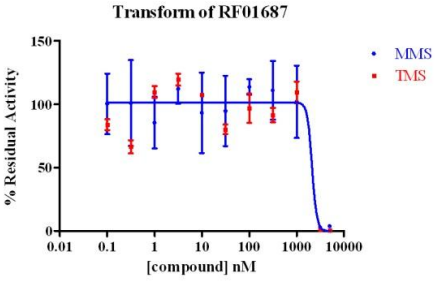
Transform of RF01687
% Residual Activity
[compound] nM
MMS
TMS

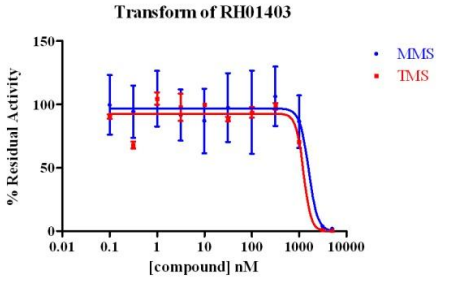
Transform of RH01403
% Residual Activity
[compound] nM
MMS
TMS

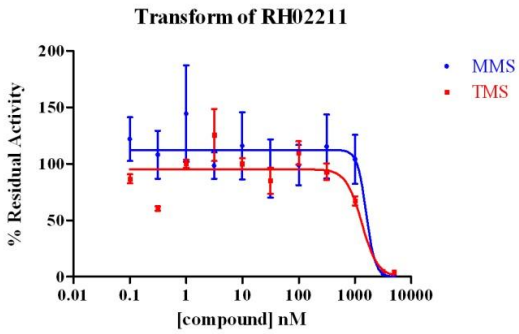
Transform of RH02211
% Residual Activity
[compound] nM
MMS
TMS

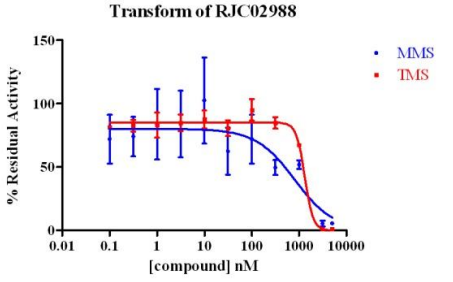
Transform of RJC02988
% Residual Activity
[compound] nM
MMS
TMS

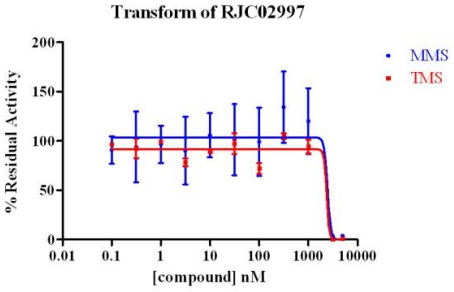
Transform of RJC02997
% Residual Activity
[compound] nM
MMS
TMS

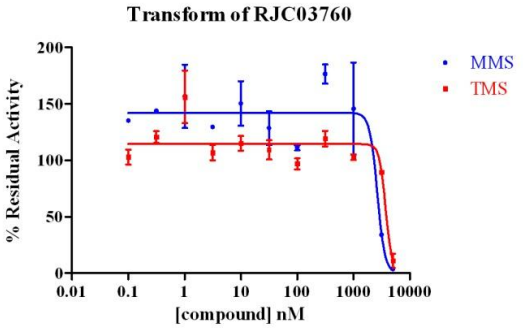
Transform of RJC03760
% Residual Activity
[compound] nM
MMS
TMS

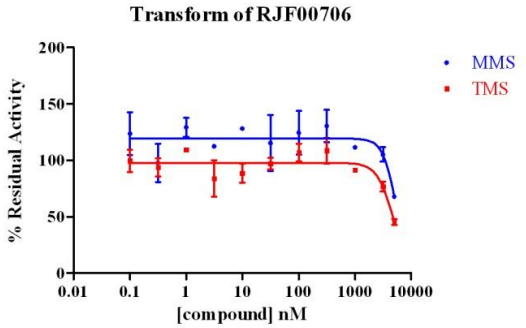
Transform of RJF00706
% Residual Activity
[compound] nM
MMS
TMS

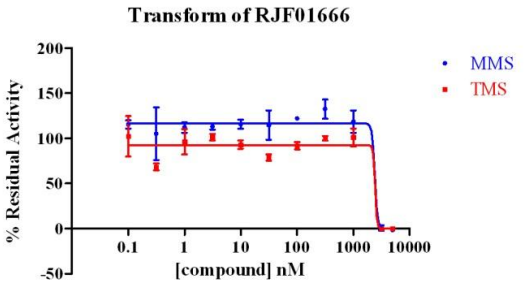
Transform of RJF01666
% Residual Activity
[compound] nM
MMS
TMS

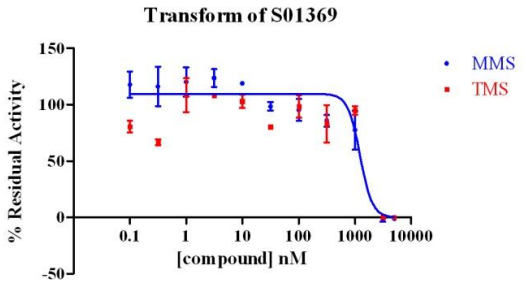
Transform of S01369
% Residual Activity
[compound] nM
MMS
TMS

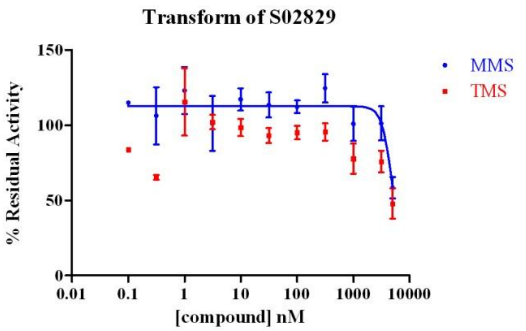
Transform of S02829
% Residual Activity
[compound] nM
MMS
TMS

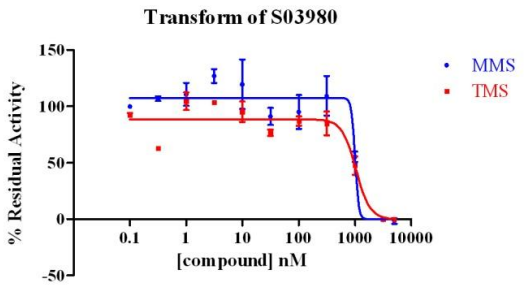
Transform of S03980
% Residual Activity
[compound] nM
MMS
TMS

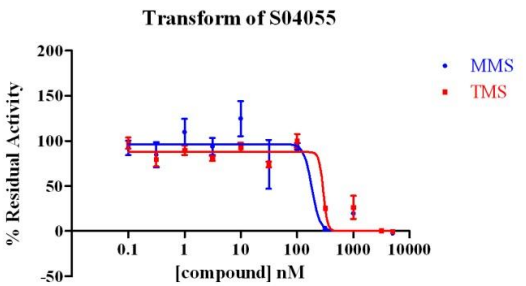
Transform of S04055
% Residual Activity
[compound] nM
MMS
TMS

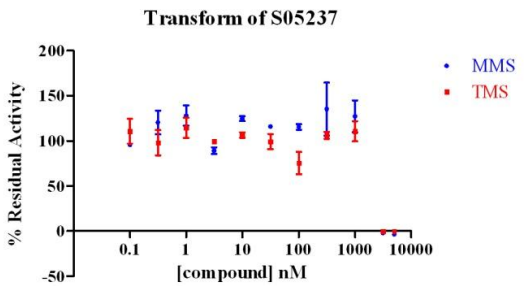
Transform of S05237
% Residual Activity
[compound] nM
MMS
TMS

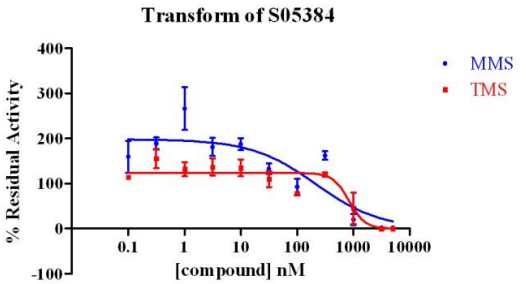
Transform of S05384
% Residual Activity
[compound] nM
MMS
TMS

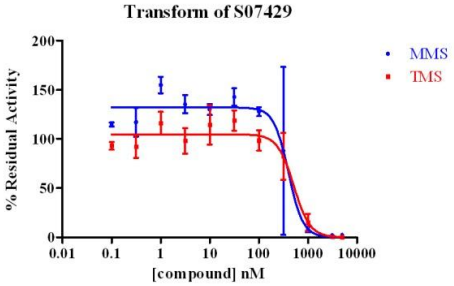
Transform of S07429
% Residual Activity
[compound] nM
MMS
TMS

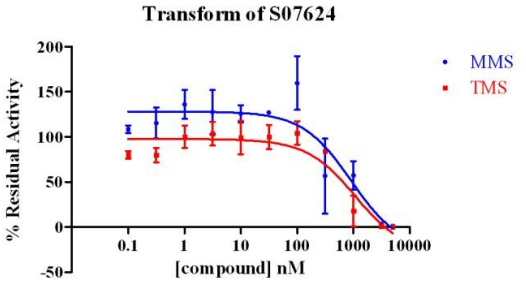
Transform of S07624
% Residual Activity
[compound] nM
MMS
TMS

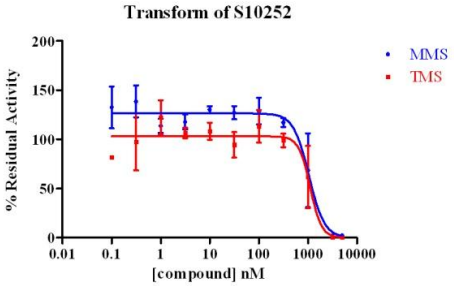
Transform of S10252
% Residual Activity
[compound] nM
MMS
TMS

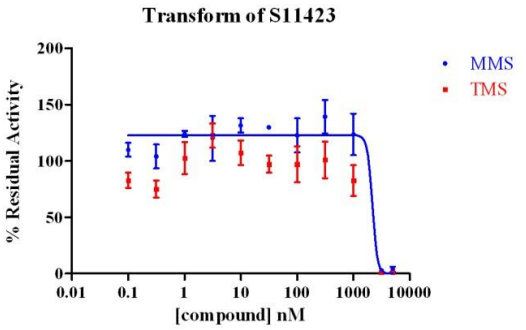
Transform of S11423
% Residual Activity
[compound] nM
MMS
TMS

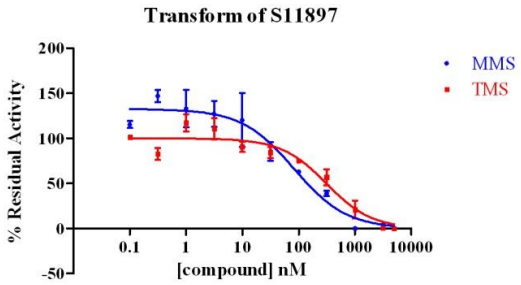
Transform of S11897
% Residual Activity
[compound] nM
MMS
TMS

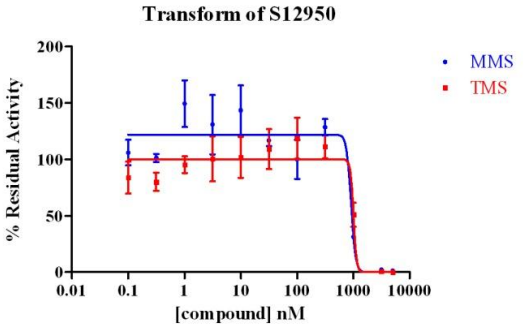
Transform of S12950
% Residual Activity
[compound] nM
MMS
TMS

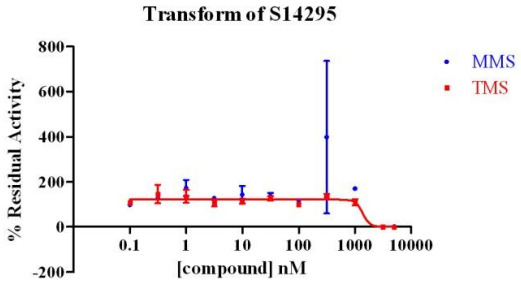
Transform of S14295
% Residual Activity
[compound] nM
MMS
TMS

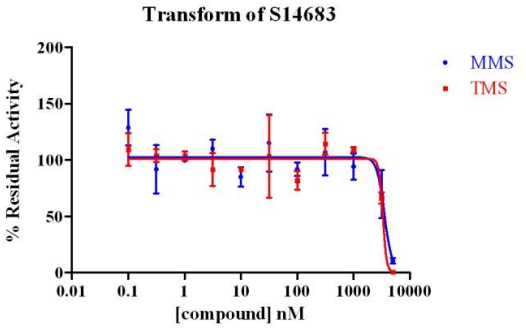
Transform of S14683
% Residual Activity
[compound] nM
MMS
TMS

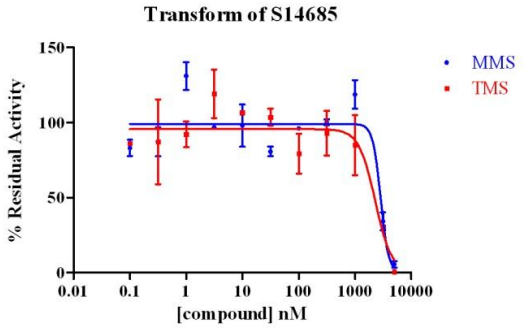
Transform of S14685
% Residual Activity
[compound] nM
MMS
TMS

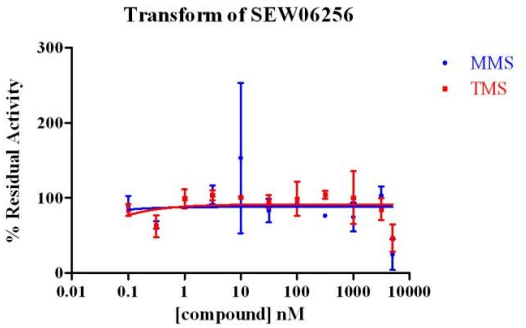
Transform of SEW06256
% Residual Activity
[compound] nM
MMS
TMS

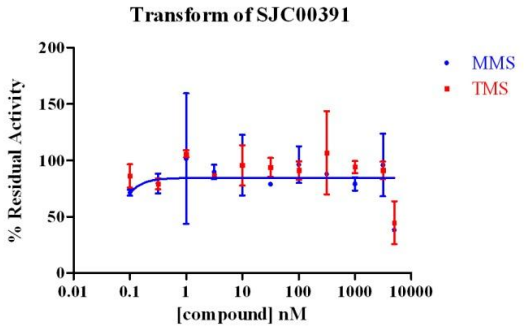
Transform of SJC00391
% Residual Activity
[compound] nM
MMS
TMS

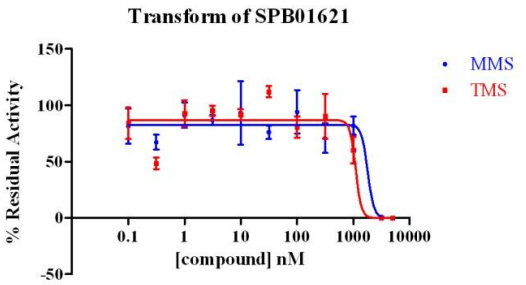
Transform of SPB01621
% Residual Activity
[compound] nM
MMS
TMS

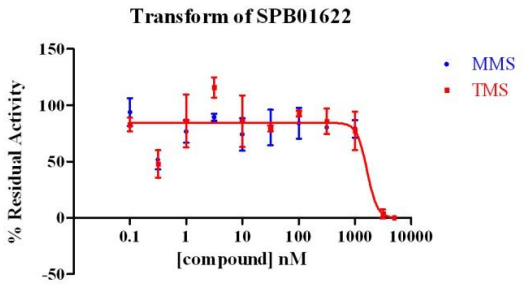
Transform of SPB01622
% Residual Activity
[compound] nM
MMS
TMS

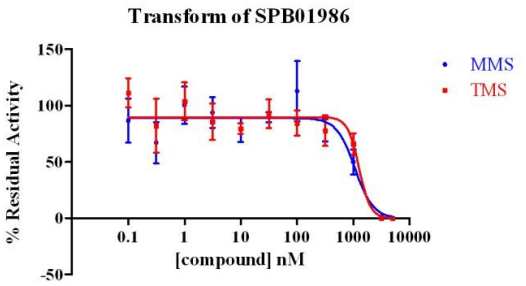
Transform of SPB01986
% Residual Activity
[compound] nM
MMS
TMS

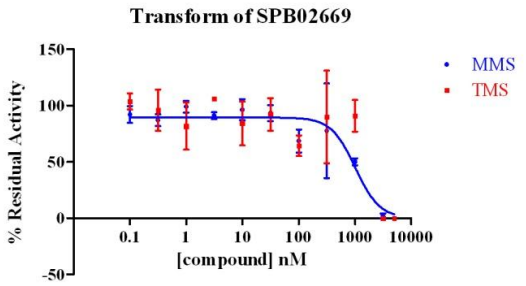
Transform of SPB02669
% Residual Activity
[compound] nM
MMS
TMS

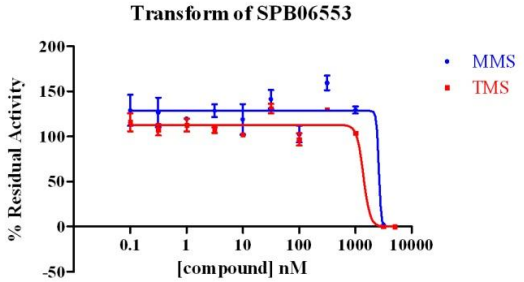
Transform of SPB06553
% Residual Activity
[compound] nM
MMS
TMS

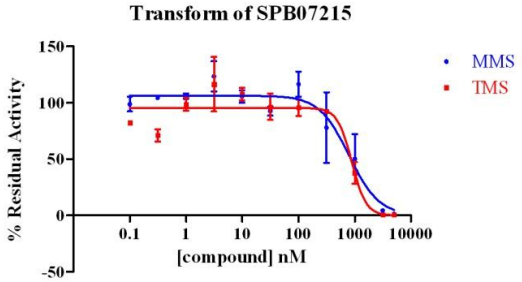
Transform of SPB07215
% Residual Activity
[compound] nM
MMS
TMS

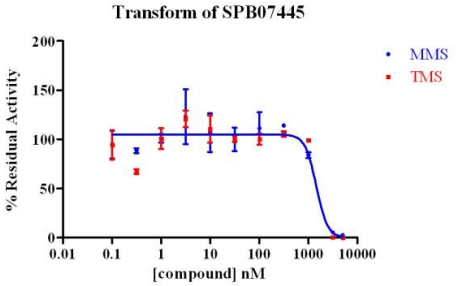
Transform of SPB07445
% Residual Activity
[compound] nM
MMS
TMS

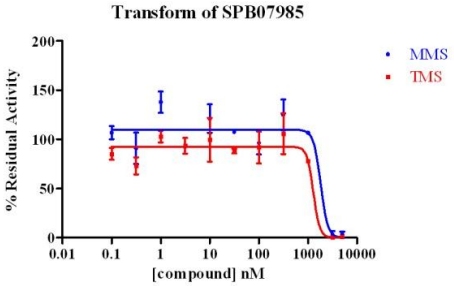
Transform of SPB07985
% Residual Activity
[compound] nM
MMS
TMS

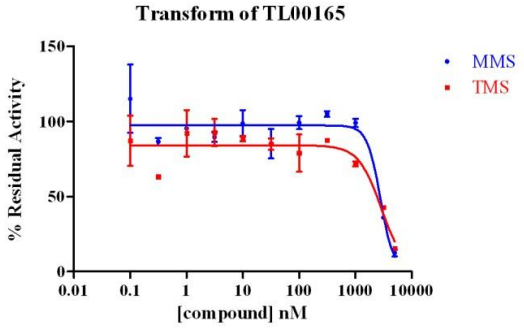
Transform of TL00165
% Residual Activity
[compound] nM
MMS
TMS

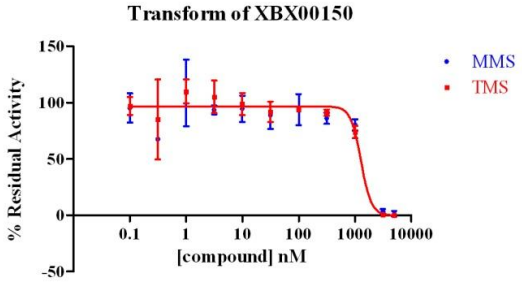
Transform of XBX00150
% Residual Activity
[compound] nM
MMS
TMS

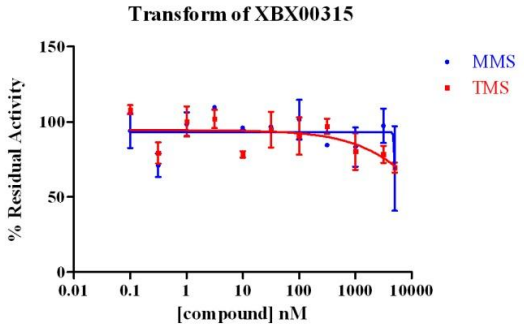
Transform of XBX00315
% Residual Activity
[compound] nM
MMS
TMS

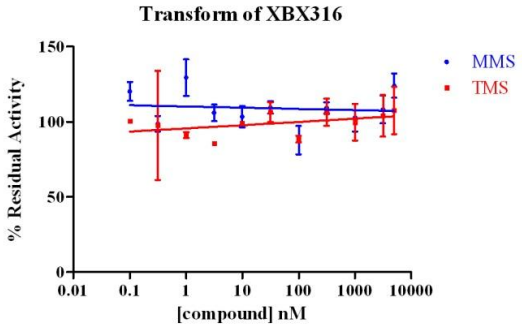
Transform of XBX316
% Residual Activity
[compound] nM
MMS
TMS

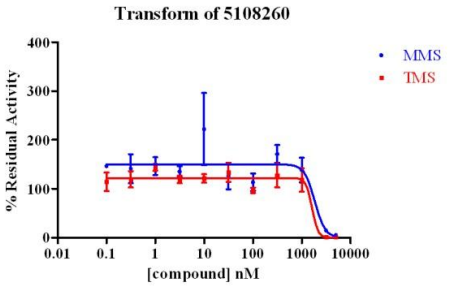
Transform of 5108260
MMS
TMS
% Residual Activity
[compound] nM

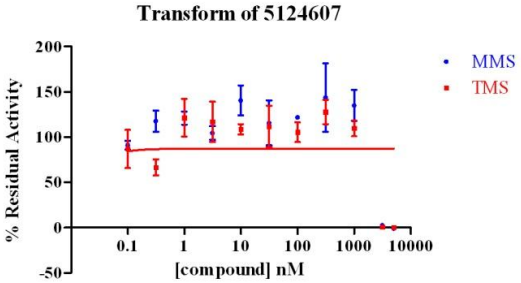
Transform of 5124607
MMS
TMS
% Residual Activity
[compound] nM

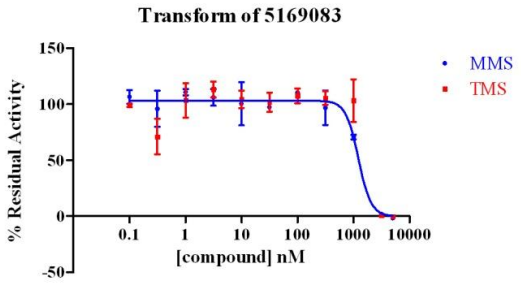
Transform of 5169083
MMS
TMS
% Residual Activity
[compound] nM

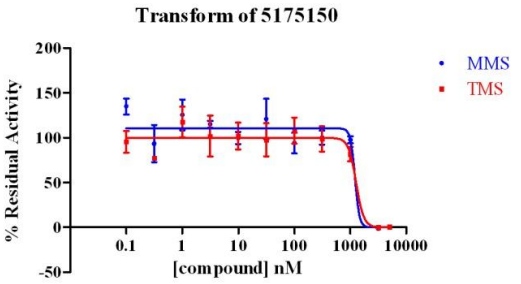
Transform of 5175150
MMS
TMS
% Residual Activity
[compound] nM

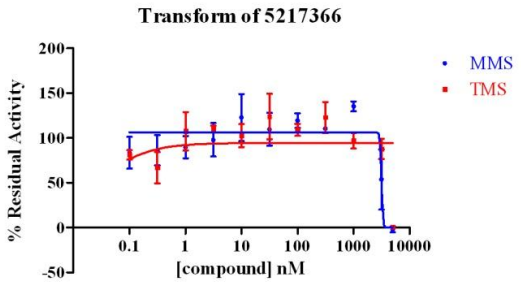
Transform of 5217366
MMS
TMS
% Residual Activity
[compound] nM

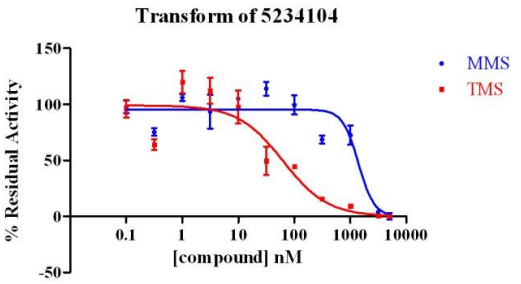
Transform of 5234104
MMS
TMS
% Residual Activity
[compound] nM

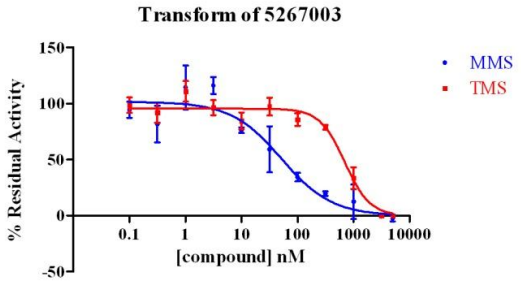
Transform of 5267003
MMS
TMS
% Residual Activity
[compound] nM

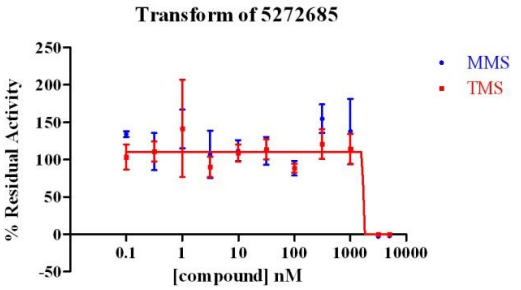
Transform of 5272685
MMS
TMS
% Residual Activity
[compound] nM

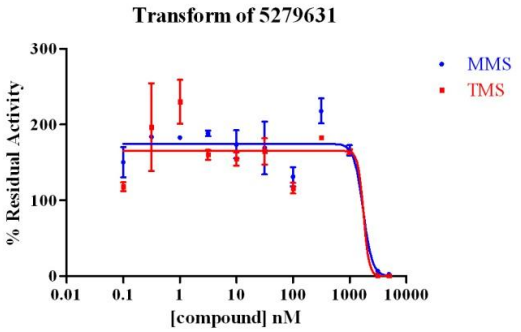
Transform of 5279631
% Residual Activity
[compound] nM
MMS
TMS

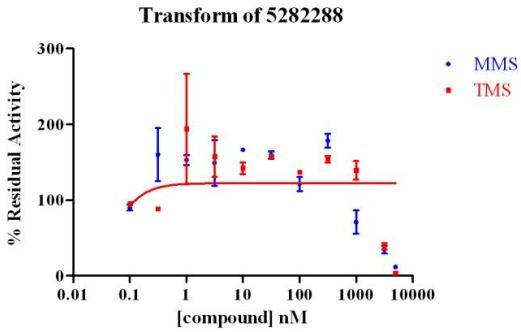
Transform of 5282288
% Residual Activity
[compound] nM
MMS
TMS

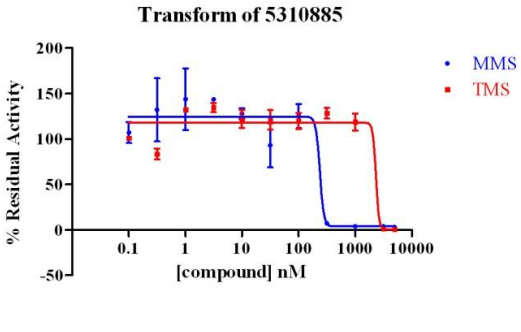
Transform of 5310885
% Residual Activity
[compound] nM
MMS
TMS

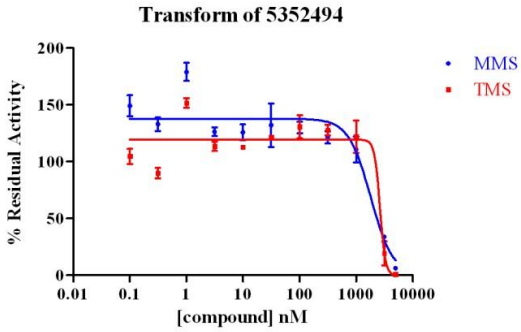
Transform of 5352494
% Residual Activity
[compound] nM
MMS
TMS

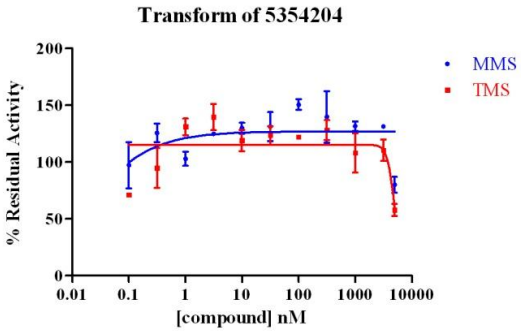
Transform of 5354204
% Residual Activity
[compound] nM
MMS
TMS

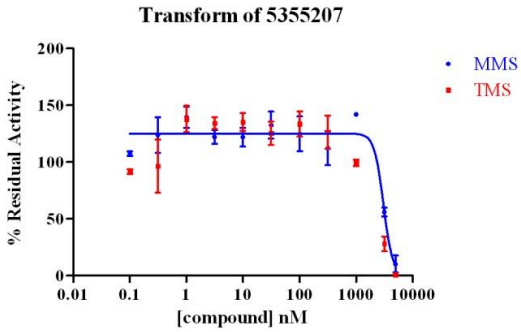
Transform of 5355207
% Residual Activity
[compound] nM
MMS
TMS

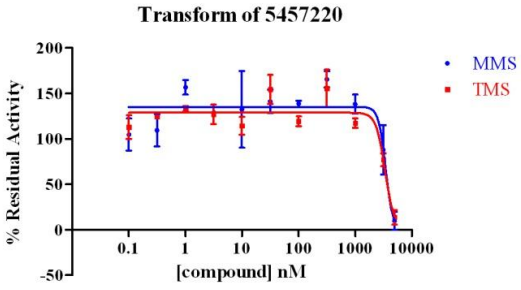
Transform of 5457220
% Residual Activity
[compound] nM
MMS
TMS

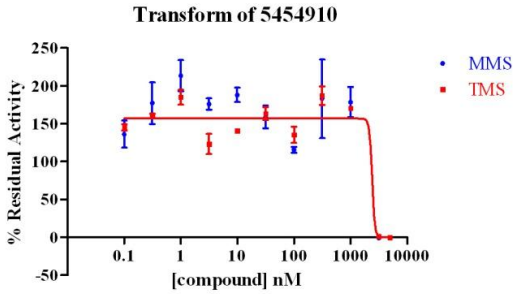
Transform of 5454910
% Residual Activity
[compound] nM
MMS
TMS

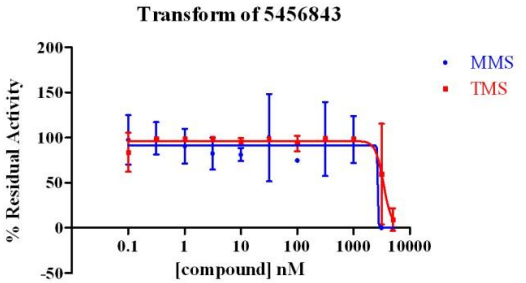
Transform of 5456843
% Residual Activity
[compound] nM
MMS
TMS

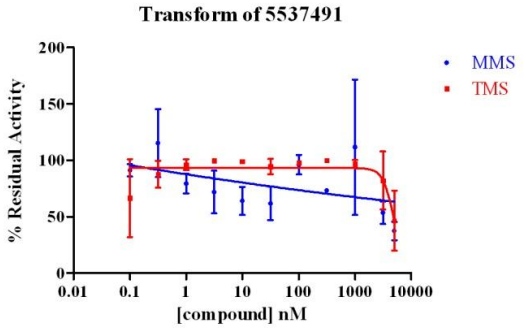
Transform of 5537491
% Residual Activity
[compound] nM
MMS
TMS

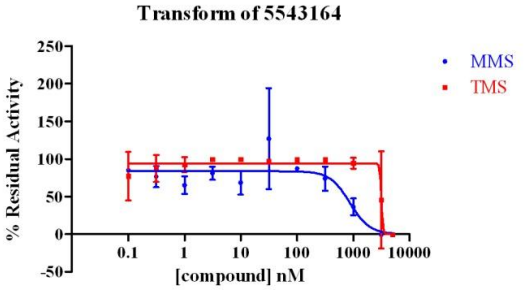
Transform of 5543164
% Residual Activity
[compound] nM
MMS
TMS

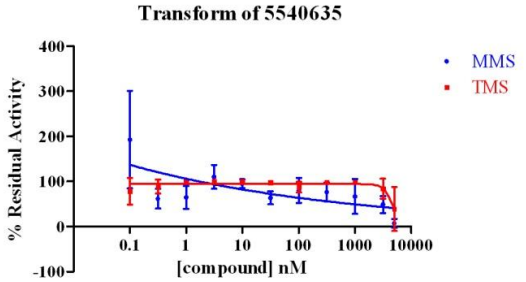
Transform of 5540635
% Residual Activity
[compound] nM
MMS
TMS

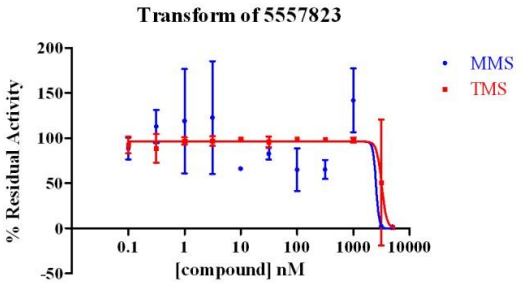
Transform of 5557823
% Residual Activity
[compound] nM
MMS
TMS

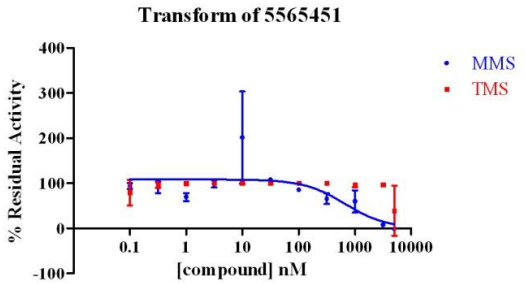
Transform of 5565451
% Residual Activity
[compound] nM
MMS
TMS

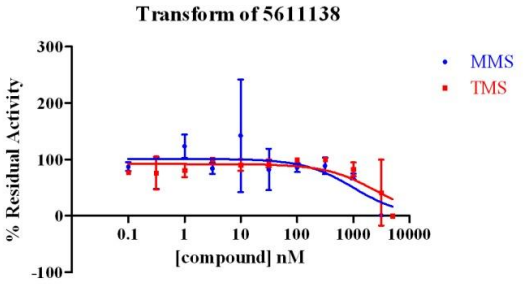
Transform of 5611138
% Residual Activity
[compound] nM
MMS
TMS

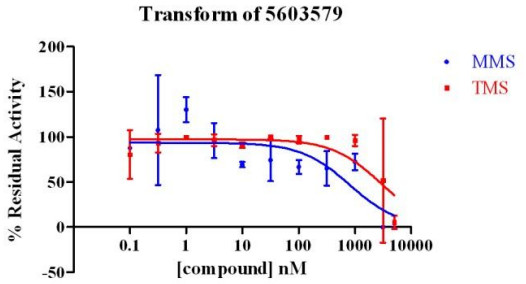
Transform of 5603579
% Residual Activity
[compound] nM
MMS
TMS

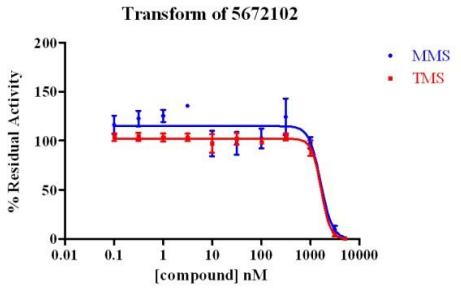
Transform of 5672102
% Residual Activity
[compound] nM
MMS
TMS

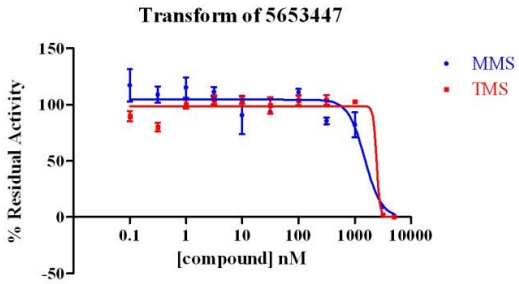
Transform of 5653447
% Residual Activity
[compound] nM
MMS
TMS

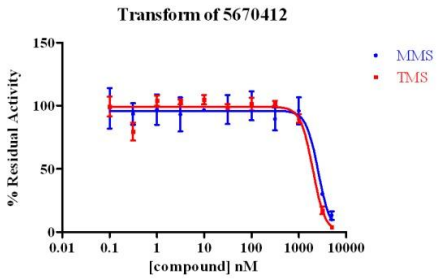
Transform of 5670412
% Residual Activity
[compound] nM
MMS
TMS

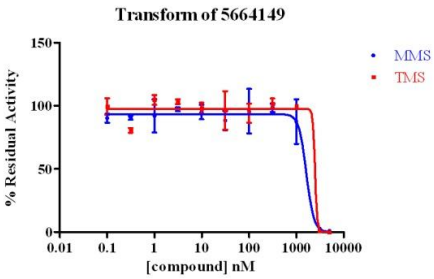
Transform of 5664149
% Residual Activity
[compound] nM
MMS
TMS

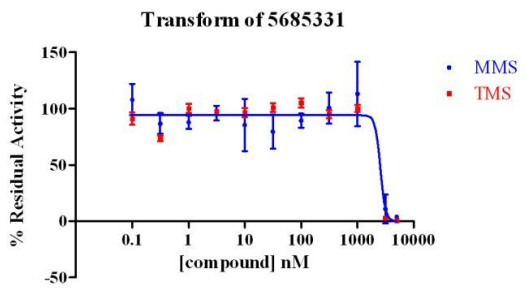
Transform of 5685331
% Residual Activity
[compound] nM
MMS
TMS

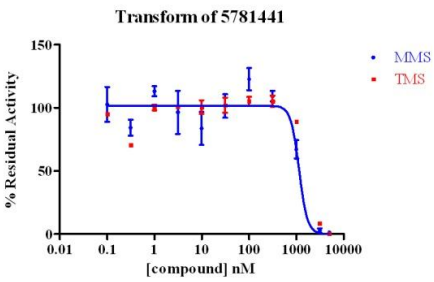
Transform of 5781441
% Residual Activity
[compound] nM
MMS
TMS

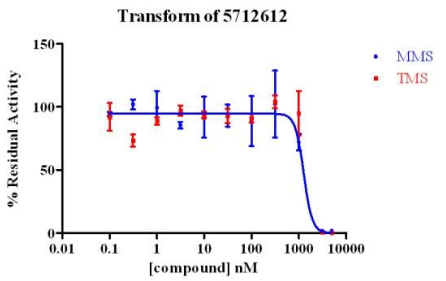
Transform of 5712612
% Residual Activity
[compound] nM
MMS
TMS

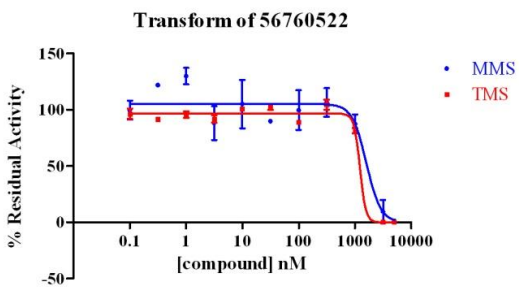
Transform of 56760522
% Residual Activity
[compound] nM
MMS
TMS

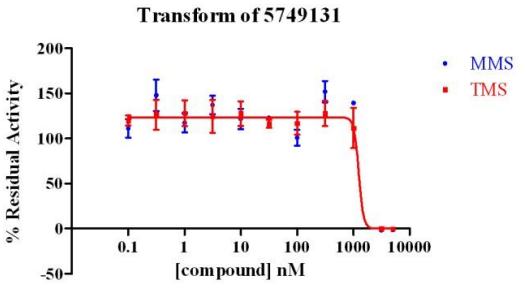
Transform of 5749131
% Residual Activity
[compound] nM
MMS
TMS

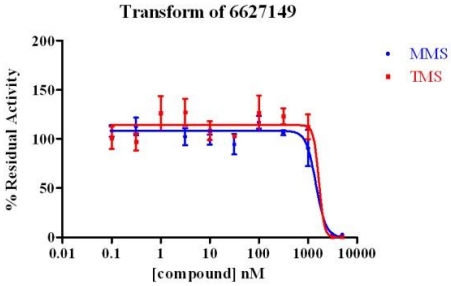
Transform of 6627149
% Residual Activity
[compound] nM
MMS
TMS

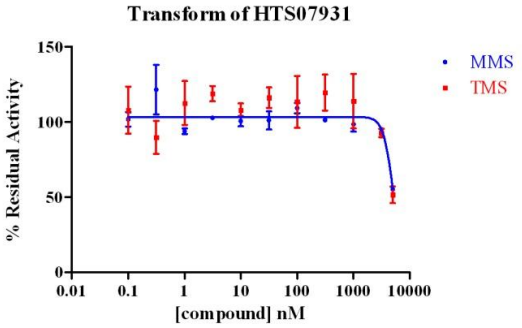
Transform of HTS07931
% Residual Activity
[compound] nM
MMS
TMS

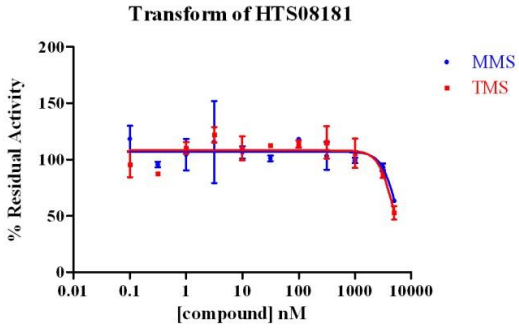
Transform of HTS08181
% Residual Activity
[compound] nM
MMS
TMS

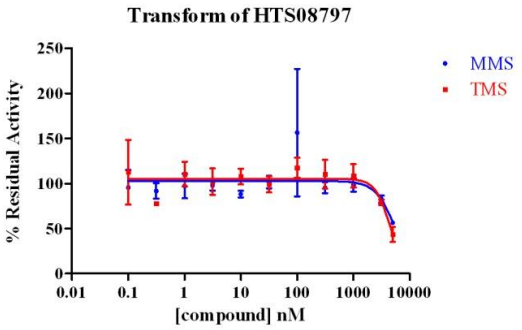
Transform of HTS08797
% Residual Activity
[compound] nM
MMS
TMS

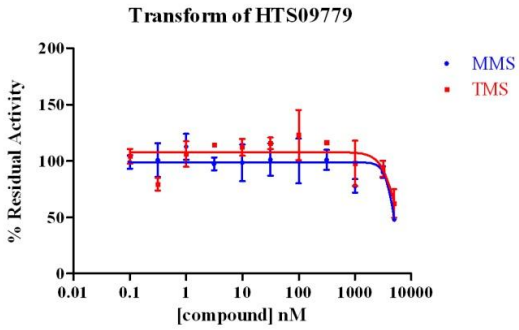
Transform of HTS09779
% Residual Activity
[compound] nM
MMS
TMS

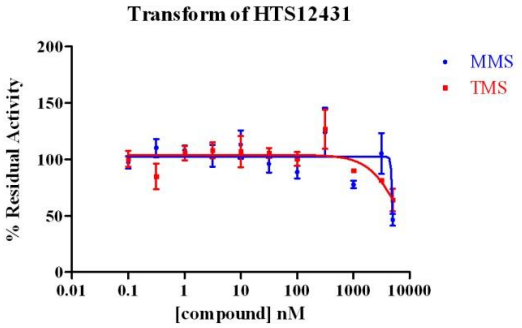
Transform of HTS12431
% Residual Activity
[compound] nM
MMS
TMS

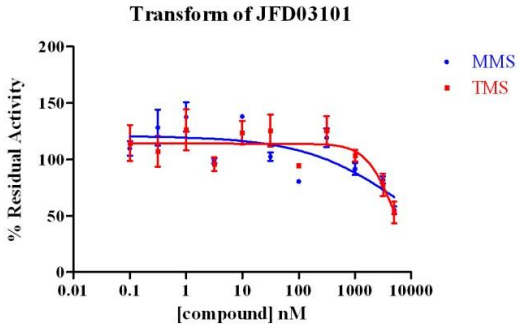
Transform of JFD03101
% Residual Activity
[compound] nM
MMS
TMS

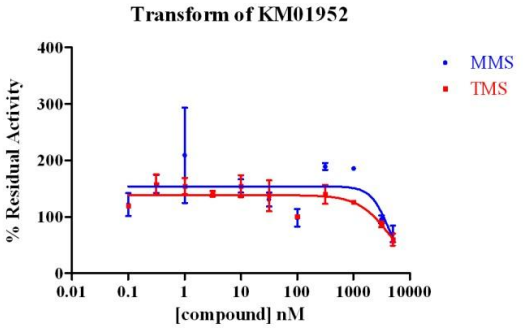
Transform of KM01952
% Residual Activity
[compound] nM
MMS
TMS

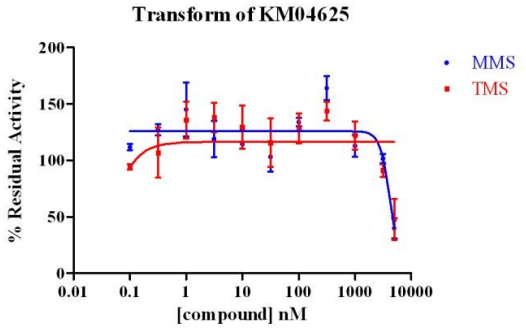
Transform of KM04625
% Residual Activity
[compound] nM
MMS
TMS

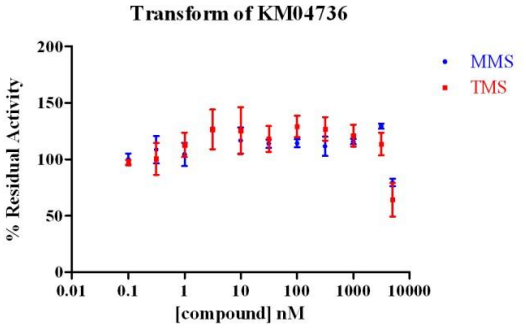
Transform of KM04736
% Residual Activity
[compound] nM
MMS
TMS

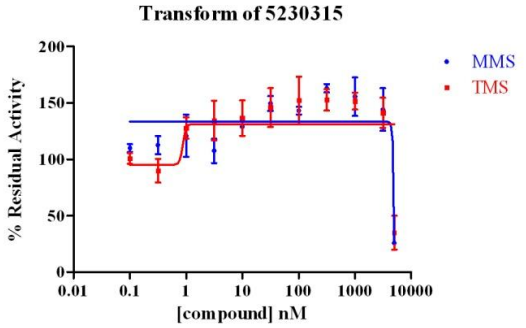
Transform of 5230315
% Residual Activity
[compound] nM
MMS
TMS

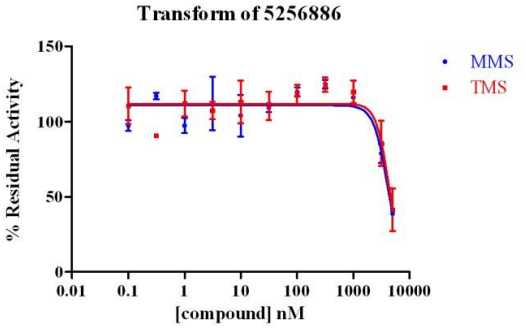
Transform of 5256886
% Residual Activity
[compound] nM
MMS
TMS

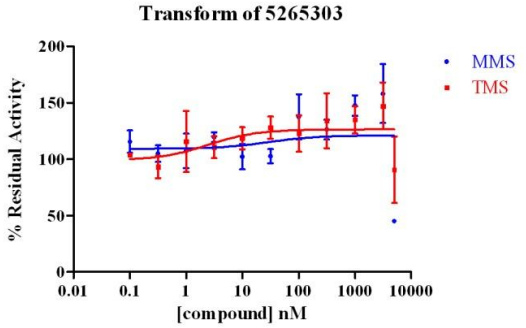
Transform of 5265303
% Residual Activity
[compound] nM
MMS
TMS

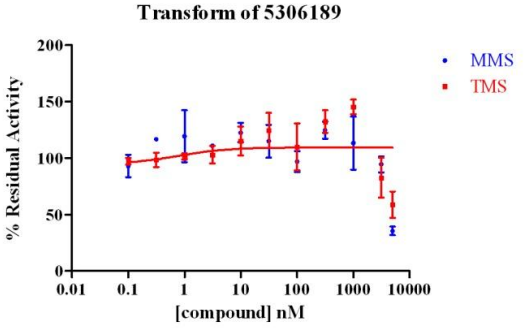
Transform of 5306189
% Residual Activity
[compound] nM
MMS
TMS

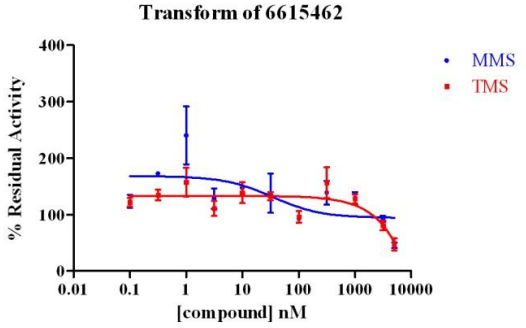
Transform of 6615462
% Residual Activity
[compound] nM
MMS
TMS

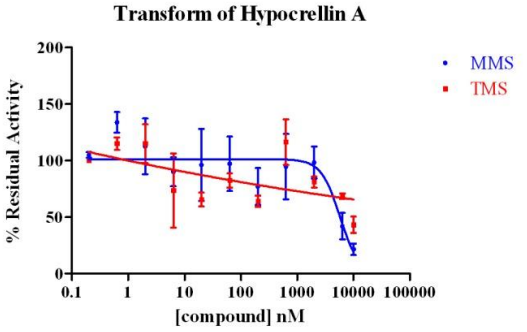
Transform of Hypocrellin A
% Residual Activity
[compound] nM
MMS
TMS

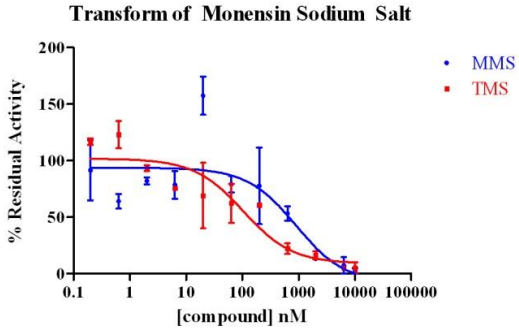
Transform of Monensin Sodium Salt
% Residual Activity
[compound] nM
MMS
TMS

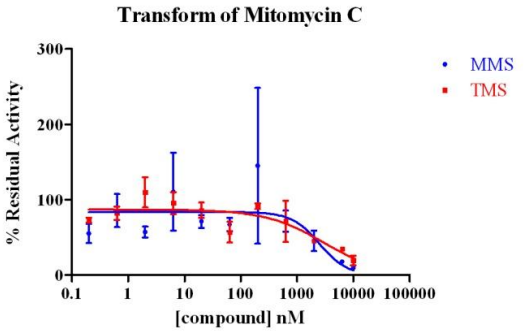
Transform of Mitomycin C
% Residual Activity
[compound] nM
MMS
TMS

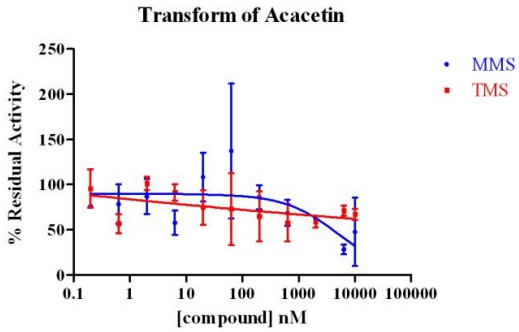
Transform of Acacetin
% Residual Activity
[compound] nM
MMS
TMS

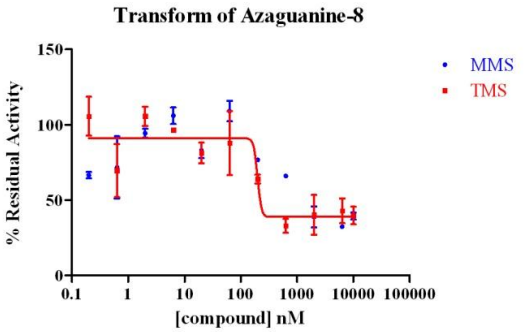
Transform of Azaguanine-8
% Residual Activity
[compound] nM
MMS
TMS

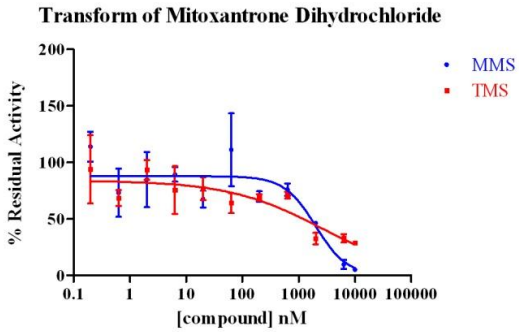
Transform of Mitoxantrone Dihydrochloride
% Residual Activity
[compound] nM
MMS
TMS

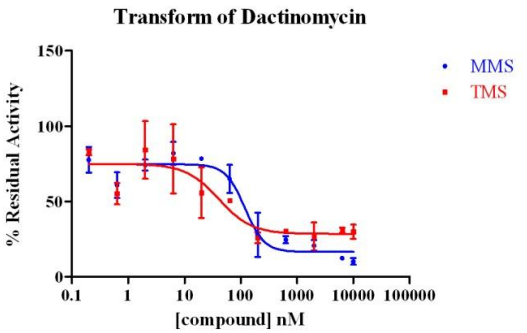
Transform of Dactinomycin
% Residual Activity
[compound] nM
MMS
TMS

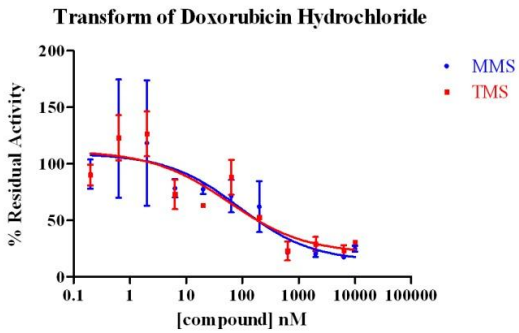
Transform of Doxorubicin Hydrochloride
% Residual Activity
[compound] nM
MMS
TMS

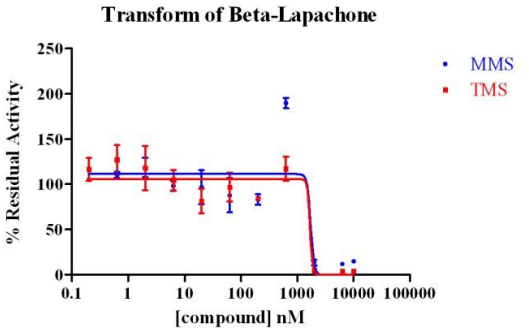
Transform of Beta-Lapachone
% Residual Activity
[compound] nM
MMS
TMS

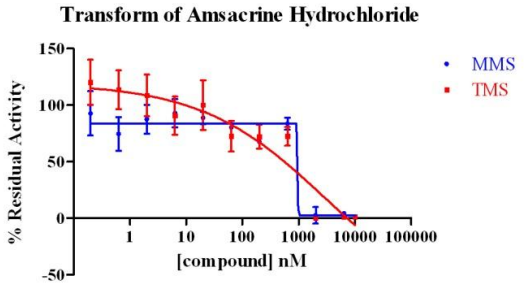
Transform of Amsacrine Hydrochloride
% Residual Activity
[compound] nM
MMS
TMS

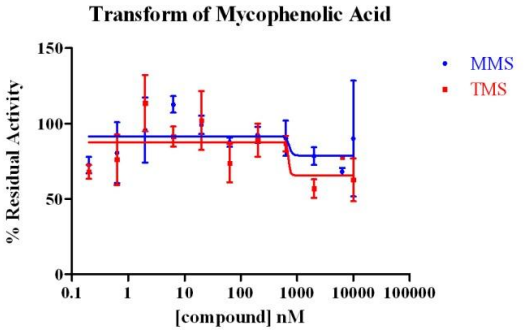
Transform of Mycophenolic Acid
% Residual Activity
[compound] nM
MMS
TMS

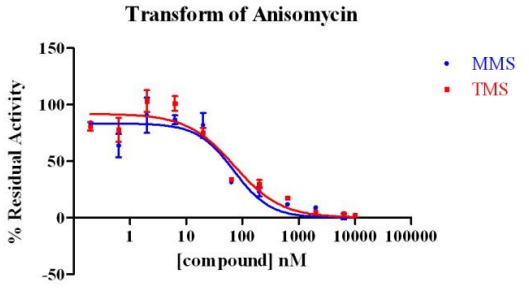
Transform of Anisomycin
% Residual Activity
[compound] nM
MMS
TMS

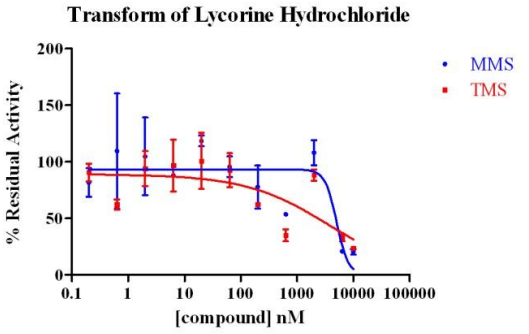
Transform of Lycorine Hydrochloride
% Residual Activity
[compound] nM
MMS
TMS

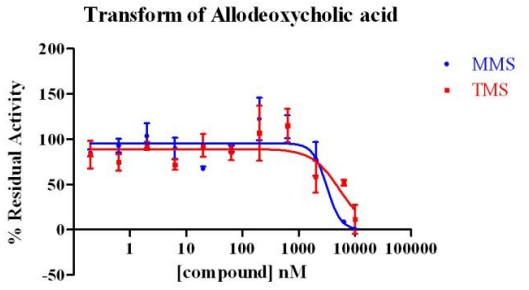
Transform of Allodeoxycholic acid
% Residual Activity
[compound] nM
MMS
TMS

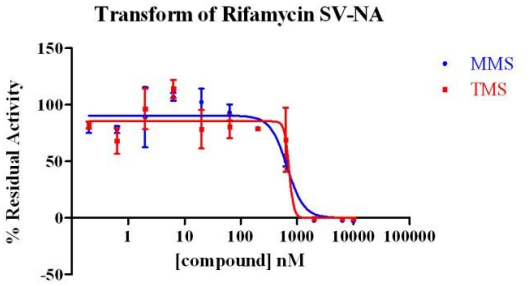
Transform of Rifamycin SV-NA
% Residual Activity
[compound] nM
MMS
TMS

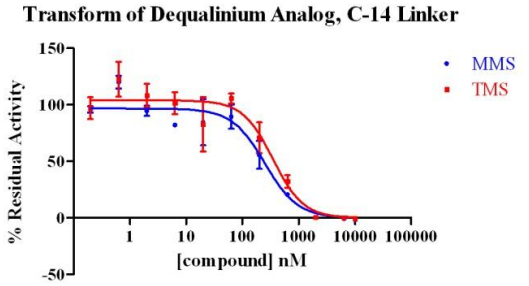
Transform of Dequalinium Analog, C-14 Linker
% Residual Activity
[compound] nM
MMS
TMS

Transform of 4-Alpha-Phorbol 12-myristate 13-acetate

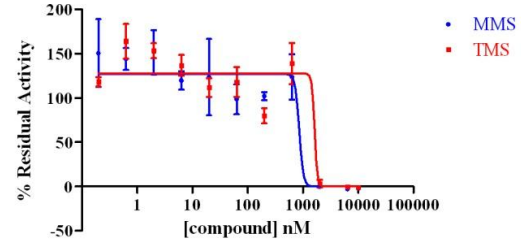


Transform of Sanguinarine Sulfate

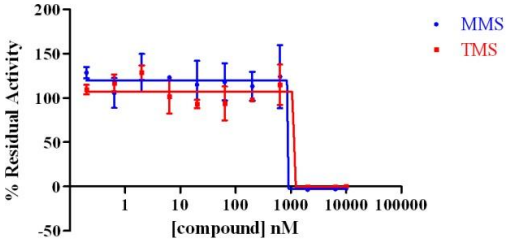


Transform of Tetrachloroisophthalonitrile

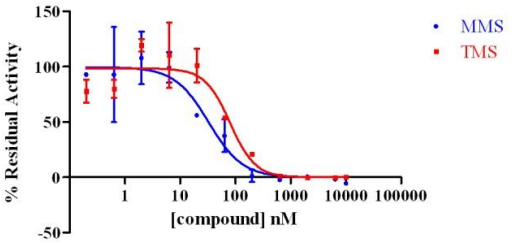


Transform of Pristimerin

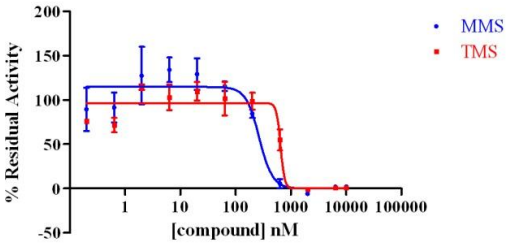


Transform of Pristimerol

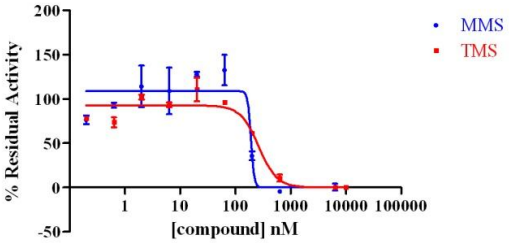


Transform of Terconazole

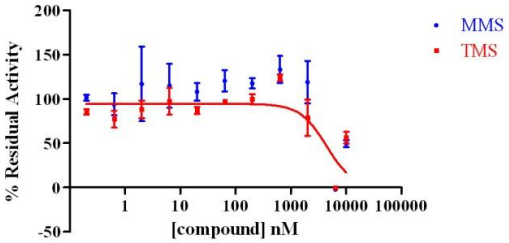


Transform of Obtusaquinone

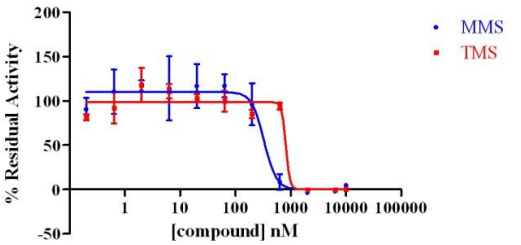


Transform of Amodiaquin Dihydrochloride Dihydrate

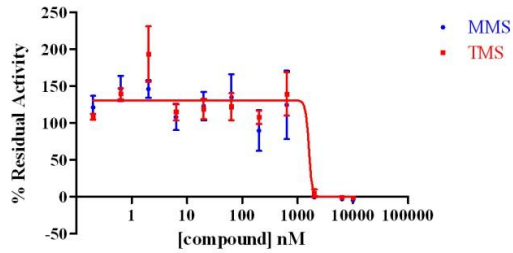

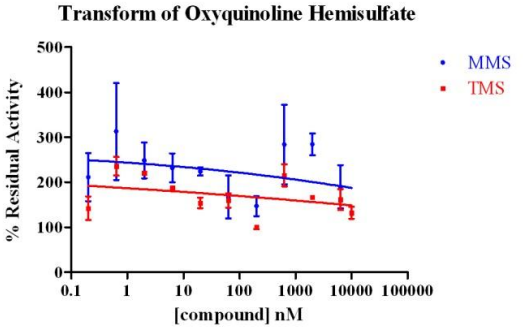
Transform of Oxyquinoline Hemisulfate
% Residual Activity
[compound] nM
MMS
TMS

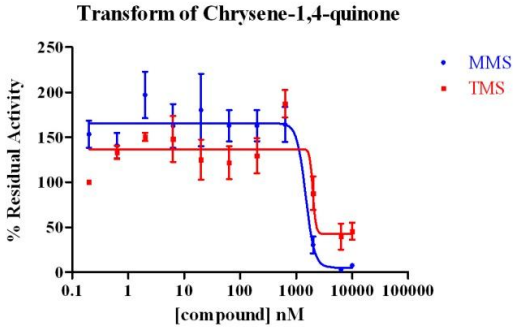
Transform of Chrysene-1,4-quinone
% Residual Activity
[compound] nM
MMS
TMS

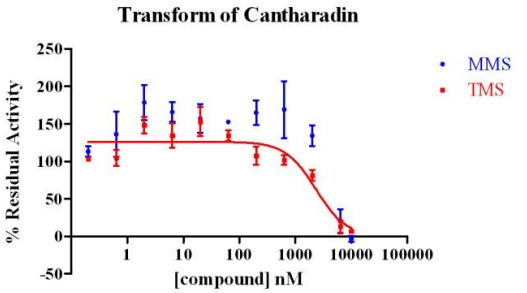
Transform of Cantharadin
% Residual Activity
[compound] nM
MMS
TMS

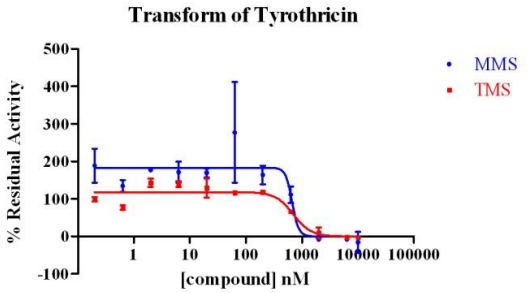
Transform of Tyrothricin
% Residual Activity
[compound] nM
MMS
TMS

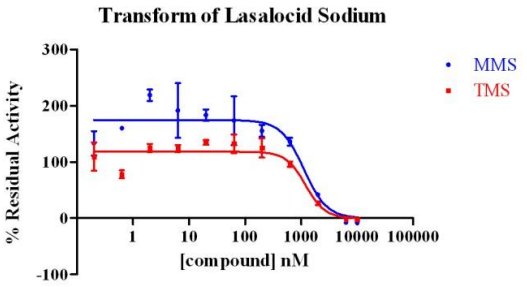
Transform of Lasalocid Sodium
% Residual Activity
[compound] nM
MMS
TMS

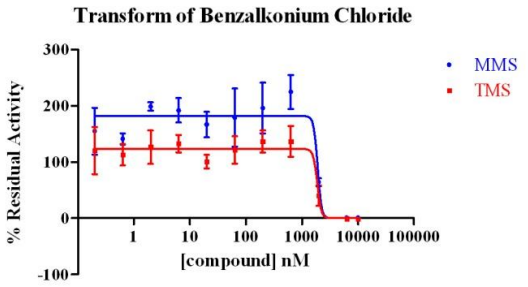
Transform of Benzalkonium Chloride
% Residual Activity
[compound] nM
MMS
TMS

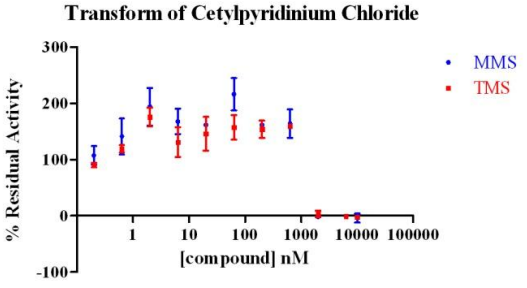
Transform of Cetylpyridinium Chloride
% Residual Activity
[compound] nM
MMS
TMS

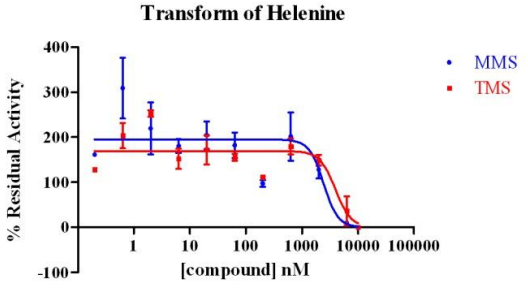
Transform of Helenine
% Residual Activity
[compound] nM
MMS
TMS

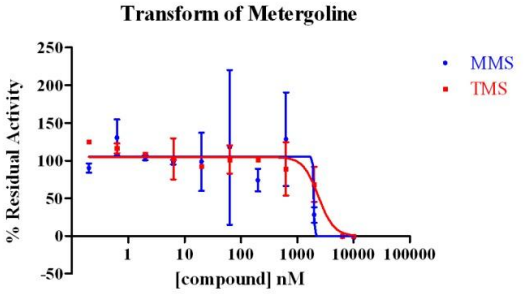
Transform of Metergoline
% Residual Activity
[compound] nM
MMS
TMS

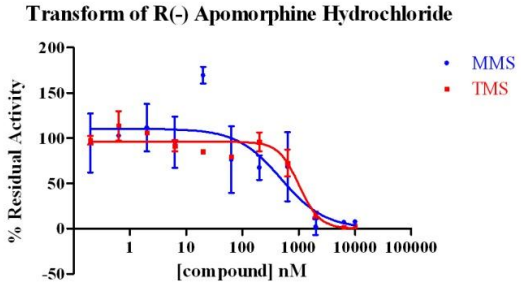
Transform of R(-) Apomorphine Hydrochloride
% Residual Activity
[compound] nM
MMS
TMS

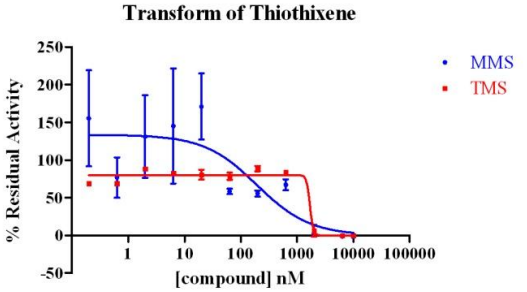
Transform of Thiothixene
% Residual Activity
[compound] nM
MMS
TMS

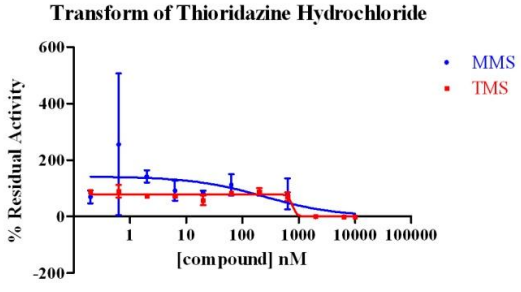
Transform of Thioridazine Hydrochloride
% Residual Activity
[compound] nM
MMS
TMS

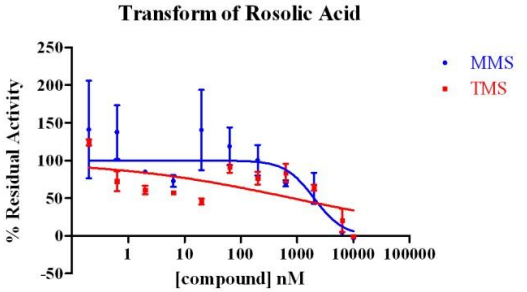
Transform of Rosolic Acid
% Residual Activity
[compound] nM
MMS
TMS

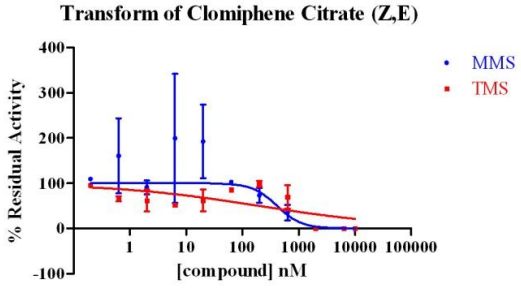
Transform of Clomiphene Citrate (Z,E)
% Residual Activity
[compound] nM
MMS
TMS

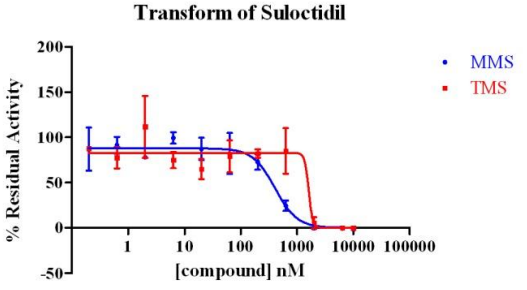
Transform of Suloctidil
% Residual Activity
[compound] nM
MMS
TMS

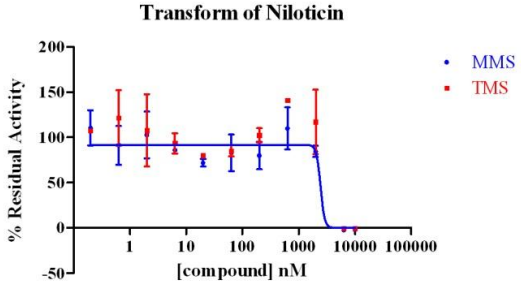
Transform of Niloticin
% Residual Activity
[compound] nM
MMS
TMS

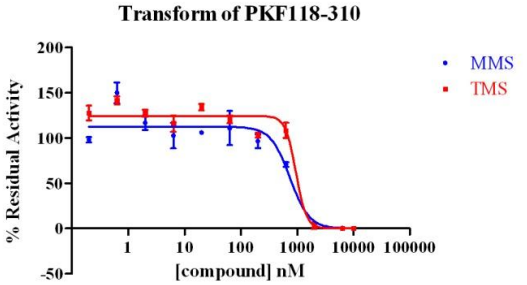
Transform of PKF118-310
% Residual Activity
[compound] nM
MMS
TMS

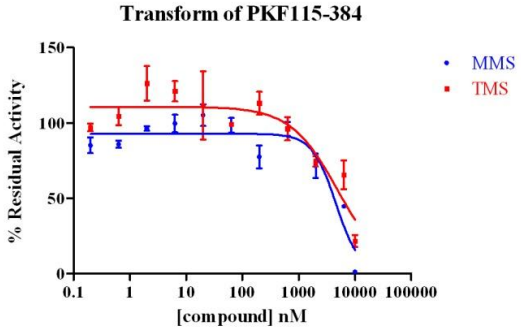
Transform of PKF115-384
% Residual Activity
[compound] nM
MMS
TMS

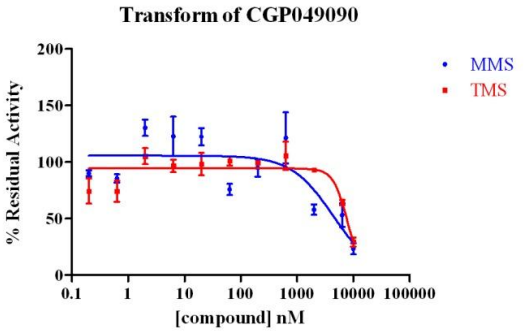
Transform of CGP049090
% Residual Activity
[compound] nM
MMS
TMS

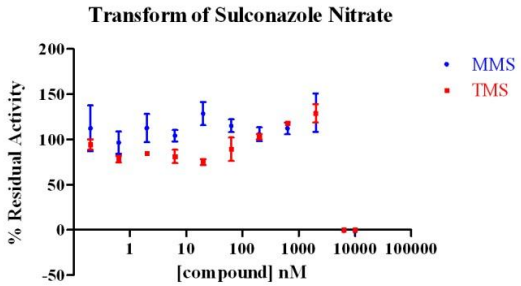
Transform of Sulconazole Nitrate
% Residual Activity
[compound] nM
MMS
TMS

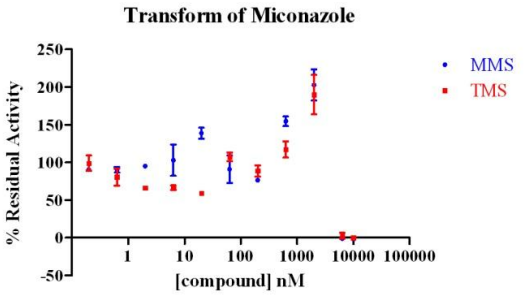
Transform of Miconazole
% Residual Activity
[compound] nM
MMS
TMS

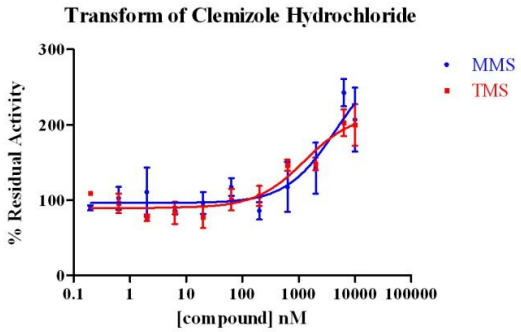
Transform of Clemizole Hydrochloride
% Residual Activity
[compound] nM
MMS
TMS

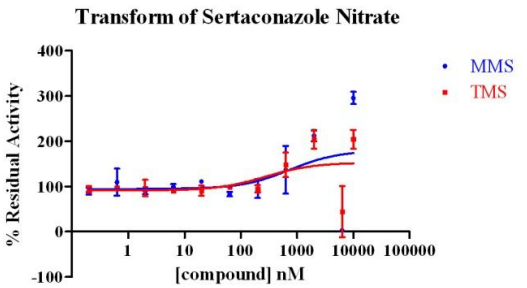
Transform of Sertaconazole Nitrate
% Residual Activity
[compound] nM
MMS
TMS

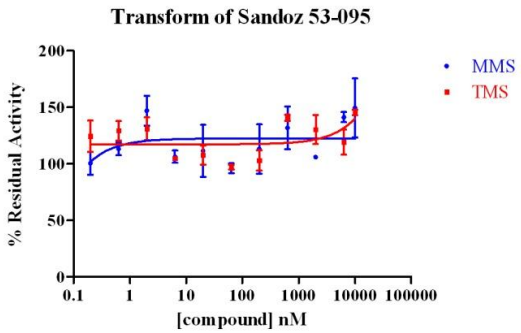
Transform of Sandoz 53-095
% Residual Activity
[compound] nM
MMS
TMS

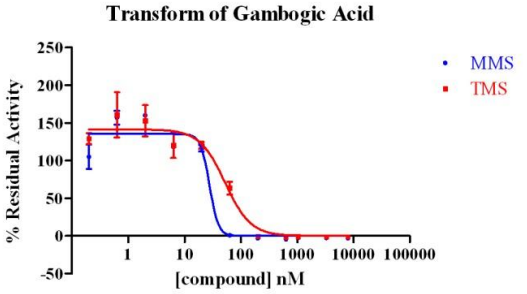
Transform of Gambogic Acid
% Residual Activity
[compound] nM
MMS
TMS

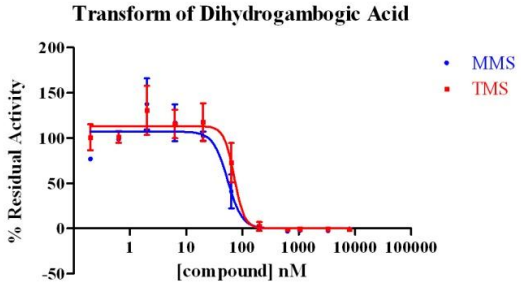
Transform of Dihydrogambogic Acid
% Residual Activity
[compound] nM
MMS
TMS

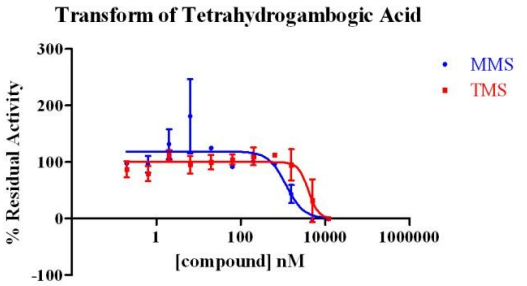
Transform of Tetrahydrogambogic Acid
% Residual Activity
[compound] nM
MMS
TMS

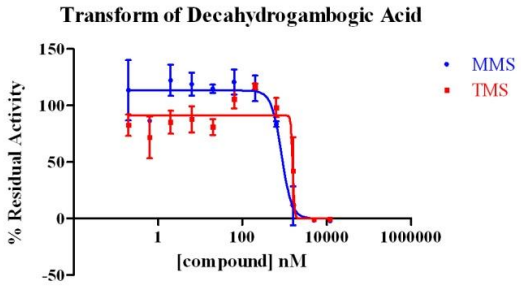
Transform of Decahydrogambogic Acid
% Residual Activity
[compound] nM
MMS
TMS

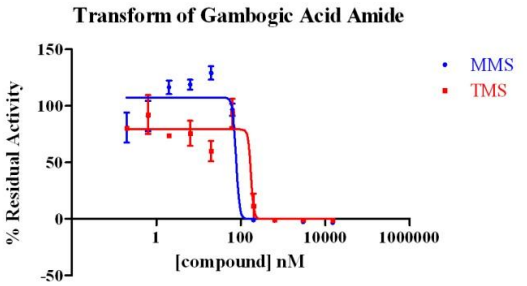
Transform of Gambogic Acid Amide
% Residual Activity
[compound] nM
MMS
TMS

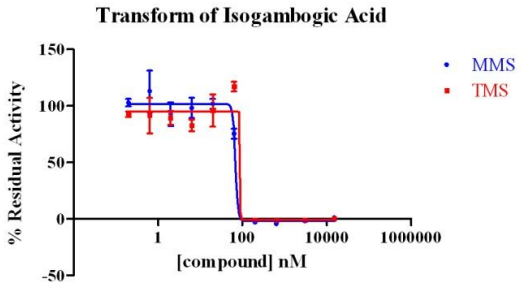
Transform of Isogambogic Acid
% Residual Activity
[compound] nM
MMS
TMS

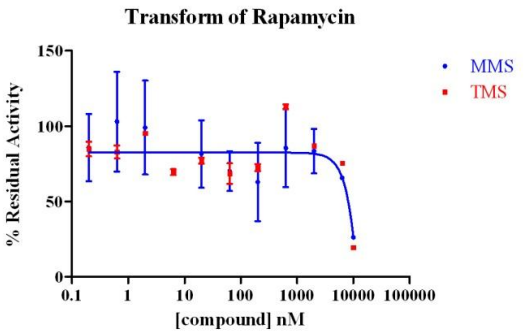
Transform of Rapamycin
% Residual Activity
[compound] nM
MMS
TMS

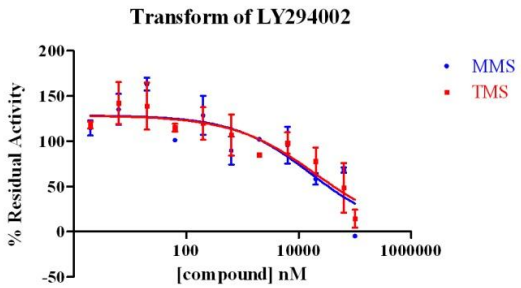
Transform of LY294002
% Residual Activity
[compound] nM
MMS
TMS

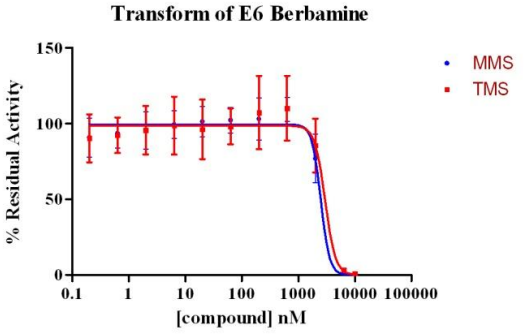
Transform of E6 Berbamine
% Residual Activity
[compound] nM
MMS
TMS

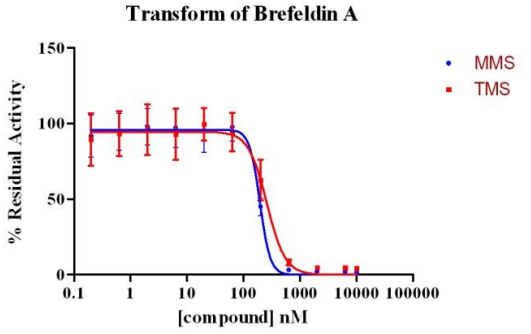
Transform of Brefeldin A
% Residual Activity
[compound] nM
MMS
TMS

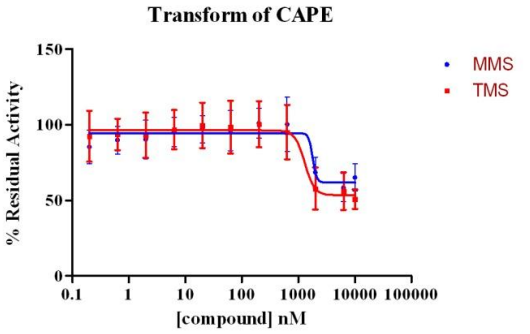
Transform of CAPE
% Residual Activity
[compound] nM
MMS
TMS

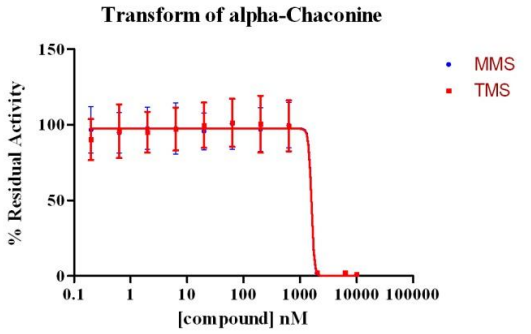
Transform of alpha-Chaconine
% Residual Activity
[compound] nM
MMS
TMS

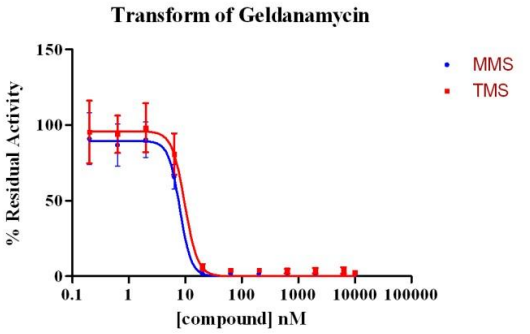
Transform of Geldanamycin
% Residual Activity
[compound] nM
MMS
TMS

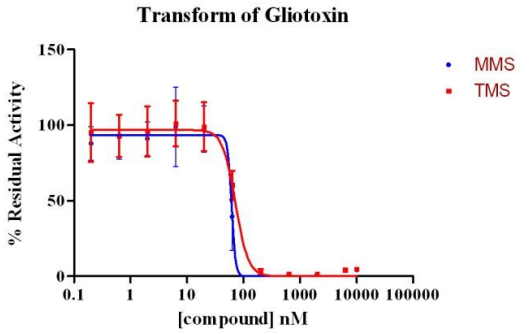
Transform of Gliotoxin
% Residual Activity
[compound] nM
MMS
TMS

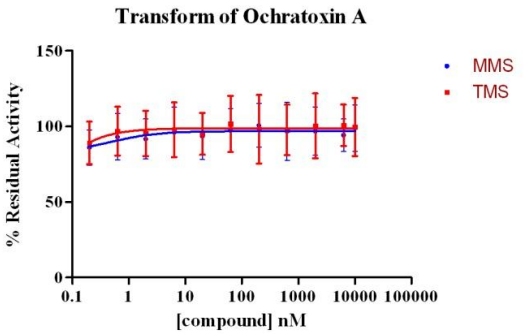
Transform of Ochratoxin A
% Residual Activity
[compound] nM
MMS
TMS

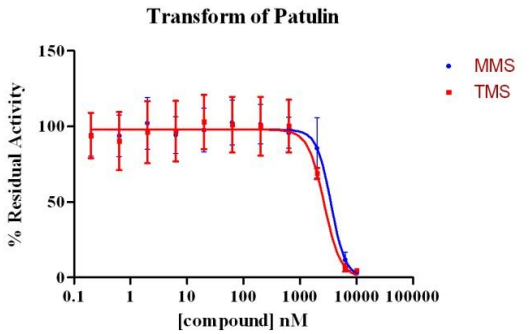
Transform of Patulin
% Residual Activity
[compound] nM
MMS
TMS

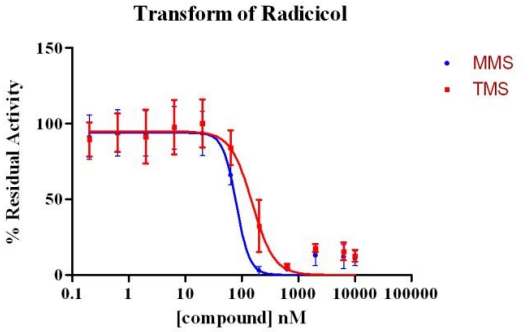
Transform of Radicicol
% Residual Activity
[compound] nM
MMS
TMS

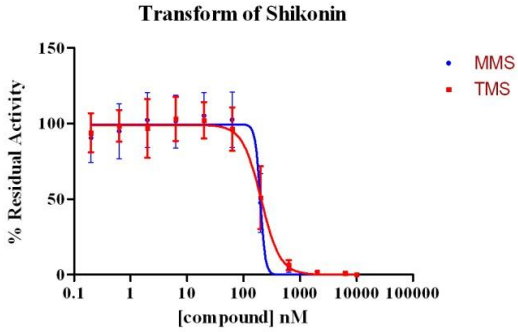
Transform of Shikonin
% Residual Activity
[compound] nM
MMS
TMS

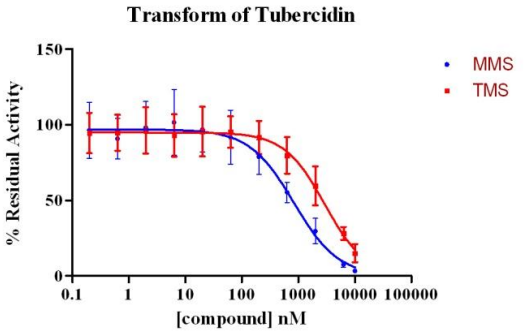
Transform of Tubercidin
% Residual Activity
[compound] nM
MMS
TMS

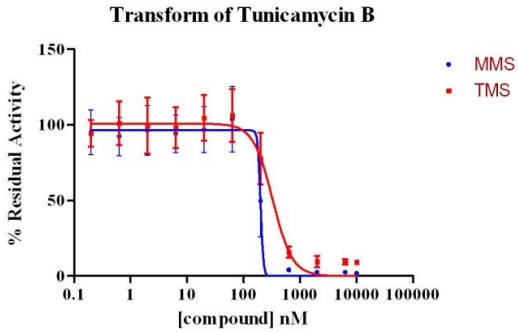
Transform of Tunicamycin B
% Residual Activity
[compound] nM
MMS
TMS

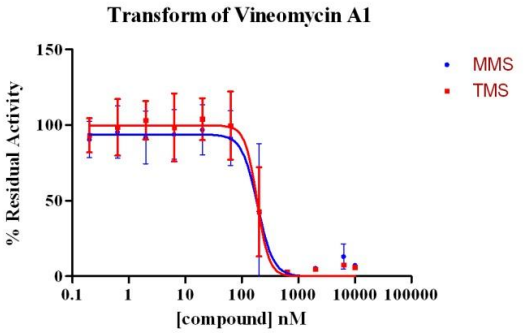
Transform of Vineomycin A1
% Residual Activity
[compound] nM
MMS
TMS

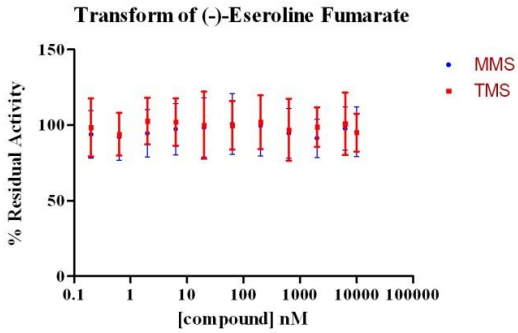
Transform of (-)-Eseroline Fumarate
% Residual Activity
[compound] nM
MMS
TMS

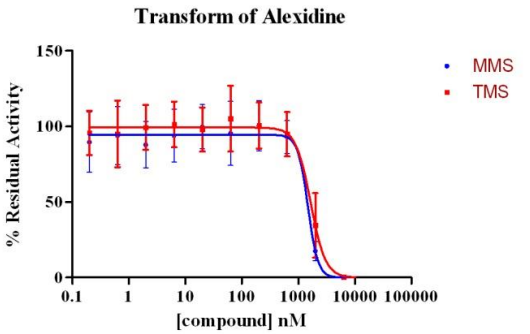
Transform of Alexidine
% Residual Activity
[compound] nM
MMS
TMS

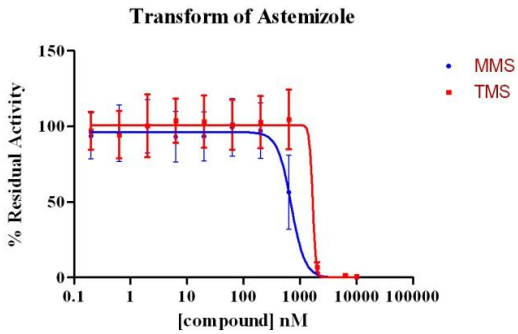
Transform of Astemizole
% Residual Activity
[compound] nM
MMS
TMS

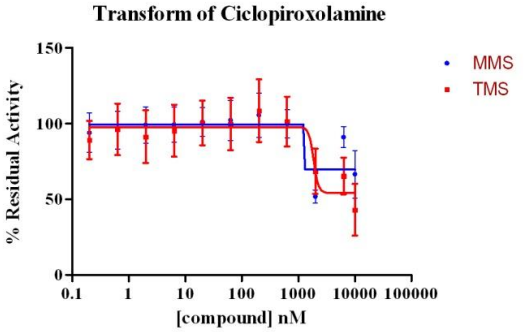
Transform of Ciclopiroxolamine
% Residual Activity
[compound] nM
MMS
TMS

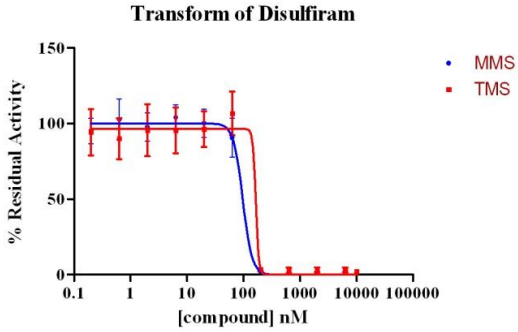
Transform of Disulfiram
% Residual Activity
[compound] nM
MMS
TMS

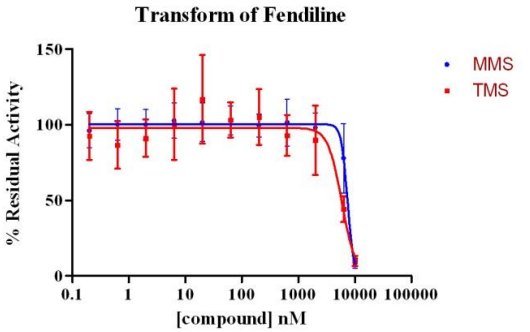
Transform of Fendiline
% Residual Activity
[compound] nM
MMS
TMS

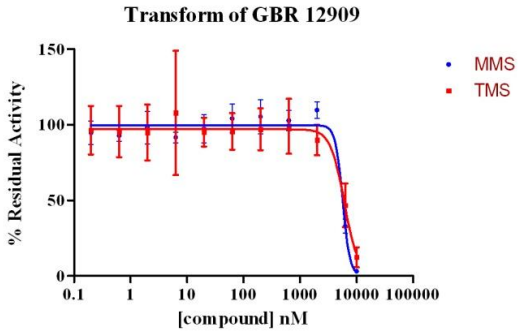
Transform of GBR 12909
% Residual Activity
[compound] nM
MMS
TMS

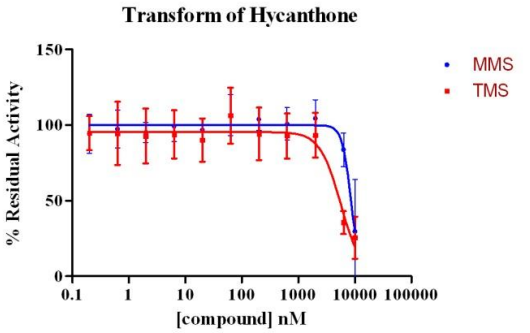
Transform of Hycanthone
% Residual Activity
[compound] nM
MMS
TMS

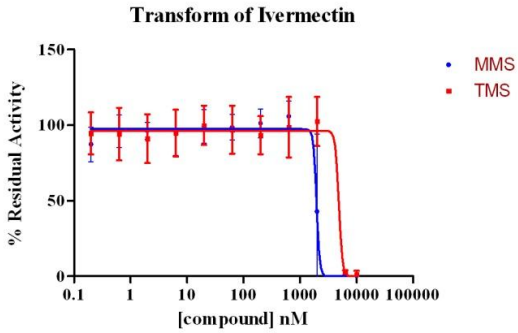
Transform of Ivermectin
% Residual Activity
[compound] nM
MMS
TMS

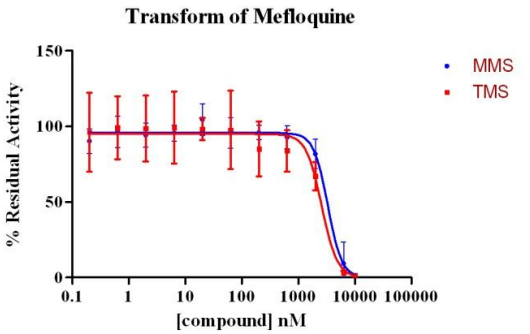
Transform of Mefloquine
% Residual Activity
[compound] nM
MMS
TMS

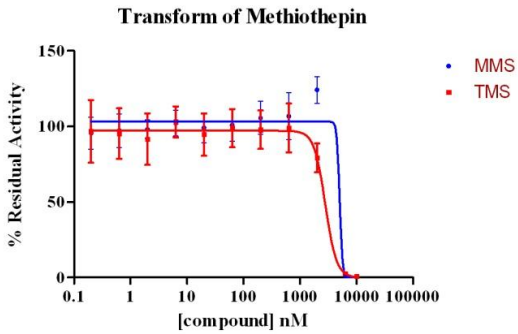
Transform of Methiothepin
% Residual Activity
[compound] nM
MMS
TMS

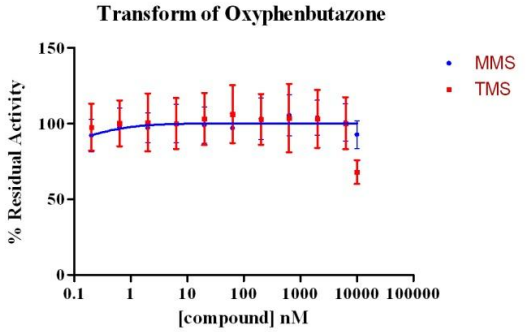
Transform of Oxyphenbutazone
% Residual Activity
150
100
50
0
0.1
1
10
100
1000
10000
100000
[compound] nM
MMS
TMS

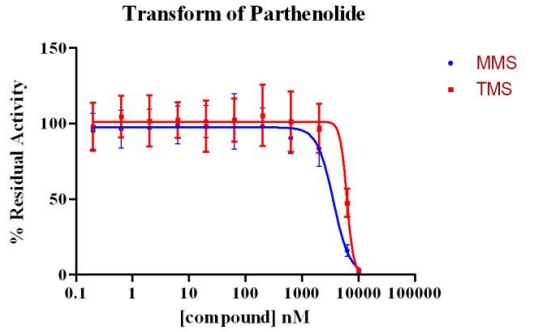
Transform of Parthenolide
% Residual Activity
150
100
50
0
0.1
1
10
100
1000
10000
100000
[compound] nM
MMS
TMS

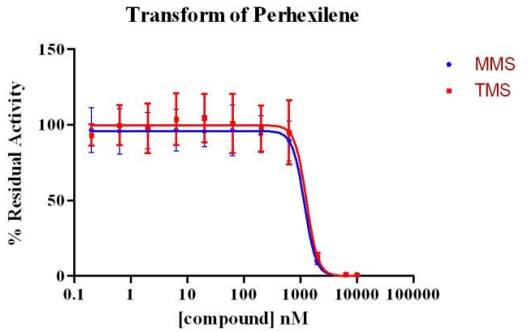
Transform of Perhexilene
% Residual Activity
150
100
50
0
0.1
1
10
100
1000
10000
100000
[compound] nM
MMS
TMS

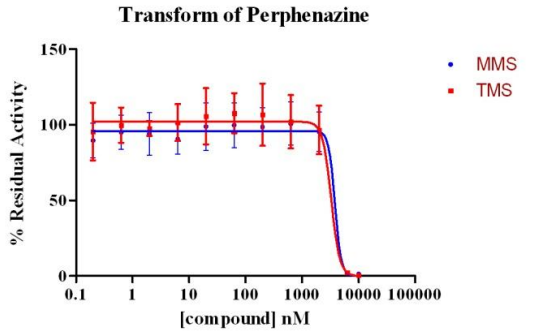
Transform of Perphenazine
% Residual Activity
150
100
50
0
0.1
1
10
100
1000
10000
100000
[compound] nM
MMS
TMS

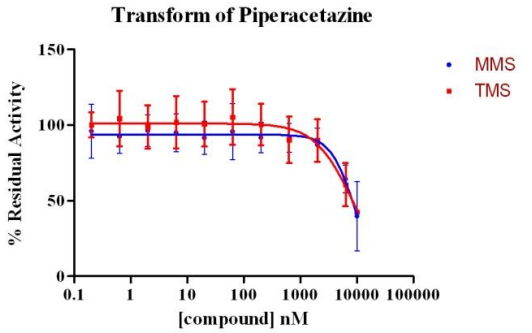
Transform of Piperacetazine
% Residual Activity
150
100
50
0
0.1
1
10
100
1000
10000
100000
[compound] nM
MMS
TMS

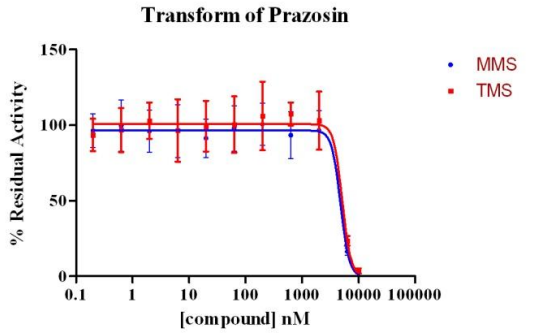
Transform of Prazosin
% Residual Activity
150
100
50
0
0.1
1
10
100
1000
10000
100000
[compound] nM
MMS
TMS

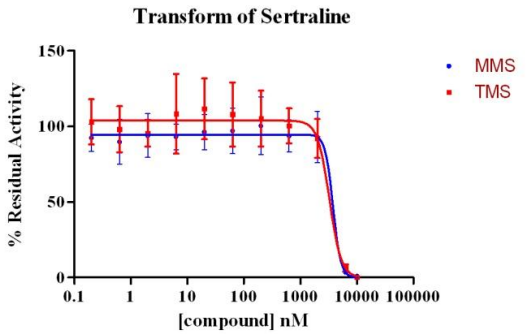
Transform of Sertraline
% Residual Activity
150
100
50
0
0.1
1
10
100
1000
10000
100000
[compound] nM
MMS
TMS

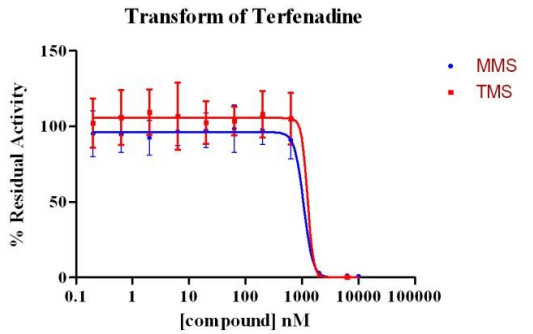
Transform of Terfenadine
% Residual Activity
150
100
50
0
0.1
1
10
100
1000
10000
100000
[compound] nM
MMS
TMS

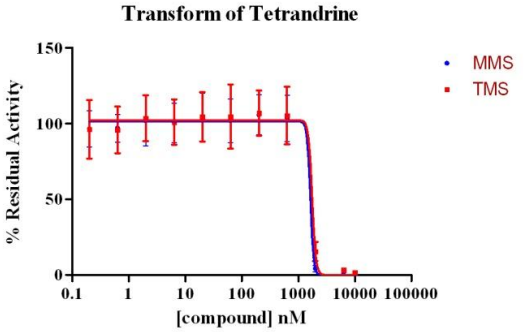
Transform of Tetrandrine
% Residual Activity
[compound] nM
MMS
TMS

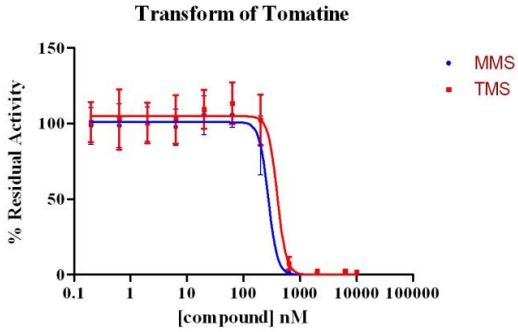
Transform of Tomatine
% Residual Activity
[compound] nM
MMS
TMS

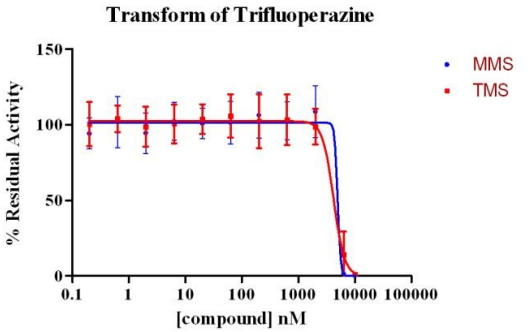
Transform of Trifluoperazine
% Residual Activity
[compound] nM
MMS
TMS

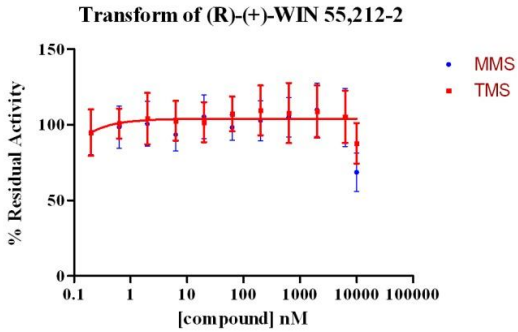
Transform of (R)-(+)-WIN 55,212-2
% Residual Activity
[compound] nM
MMS
TMS

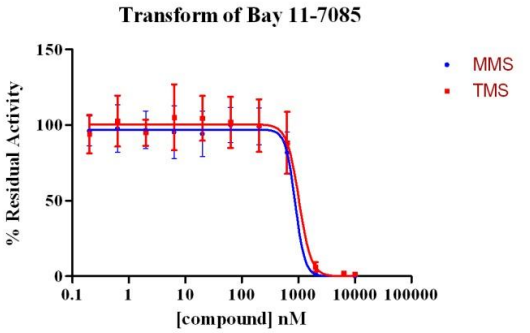
Transform of Bay 11-7085
% Residual Activity
[compound] nM
MMS
TMS

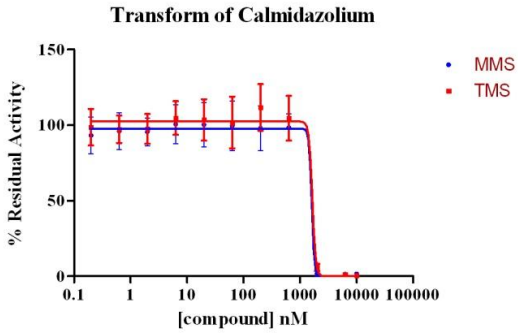
Transform of Calmidazolium
% Residual Activity
[compound] nM
MMS
TMS

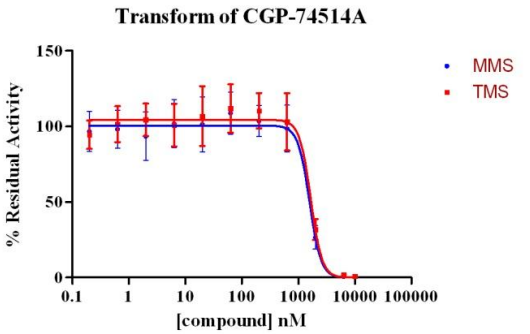
Transform of CGP-74514A
% Residual Activity
[compound] nM
MMS
TMS

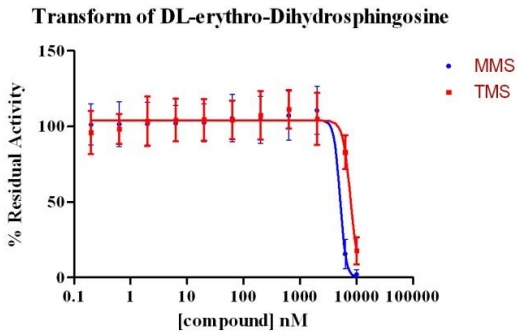
Transform of DL-erythro-Dihydrosphingosine
% Residual Activity
[compound] nM
MMS
TMS

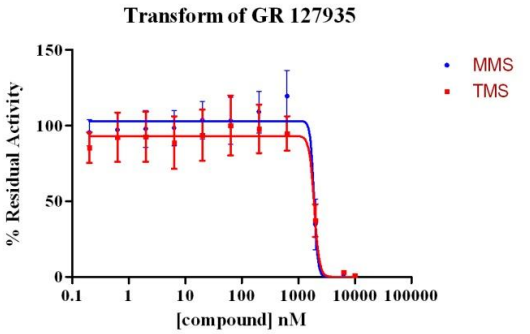
Transform of GR 127935
% Residual Activity
[compound] nM
MMS
TMS

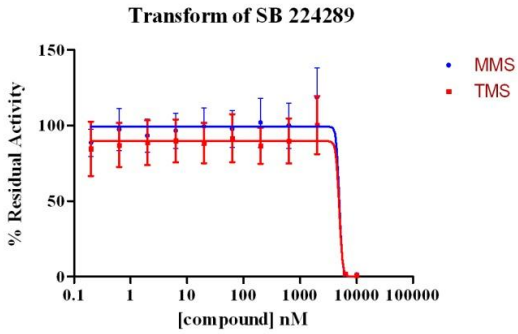
Transform of SB 224289
% Residual Activity
[compound] nM
MMS
TMS

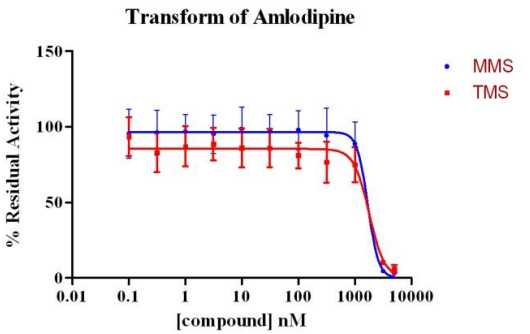
Transform of Amlodipine
% Residual Activity
[compound] nM
MMS
TMS

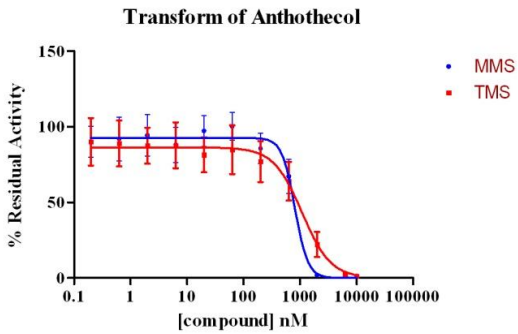
Transform of Anthothecol
% Residual Activity
[compound] nM
MMS
TMS

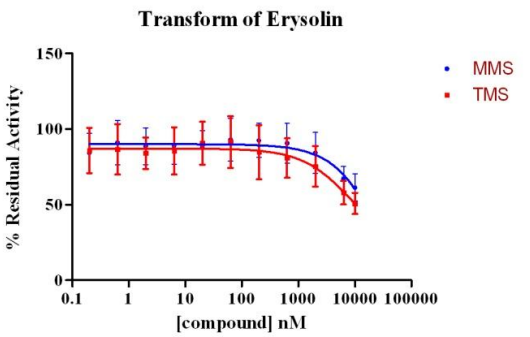
Transform of Erysolin
% Residual Activity
[compound] nM
MMS
TMS

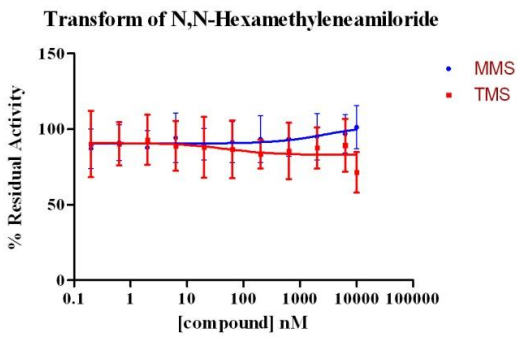
Transform of N,N-Hexamethyleneamiloride
% Residual Activity
[compound] nM
MMS
TMS

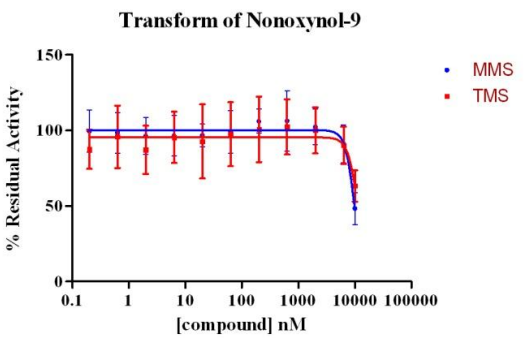
Transform of Nonoxynol-9
% Residual Activity
[compound] nM
MMS
TMS

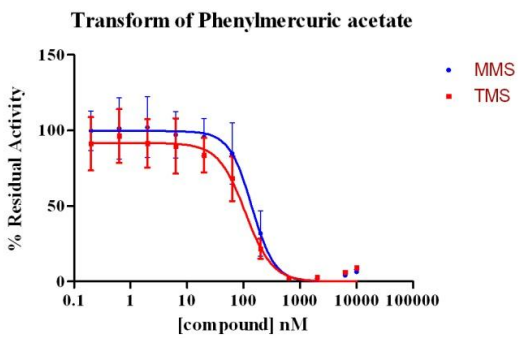
Transform of Phenylmercuric acetate
% Residual Activity
[compound] nM
MMS
TMS

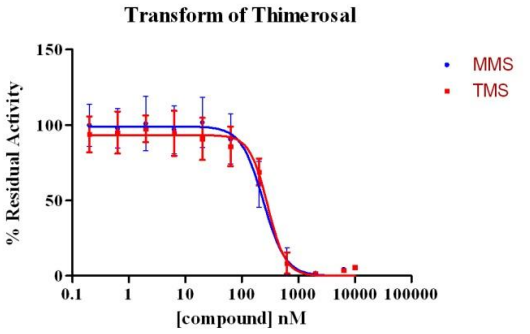
Transform of Thimerosal
% Residual Activity
150
100
50
0
0.1
1
10
100
1000
10000
100000
[compound] nM
MMS
TMS

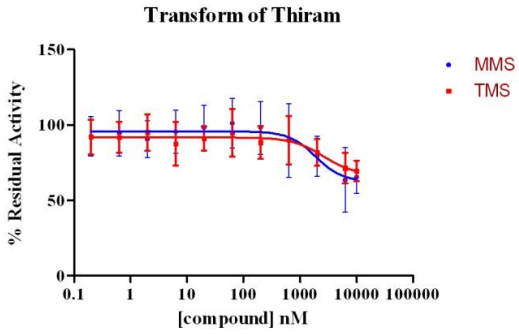
Transform of Thiram
% Residual Activity
150
100
50
0
0.1
1
10
100
1000
10000
100000
[compound] nM
MMS
TMS

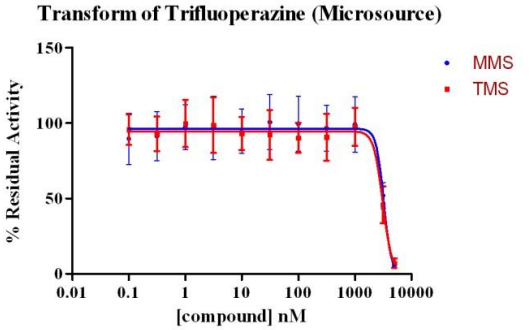
Transform of Trifluoperazine (Microsource)
% Residual Activity
150
100
50
0
0.01
0.1
1
10
100
1000
10000
[compound] nM
MMS
TMS

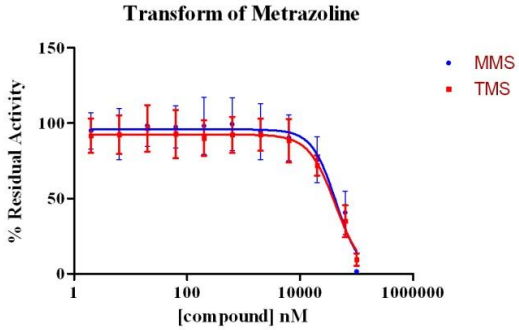
Transform of Metrazoline
% Residual Activity
150
100
50
0
1
100
10000
1000000
[compound] nM
MMS
TMS

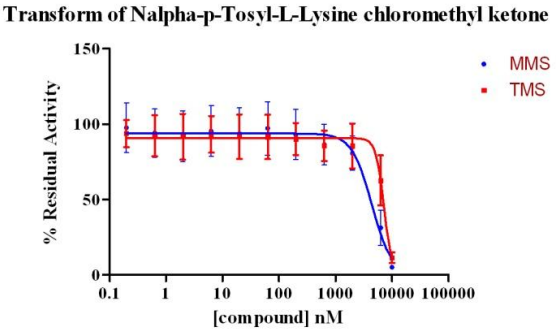
Transform of Nalpha-p-Tosyl-L-Lysine chloromethyl ketone
% Residual Activity
150
100
50
0
0.1
1
10
100
1000
10000
100000
[compound] nM
MMS
TMS

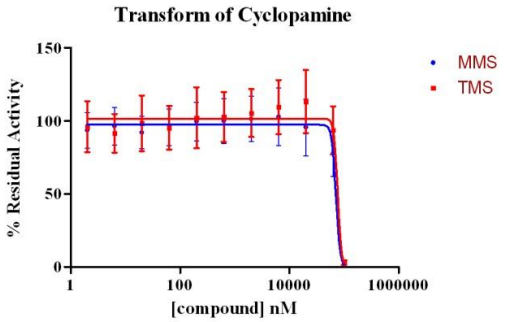
Transform of Cyclopamine
% Residual Activity
[compound] nM
MMS
TMS

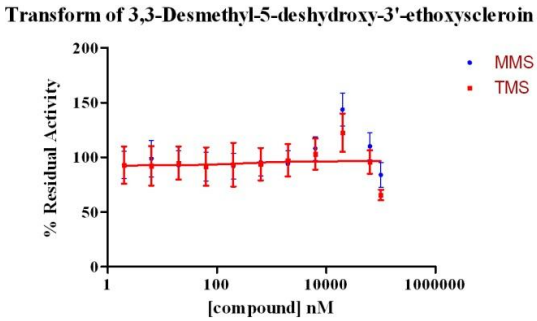
Transform of 3,3-Desmethyl-5-deshydroxy-3'-ethoxyscleroin
% Residual Activity
[compound] nM
MMS
TMS

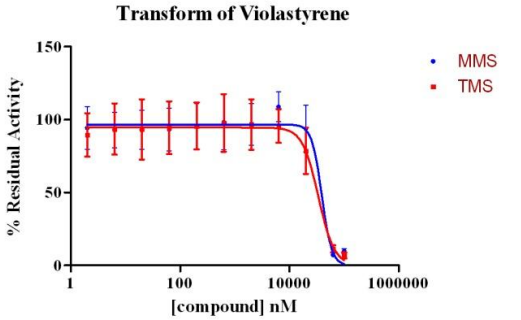
Transform of Violastyrene
% Residual Activity
[compound] nM
MMS
TMS

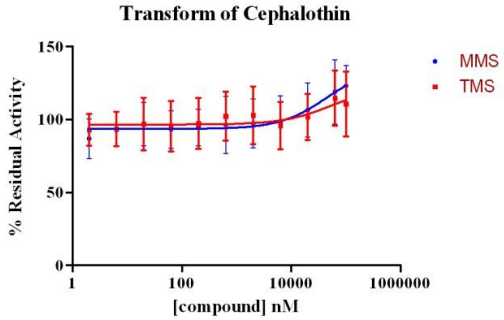
Transform of Cephalothin
% Residual Activity
[compound] nM
MMS
TMS

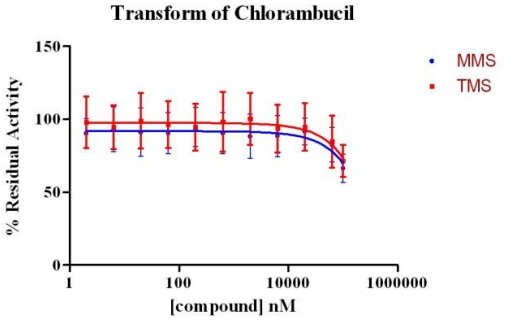
Transform of Chlorambucil
% Residual Activity
[compound] nM
MMS
TMS

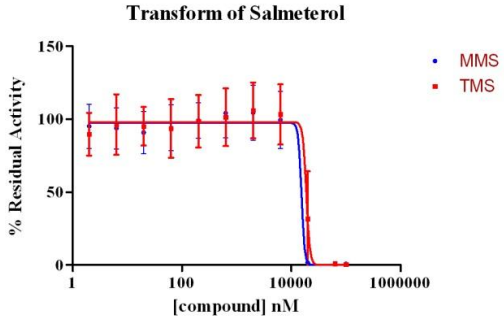
Transform of Salmeterol
% Residual Activity
[compound] nM
MMS
TMS

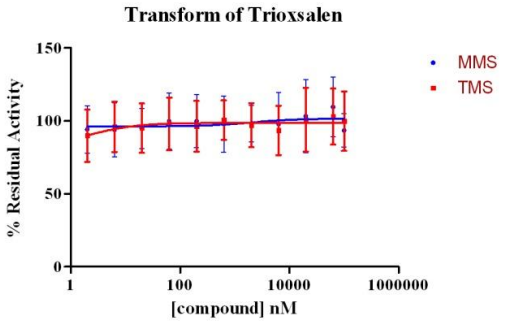
Transform of Trioxsalen
% Residual Activity
[compound] nM
MMS
TMS

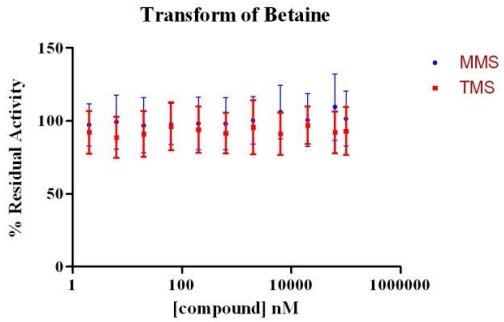
Transform of Betaine
% Residual Activity
[compound] nM
MMS
TMS

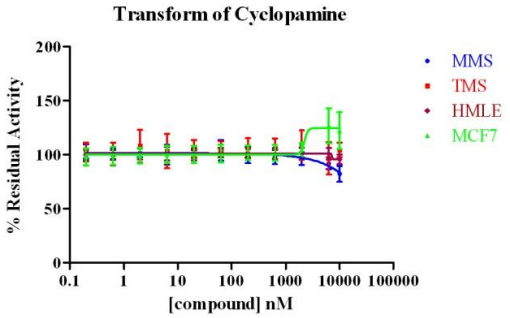
Transform of Cyclopamine
% Residual Activity
[compound] nM
MMS
TMS
HMLE
MCF7

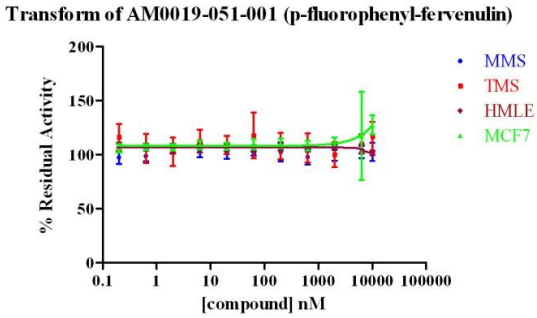
Transform of AM0019-051-001 (p-fluorophenyl-fervenulin)
% Residual Activity
[compound] nM
MMS
TMS
HMLE
MCF7

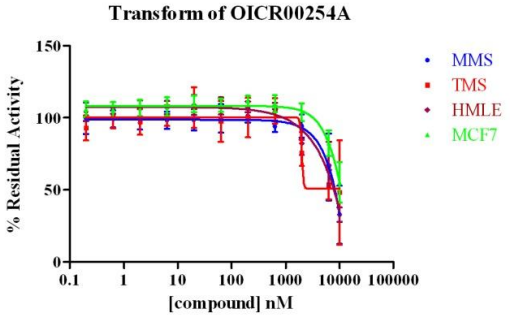
Transform of OICR00254A
% Residual Activity
[compound] nM
MMS
TMS
HMLE
MCF7

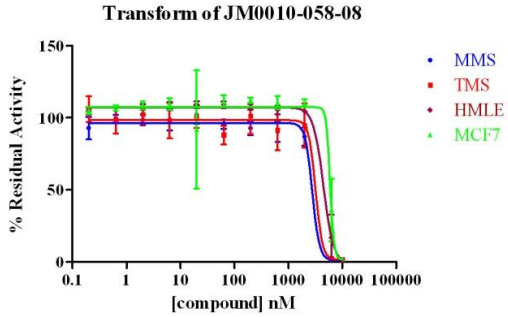
Transform of JM0010-058-08
% Residual Activity
[compound] nM
MMS
TMS
HMLE
MCF7

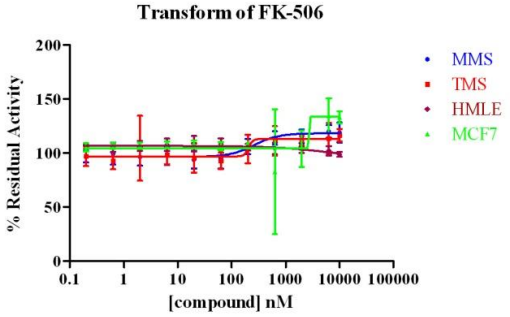
Transform of FK-506
% Residual Activity
[compound] nM
MMS
TMS
HMLE
MCF7

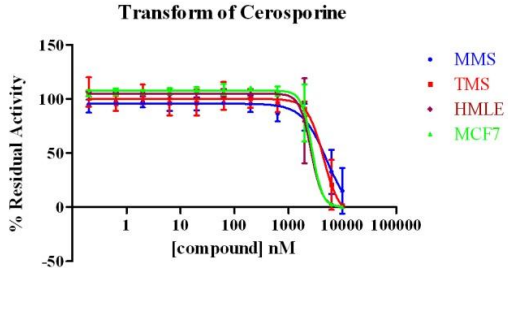
Transform of Cerosporine
% Residual Activity
[compound] nM
MMS
TMS
HMLE
MCF7

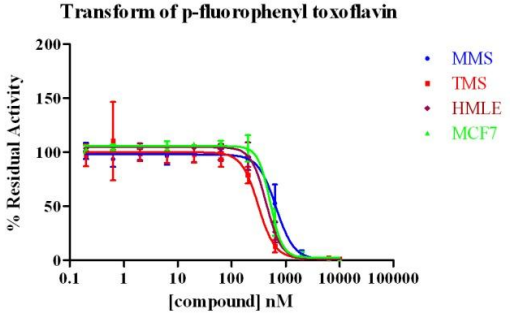
Transform of p-fluorophenyl toxoflavin
% Residual Activity
[compound] nM
MMS
TMS
HMLE
MCF7

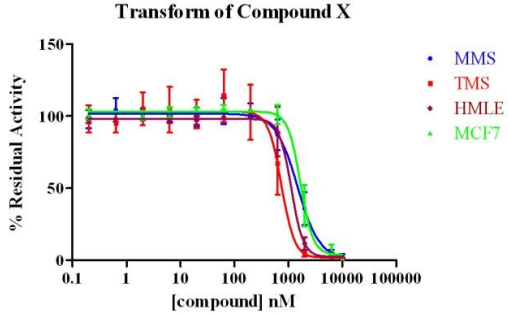
Transform of Compound X
% Residual Activity
[compound] nM
MMS
TMS
HMLE
MCF7

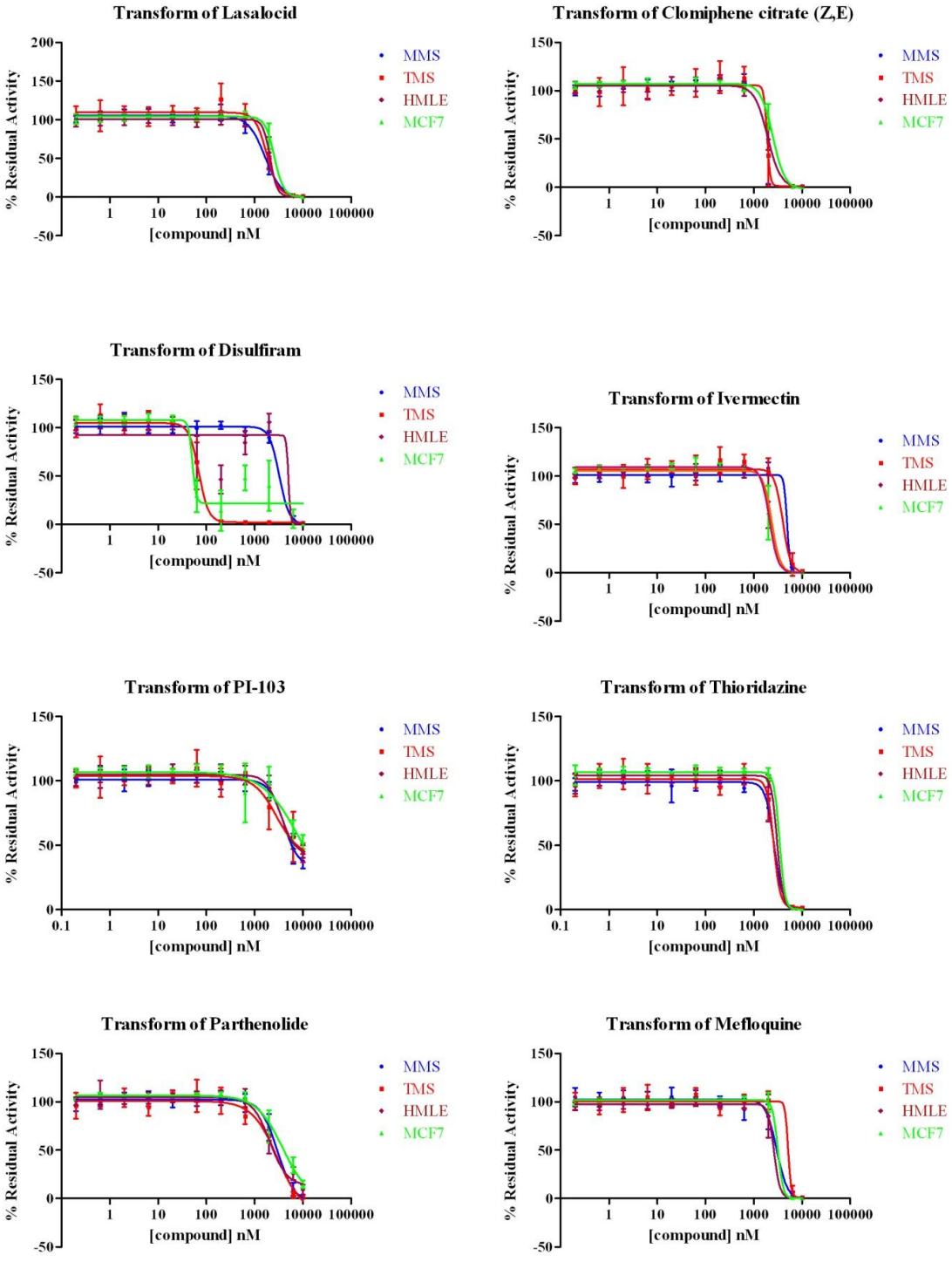
Transform of Lasalocid
Transform of Clomiphene citrate (Z,E)
Transform of Disulfiram
Transform of Ivermectin
Transform of PI-103
Transform of Thioridazine
Transform of Parthenolide
Transform of Mefloquine
% Residual Activity
[compound] nM
MMS
TMS
HMLE
MCF7

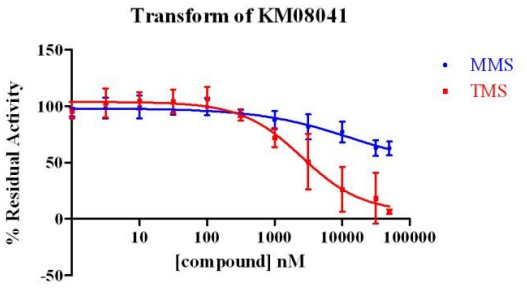
Transform of KM08041
% Residual Activity
[compound] nM
MMS
TMS

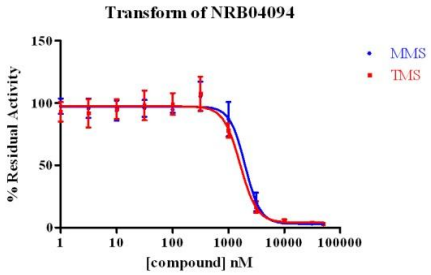
Transform of NRB04094
% Residual Activity
[compound] nM
MMS
TMS

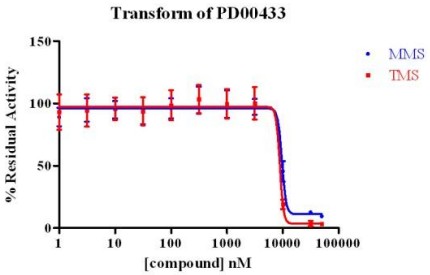
Transform of PD00433
% Residual Activity
[compound] nM
MMS
TMS

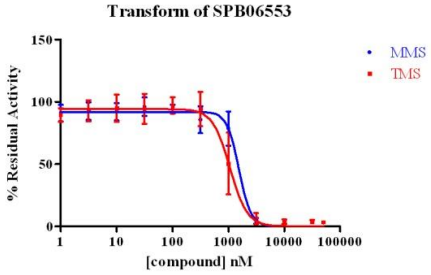
Transform of SPB06553
% Residual Activity
[compound] nM
MMS
TMS

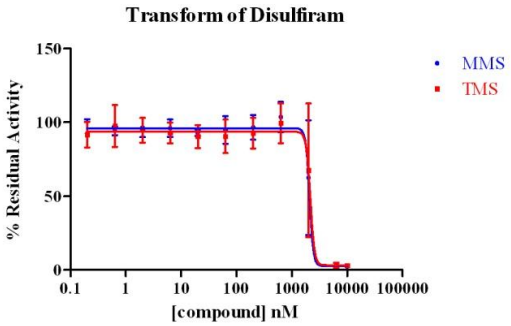
Transform of Disulfiram
% Residual Activity
[compound] nM
MMS
TMS

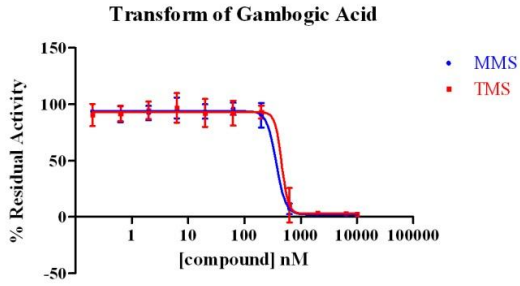
Transform of Gambogic Acid
% Residual Activity
[compound] nM
MMS
TMS

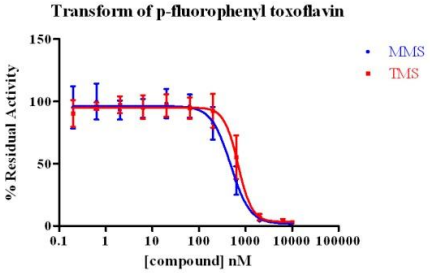
Transform of p-fluorophenyl toxoflavin
% Residual Activity
[compound] nM
MMS
TMS

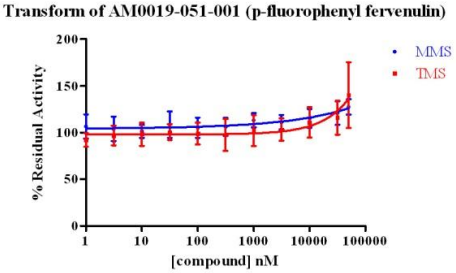
Transform of AM0019-051-001 (p-fluorophenyl fervenulin)
% Residual Activity
[compound] nM
MMS
TMS

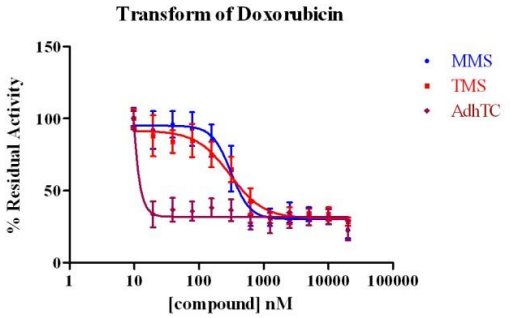
Transform of Doxorubicin
% Residual Activity
[compound] nM
MMS
TMS
AdhTC

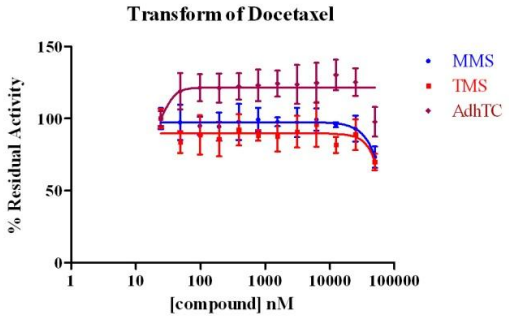
Transform of Docetaxel
% Residual Activity
[compound] nM
MMS
TMS
AdhTC

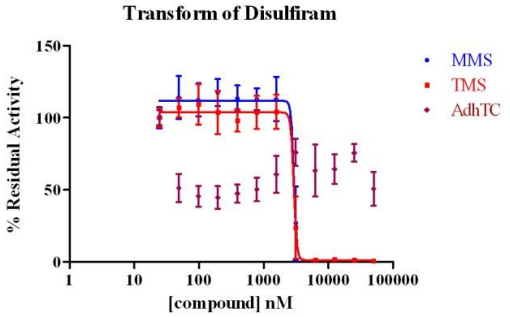
Transform of Disulfiram
% Residual Activity
[compound] nM
MMS
TMS
AdhTC

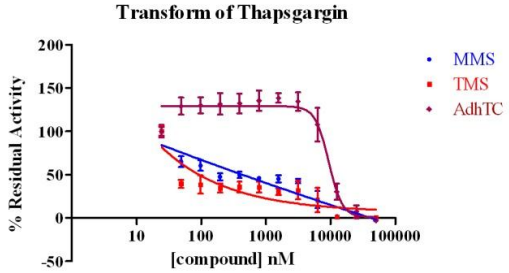
Transform of Thapsgargin
% Residual Activity
[compound] nM
MMS
TMS
AdhTC

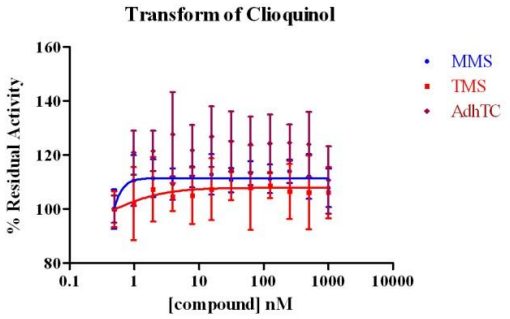
Transform of Clioquinol
% Residual Activity
[compound] nM
MMS
TMS
AdhTC

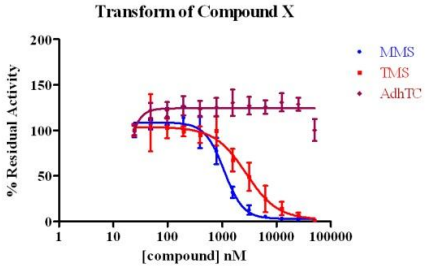
Transform of Compound X
% Residual Activity
[compound] nM
MMS
TMS
AdhTC

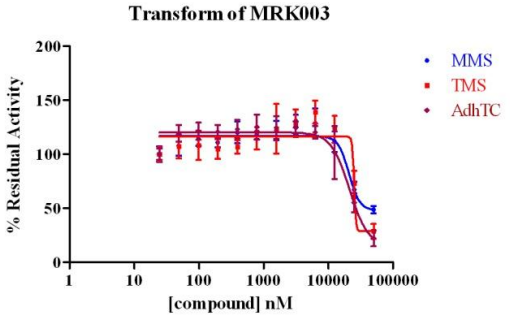
Transform of MRK003
% Residual Activity
[compound] nM
MMS
TMS
AdhTC

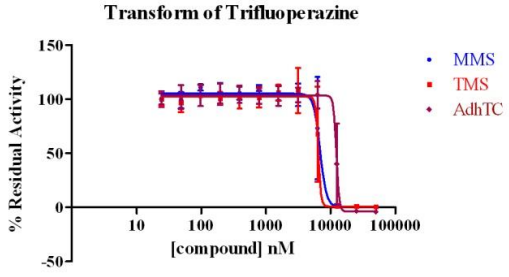
Transform of Trifluoperazine
% Residual Activity
[compound] nM
MMS
TMS
AdhTC

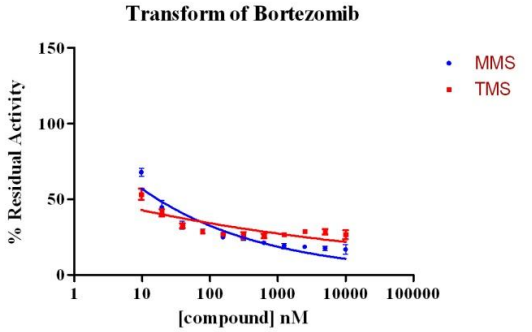
Transform of Bortezomib
% Residual Activity
[compound] nM
MMS
TMS

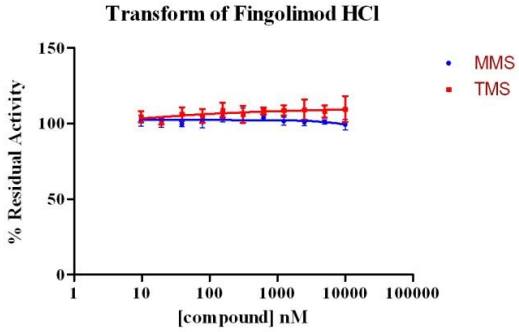
Transform of Fingolimod HCl
% Residual Activity
[compound] nM
MMS
TMS

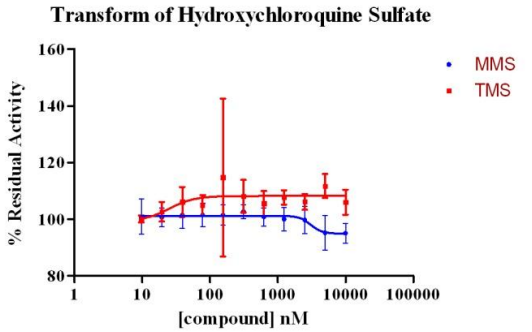
Transform of Hydroxychloroquine Sulfate
% Residual Activity
[compound] nM
MMS
TMS

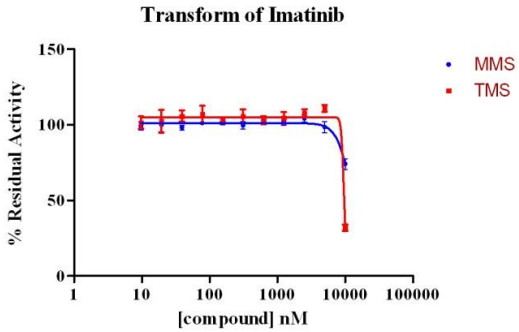
Transform of Imatinib
% Residual Activity
[compound] nM
MMS
TMS

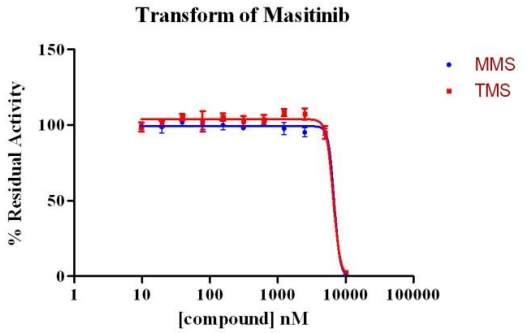
Transform of Masitinib
% Residual Activity
[compound] nM
MMS
TMS

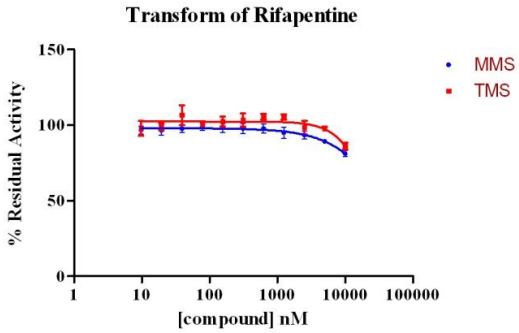
Transform of Rifapentine
% Residual Activity
[compound] nM
MMS
TMS

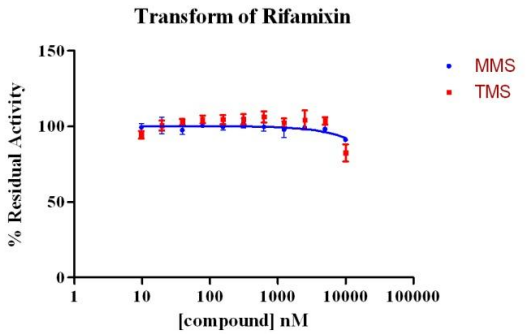
Transform of Rifamixin
% Residual Activity
[compound] nM
MMS
TMS

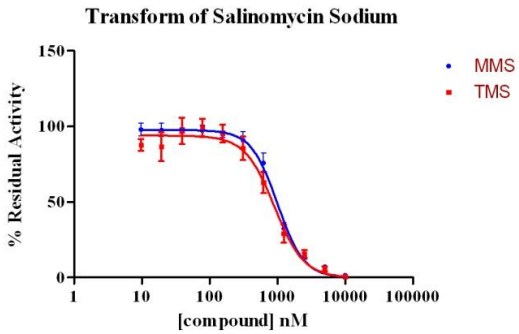
Transform of Salinomycin Sodium
% Residual Activity
[compound] nM
MMS
TMS

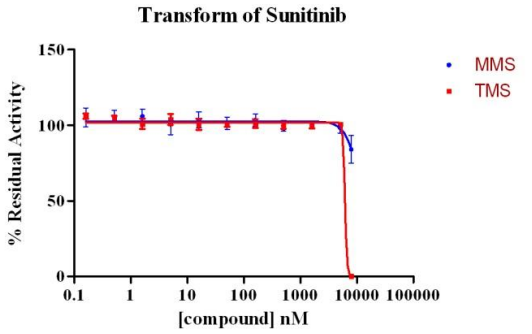
Transform of Sunitinib
% Residual Activity
150
100
50
0
0.1
1
10
100
1000
10000
100000
[compound] nM
MMS
TMS

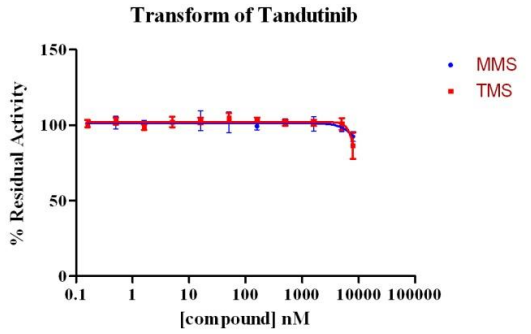
Transform of Tandutinib
% Residual Activity
150
100
50
0
0.1
1
10
100
1000
10000
100000
[compound] nM
MMS
TMS

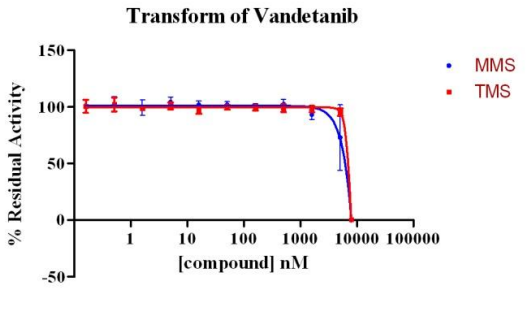
Transform of Vandetanib
% Residual Activity
150
100
50
0
-50
1
10
100
1000
10000
100000
[compound] nM
MMS
TMS

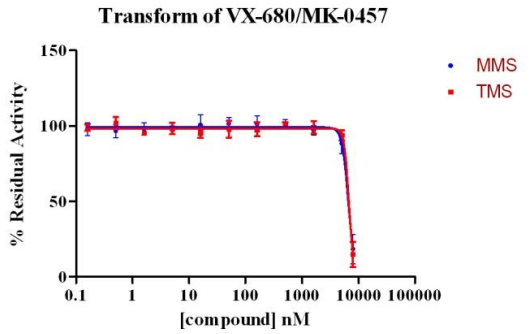
Transform of VX-680/MK-0457
% Residual Activity
150
100
50
0
0.1
1
10
100
1000
10000
100000
[compound] nM
MMS
TMS